VOLTAGE AND FREQUENCY REGULATION OF A STAND-ALONE SELF-EXCITED INDUCTION GENERATOR WITH AN UNREGULATED PRIME MOVER

Ghulam Dastagir

A Thesis

In

The Department

Of

Electrical and Computer Engineering

Presented in Partial Fulfillment of the Requirements

for the Degree of Master of Applied Science at

Concordia University

Montréal, Québec, Canada

April 2008

Your file Votre référence
ISBN: 978-0-494-40878-0
Our file Notre référence
ISBN: 978-0-494-40878-0

ABSTRACT

Voltage and Frequency Regulation of a Stand-Alone Self-Excited Induction Generator with an Unregulated Prime Mover

Ghulam Dastagir

The squirrel-cage induction machine is very attractive for small and medium power generation schemes because of its low cost, robustness and high power density (W/kg). However, the magnitude and the frequency of the generated voltage depend upon the rotor speed, the amount of capacitive excitation, and the load in stand-alone systems with unregulated prime movers. A common approach for providing regulated voltage and frequency to the load is the use of an asynchronous link (ac-dc-ac) power electronic converter. The main disadvantage of this scheme is that the two series connected ac-dc converters have to be rated at least to the rated generator output power.

This thesis investigates the use of a single reduced rating ac-dc converter, or voltage source inverter (VSI), connected to the stator of a self-excited induction generator (SEIG) for regulating purposes. Reactive power control is used to regulate the voltage magnitude while active power control, made possible by using a battery bank at the dc side of the VSI, regulates the voltage frequency. An experimental set-up is implemented for the proposed scheme operating with unregulated micro hydro and wind turbines, implemented on a prime mover emulator. The experimental results are in agreement with the simulation results, theoretical analysis and design specifications.

ACKNOWLEDGMENTS

The author would like to express his sincere gratitude to his supervisor, Dr. Luiz A. C. Lopes for his invaluable guidance, advice, friendship and financial support throughout the course of this study.

Special thanks to Mr. Joseph Woods for his technical support, friendship, kindness, and unconditional help.

The author would also like to thank his colleagues in the P. D. Ziogas Power Electronics Laboratory. Smart suggestions from and helpful discussions with Reinaldo Tonkoski, Maged Barsom, Saeed khedri and Nayeem Ahmed Ninad are unforgettable.

Last but not least, the author is very grateful towards his parents whose constant support made it possible to finish the project.

To my wife Adeeba

and kids

Zarrar and Hasnain

TABLE OF CONTENTS

LIST OF FIGURES

LIST OF TABLES

LIST OF ACRONYMS

AC	Alternating Current (*A*)
A/D	Analogue/Digital
CC-VSI	Current Controlled VSI
D/A	Digital/Analogue
DC	Direct Current (*A*)
DG	Distributed Generation
DQ	Direct Quadrature
DSP	Digital Signal Processor
IGBT	Insulated-Gate Bipolar Transistor
I/O	Input/Output
KVL	Kirchoff's Voltage Law
rms	Root-Mean-Square value
SEIG	Self Excited Induction Generator
SCIG	Squirrel-Cage Induction Generator
SPWM	Sinusoidal Pulse Width Modulation
SRG	Switched Reluctance Generator
STATCOM	STATic synchronous COMpensator
PCC	Point of Common Coupling
PMSG	Permanent Magnet Synchronous Generator
PWM	Pulse Width Modulation
PMDC	Permanent Magnet DC Machine

VARIAC	Variable Auto Transformer
VAR	Variable Reactive
VCVS	Voltage Controlled Voltage Source
VSI	Voltage Source Inverter
WECS	Wind Energy Conversion System
WRSG	Wound Rotor Synchronous Generator
WRIG	Wound Rotor Induction Generator

LIST OF PRINCIPAL SYMBOLS

a	Changes in Current during Transient (A)
A	Area (m^2)
B_{sh}	Shaft damping Constant $(N\,m\,s\,/\,rad)$
E_d	Direct Axis Inverter Voltage (V)
E_q	Quadrature Axis Inverter Voltage (V)
C	Capacitance (F)
C_T	Torque Coefficient
C_P	Power Coefficient
F	Per Unit Frequency $(p.u)$
f_x	Cross Over Frequency (Hz)
f_{sw}	Switching Frequency (Hz)
f	Frequency (Hz)
φ	Ratio of Wheel Speed to Spouting Velocity (m/sec)
$G_cV(s)$	Voltage Controller
$G_cf(s)$	Frequency Controller
$H_i\,(s)$	Current Controller
h	Effective Head (m)
H	Net Head (m)
hp	Horse Power
η	Efficiency (%)
I_A	Armature Current (A)

I_{cr}	Current Ripple (%)
I_d	Direct Axis Current (A)
I_q	Quadrature Axis Current (A)
J_{wt}	Wind Turbine Inertia $(Kg\ m^2)$
K_{sh}	Shaft Torsional Spring Coefficient $(N\ m\ /\ rad)$
kW	Kilo Watt
K_p	Proportional Gain
K_i	Integral Gain
L	Inductance (H)
λ	Tip Speed Ratio
m_a	Modulation Index
PI	Proportional Integral
P_{SCL}	Stator Copper Losses (W)
P	Active Power (W)
Q_w	Water Flow Rate $(m^3\ /\ sec)$
Q	Reactive Power (Var)
R	Resistance (Ω)
R_A	Armature Resistance (Ω)
R_r	Rotor Resistance (Ω)
R_s	Stator Resistance (Ω)
R_L	Load Resistance (Ω)
r	Radius (m)
ρ	Air Specific Density $(Kg\ /\ m^2)$

s	Slip
t	Time (sec)
T_s	Sampling time (sec)
τ	Torque $(N\,m)$
θ	Angle of Deflection (Degree)
V_d	Direct Axis Generator Voltage (V)
V_q	Quadrature Axis Generator Voltage (V)
V_m	Maximum Voltage (V)
V_g	Air Gap Voltage (V)
V_{dc}	DC voltage (V)
V	Velocity (m/sec)
ω	Angular Speed (rad/sec)
ω_n	Natural Frequency (rad/sec)
w	Weight of Water Striking Vanes (Kg/sec)
X_{ls}	Stator Leakage Reactance (Ω)
X_{lr}	Rotor Leakage Reactance (Ω)
X_m	Magnetization Reactance (Ω)
X_c	Capacitive Reactance (Ω)
X_{mo}	Unsaturated Magnetization Reactance (Ω)
ζ	Damping Factor
Z_s	Characteristics Impedance (Ω)

CHAPTER 1
INTRODUCTION

1.1 BACKGROUND

The increasing importance of fuel saving due to the present day energy crisis, the high cost of the conventional fuel, the high rate at which the conventional fuel is being consumed and the environmental issues has been responsible for the revival of interest in the so-called alternative sources of energy such as wind energy, hydro, solar, biomass, wave energy, tidal power, ocean thermal energy and geothermal energy [1]. Many of these generate electricity by means of an electro-mechanical power converter, where the mechanical input power is supplied from some sort of turbine or prime mover. This Thesis focuses on small wind and hydro energy conversion schemes for stand-alone systems which are simple, economical and yields good power quality. The major advantage of hydro and wind is that they are renewable energy resources which can be easily harnessed and used for practical purposes.

Wind is an inexhaustible source of energy. It has served the mankind for many centuries by propelling ships and driving wind mills to grind grain and pump water [2]. Interest in wind power decreased when cheap and plentiful petroleum products became available. The high installation cost and the stochastic and uncertain nature of the wind placed wind power at an economic disadvantage [1, 2]. However, in 1973, when the Arab nations placed an embargo on petroleum, the days of cheap and plentiful petroleum came to an end and people realized that an alternative energy source besides oil and natural gas

would have to be developed. The two conventional energy sources besides petroleum which can supply the long-term world energy needs are coal and nuclear energy [2]. Unfortunately, both coal and nuclear energy presents serious environmental problems along with large initial cost and waste disposal. Because of these problems, renewable energy resources like wind power, hydro power and solar power have been strongly encouraged and have become the predominant alternative energy sources.

Wind energy is being investigated as a supplemental source to meet the increasing energy demand. The use of wind turbines for the generation of electrical power was first introduced by Denmark [2]. The nature of wind energy is much different from conventional sources such as hydro and steam. Due to its intermittency one cannot guarantee that there will be enough mechanical power to be converted to electrical and supplied to a load. However, when interconnected with a power grid having a much higher capacity than that of the Wind Energy Conversion Scheme (WECS), the fluctuations in energy input of the WECS can be taken care of by the other power stations connected to the grid [3, 4]. Variations in the wind velocity will cause the wind rotor to run at different speeds affecting the efficiency of the wind turbine. In the case of stand-alone systems, the uncertainty of the wind availability presents a more serious problem requiring some sort of energy storage, supplemental source of energy or even the capability of load shedding.

Hydro power is a well-established technology, which has been producing firm power at competitive prices for about a century. It is the principal source of electric power in the world and provides about a fifth of the worlds annual electric output. The essential characteristics of a hydro site are the effective head, (H) and the water flow rate,

(Q_w). The power carried by the water is roughly 10 times the product of these two quantities and it can be calculated more accurately as: $P(\text{kW}) = \frac{\eta \times \gamma \times Q_W \times H}{1000}$.

Where, P = Generator output in (kW), η= Overall efficiency of plant, γ= Specific weight of water (N/m^3), Q = Flow of water (m^3/sec) and H = Net head (m). The electric output power will be rather less than this input power. In estimating the resource, the power available at any time is at least as important as the annual total. Resource estimates must take into account energy losses. In any real system the water will lose some energy as a result of frictional drag and turbulence as it flows in channels and through pipes, and the effective head will thus be less than the actual head. With these factors incorporated, therefore, the output power becomes: $P(kW) = \eta \times Q_W \times g \times H$. The conversion of the energy of the water into electrical energy is carried out by the turbo-generator, a rotating turbine driven by the water and connected by a common shaft to the rotor of a generator. The available head and the required power are critical in determining the most suitable type of turbine for a site [5].

As water passes through a hydro plant, its energy is converted into electrical energy by a prime mover known as a hydraulic turbine or water wheel. The turbine has vanes, blades, or buckets that rotate about an axis by the action of the water. The rotating part of the turbine or water wheel is often referred to as the runner. Hydraulic turbines are machines that develop torque from the dynamic and pressure action of water. They can be grouped into two types. One type is an impulse turbine, which utilizes the kinetic energy of a high-velocity jet of water to transform the water energy into mechanical energy. The second type is a reaction turbine, which develops power from the combined

action of pressure energy and kinetic energy of the water. Reaction turbines can be further divided into several types, of which the principle two are the Francis and the propeller type [6]. In micro hydro power plants for a fixed head usually the impulse type turbine is preferred.

In this thesis also the unregulated micro hydro turbine considered is the impulse type hydro turbine, where the speed varies linearly (decreases) with the load torque. Micro hydro power usually refers to hydraulic turbines having a capacity of less than 100 *kW*. There are generally four types of units that are most appropriate to micro hydro and mini hydro systems. Small impulse type turbines are available in numerous sizes. The higher the head available, the better the chance for a suitable installation using a small impulse type turbine. A second standard unit is a small Francis type turbine. A third type, useful for low-head installation, utilizes small propeller type units with the generator usually mounted outside the water passage and a fourth type is the cross flow turbine. Micro hydro power units can utilize belt drives to accommodate to the best turbine speed of operation while allowing for selection of an economical size and type of electric generator [6].

Micro hydro plants can be built at relatively low cost by using indigenous materials as for as possible. The cost of turbine and generator can be reduced by standardizing the sizes and other specifications of the machinery. If the plant is located in the vicinity of an existing grid, it can be designed to feed all the available energy into the grid when demand has risen and the existing grid has been expanded to the region in the future. Traditionally, synchronous generators have been used for stand-alone micro hydro systems, these generators, however require a rotating field system which can be either

wound on salient poles or in distributed slots on a cylindrical rotor, which adds to the manufacturing complexity and cost of the machine, to overcome this problem, brushless generators are often used.

However for micro hydro electric schemes, stand-alone self-excited squirrel-cage induction generators offer significant cost reductions in the system initial cost and may be advantageous compared with the synchronous generators, due to the ruggedness and low maintenance requirements of induction machines [7]. However this type of machine does not allow the regulation of the output voltage and frequency. Some sort of power electronic regulators should be added to the system.

1.2 ELECTRO-MECHANICAL ENERGY CONVERSION SYSTEMS

The basic components of an electro-mechanical energy conversion system used for electric power generations are a prime mover or a source of mechanical power, and an electrical generator that are connected by a shaft. Whenever the speed of the prime mover is lower than the required speed of the generator a gear box is used. This can be avoided by using a generator with a large number of poles. The prime mover can be regulated or unregulated. That is, the amount of power it supplies to the electrical generator can be controlled and adjusted to the amount of power demanded from the electrical generator by a load. In such a case, the shaft speed will be constant which will help to keep the magnitude and frequency of the generated voltage regulated. Power electronic converters are frequently included at the electrical side of the generating system to provide an additional means for regulating the magnitude and the frequency of the generated voltage.

Power generation schemes for stand-alone applications with regulated prime movers can be achieved by using common diesel generator sets (gensets) that employ internal combustion engines and synchronous generators. The frequency of the output voltage can be regulated by regulating the shaft speed of the generator by means of a speed governor that controls the amount of fuel injected into the engine. The magnitude of the output voltage can be regulated by adjusting the dc current applied to the field circuit of the synchronous machine. This system presents a certain degree of complexity and requires frequent maintenance service. Squirrel-cage induction generators have been proposed as a replacement for the more costly and sophisticated synchronous generators. In such a case, the voltage magnitude can be controlled by means of reactive power with either a STATCOM or a SVC but a speed governor is still required for frequency regulation. The system investigated in this thesis assumes that the prime over is unregulated, that is, no speed governor is used thus further decreasing the cost and complexity of the system. A single power electronic converter placed in the stator side of the induction generator is used to provide both frequency and voltage regulation.

In the following section, we will discuss in more detail the basic characteristics of the main components of an electro-mechanical energy generating system.

1.2.1 THE PRIME MOVER

In this thesis the main focus is on the unregulated micro hydro turbine and also the wind turbine. So both the prime movers, unregulated type can be used in conjunction with the induction generator in stand-alone applications. The following subsection

explains the relevant theory and important torque-speed characteristics of both the wind and micro hydro prime mover.

1.2.1.1 Characteristics of a Micro Hydro Turbine

In this study, a micro hydro turbine is assumed to operate with constant input power ($P = \eta\ Q\ g\ H$) resulting from the operation with a fully opened gate valve and a constant water head. Since the speed of the turbine is not regulated therefore both the speed and the shaft torque will vary with the variations of the consumer load. So for a given input power, the possible operating speed and torque can be specified by the torque-speed characteristics of the micro hydro turbine. Usually for an impulse type turbine, the theoretical torque exerted on the shaft is determined in [6, 8] as,

$$\tau = \frac{w}{g} r(1 - k\cos\theta)v(1 - \phi) \tag{1-1}$$

Where,

τ =Torque (*N-m*), w =Weight of water striking vane (*Kg/sec*)

r = Radius of runner (*m*), g = Acceleration of gravity (m/sec^2)

k = Coefficient accounting for loss of velocity moving across vane

θ = Angle of deflection of jet (degree), v = Velocity of water jet (*m/sec*)

ϕ = Ratio of wheel speed to the spouting velocity, $\sqrt{2gh}$ and h = Effective head in (*m*)

Under the above mentioned conditions all the parameters in (1-1) are constants except for the speed related variable (ϕ). Since the effective head is assumed constant, ϕ varies only due to changes of turbine speed. Thus, the theoretical value of torque with speed can be modeled by a linear relationship as shown in Fig. 1-1. This figure also

shows the deviation of the actual torque of an impulse type turbine from the theoretical values [8, 9].

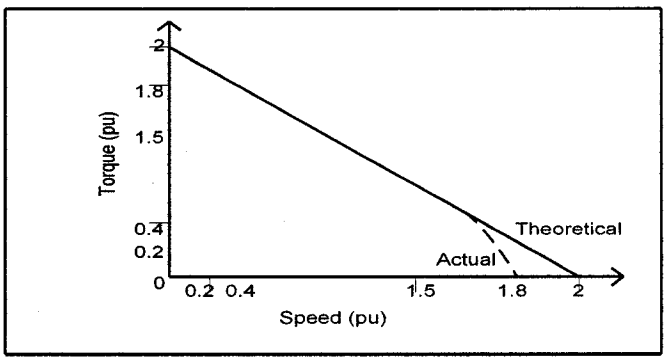

Fig. 1-1 Theoretical and actual variable-speed performance for an unregulated impulse type hydro turbine

Therefore, the shaft torque for a given speed of micro hydro turbine can be determined as, $\tau = \tau_o - m(\omega - \omega_o)$ (1-2)

Where, τ_o and ω_o are any points on the straight line torque-speed characteristics corresponding to the given input hydro power and m is the negative gradient of the characteristics. The theoretical ratio of runaway speed to the normal operating speed is 2.0 for an impulse turbine. Therefore, the theoretical gradient of torque-speed characteristics of an impulse turbine is 1.0 p.u. In the case of reaction type turbines, the runaway speed is dependent on several factors such as the type of turbine, head and the runner blade angle etc. In impulse type turbine the actual value of the gradient may slightly vary from the theoretical predictions. Since the operating torque and speed of the generator under normal conditions are generally known, the variation of torque with varying speed can easily be determined by using (1.2) [8].

1.2.1.2 Characteristics of a Wind Turbine

A horizontal axis wind turbine is used as the prime mover to drive the self-excited induction generator. The kinetic energy available in wind is converted to mechanical energy and transferred as shaft torque input to the induction generator, which in turn converts it to electrical energy. The torque τ on the low speed side, available from a wind turbine is a function of the wind velocity V and the torque conversion coefficient C_T and can be mathematically represented by [4],

$$\tau = \frac{1}{2}\rho ARC_T V^2 \tag{1-3}$$

Where,

ρ = specific density of air (1.25 kg/m^2), A= swept area of the blades (m^2)

R= radius of the rotor blade (m)

A wind turbine can be characterized by its torque and or power versus speed characteristics. For a horizontal axis wind turbine, the amount of power (P) that a turbine is capable of producing is given by,

$$P = \frac{1}{2}C_p \rho A V^3 \tag{1-4}$$

$$\tau = \frac{P}{\omega_m} \tag{1-5}$$

Where,

C_p = power coefficient, it can be related to torque coefficient by $C_P = \lambda C_T$

ρ =Air density (kg/m^2), V =Wind velocity (m/sec)

A =Swept area (cross sectional area) of turbine (m^2) and ω_m = Rotor speed (rad/sec)

The power coefficient of the wind turbine (C_p) varies non-linearly with the tip speed ratio (λ) and is a characteristic of wind turbine. The tip speed ratio is defined as the ratio of the linear speed at the tip of the blade $(\omega_t R)$ and the wind speed (V) where (ω_t) being the rotational tip speed of the blade. A typical $C_p - \lambda$ curve is shown in Fig. 1-2 and the power as well as torque versus speed characteristics of the wind turbine is shown in Fig. 1-3.

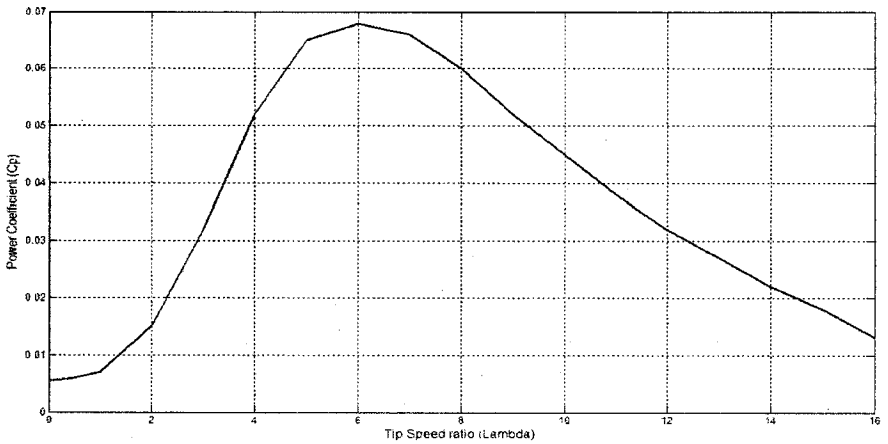

Fig. 1-2 The C_p versus λ curve

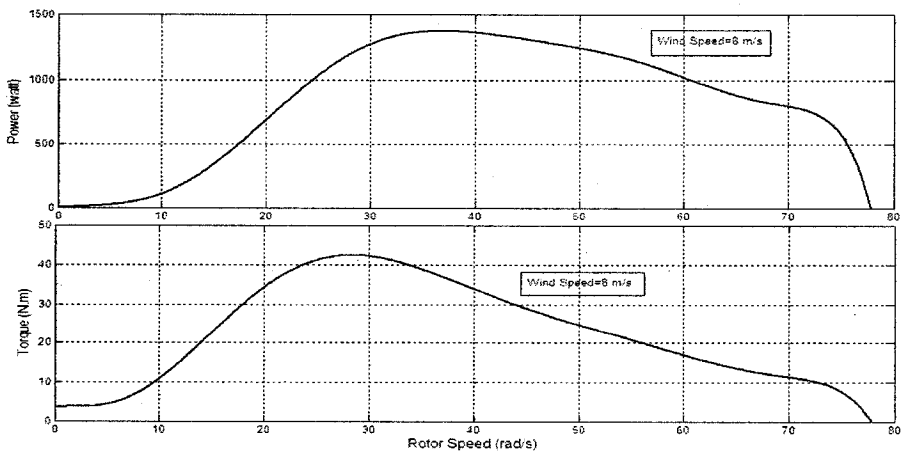

Fig. 1-3 Power and torque versus speed characteristics of wind turbine

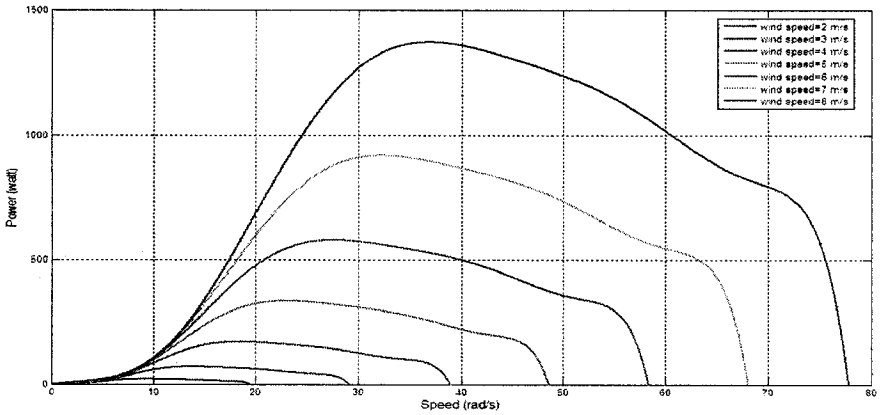

Fig. 1-4 Power versus speed characteristics of wind turbine for different wind speeds

Fig. 1-2 shows that the power coefficient (C_p) reaches a maximum value for a tip speed ratio (λ_m), which in turn yields the maximum mechanical power available in the wind turbine for a given wind speed. The steady-state turbine speed is determined by the power balance at the wind turbine. That is, for a given wind speed and a required input mechanical power in the generator to supply a given load, the steady-state value of (λ) is obtained from the (C_p) versus λ curve with the (C_p), that results $P_{wt} = P_{in}$. This value of (λ) must be larger than (λ_m) for a stable operation where (λ_m) is the maximum tip speed ratio as shown in the Fig. 1-2 [10]. A typical wind turbine power versus speed characteristics for variable wind velocities are also shown in Fig. 1-4, as one can see from (1-4) that power is increasing almost eight times for every doubling of wind speed and decreases eight times for every halving of the wind speed.

1.2.2 GENERATOR TYPES AND POWER ELECTRONIC CONVERTERS

Several types of ac generators are being used in renewable energy systems. This can be classified in three large groups that are:

(A) Asynchronous generator:-

(i) Squirrel-cage induction generator (SCIG)

(ii) Wound rotor induction generator (WRIG)

(B) Synchronous generator:-

(i) Wound rotor synchronous generator (WRSG)

(ii) Permanent magnet synchronous generator (PMSG)

(C) Switched reluctance generator (SRG)

We will now review the features of different generator technologies for comparison:

The technology of induction generator is based on the relatively mature electric motor technology. Induction motors are perhaps the most common types of electric motors used throughout the industry. The most common generator used in wind turbines is the induction generator. It has several advantages, such as robustness and mechanical simplicity and it is produced in large series, it also has a low price. The major disadvantage is that the stator needs a reactive magnetizing current. Induction generator has two electromagnetic components, the rotating magnetic field constructed using high conductivity, high strength bars located in a slotted iron core to form a squirrel-cage and the stationary armature is constructed using electrical windings located in a slotted iron core. Early developments in induction generators were made using fixed capacitors for excitation. With the availability of power electronic converters, induction generators can

be provided with adjustable excitation and operate in stand-alone in a stable manner with appropriate controls. The rotor of an induction generator can be designed as so-called short-circuit rotor (squirrel-cage rotor) or as a wound rotor. The squirrel-cage induction generator (SCIG) has been the prevalent choice because of its mechanical simplicity, high efficiency and low maintenance requirements. The generator and the wind turbine rotor are coupled through a gearbox, as the optimal rotor and generator speed ranges are different. Wind turbines based on a SCIG are typically equipped with a soft-starter mechanism and an installation for reactive power compensation, as SCIG consume reactive power. While in the case of wound rotor induction generator (WRIG), the electrical characteristics of the rotor can be controlled from the outside, and thereby a rotor voltage is impressed. The windings of the wound rotor can be externally connected through slip rings and brushes or by means of power electronic equipment, which may or may not require slip rings and brushes. By using power electronic converter, the power can be extracted or impressed to the rotor circuit and the generator can be magnetized from either the stator circuit or the rotor circuit. The disadvantage of WRIG is that it is more expensive than and not as robust as SCIG.

In the case of synchronous generators, the magnetic field on the rotor is developed in discrete north and south poles usually through the action of passing the dc current through insulated rotor windings. Power to the rotor is fed via slip rings or by a brushless exciter system and the stator construction is the same as for the induction generator.
The synchronous generator is much more expensive and mechanically more complicated than an induction generator of same size. However, it has one clear advantage compared with the induction generator is that it does not need a reactive magnetizing current. The

magnetic field in the synchronous generator can be created by using permanent magnets or with conventional field windings. If the synchronous generator has a suitable number of poles, it can be used for direct-drive application without any gearbox. As a synchronous generator, it is probably most suited for full power control as it is connected to the grid through a power electronic converter.

Micro power systems currently in the market use the generator designs based on the permanent magnet technology. In the permanent magnet machines (PMSG), the efficiency is usually higher than the induction machine, as the excitation is provided without any energy supply. The PMSG generator also has two electromagnetic components. The rotating magnetic field constructed using permanent magnets and may have salient poles or may be cylindrical. The salient pole machines are more common in low speed applications. While the stationary armature is of wound type that is similar to the one described for the induction generator. The benefit is that power can be generated at any speed to meet the current conditions. The voltage output from the generator is unregulated, multiple phase ac. This voltage varies as a function of the speed and load. This voltage output is connected to a solid state power conditioning system and regulates the entire power output.

The technology of switched reluctance generator is based on the concepts that magnetically charged opposite poles attracts. The SRG is a synchronous generator with a doubly salient construction, with salient poles on both the stator and the rotor. Excitation of the magnetic field is provided by the stator current in the same way as it is provided for the induction generator. Typically, there are unequal number of salient poles on the stator and rotor. Both are constructed by using laminated electrical grade steel and there

is no winding on the rotor. Armature coils located on the stator poles are concentric and are isolated from one another. The voltage output from the SR generator is dc and has high ripple content. The voltage output can be filtered, and is regulated by adjusting the duration of the excitation current. The SRG is considered inferior to the PMSG because of its lower power density and it has a lower efficiency than PMSG. The commutation of the stator coil is accomplished by the controller [11, 12].

The most common configurations of generators and connverters for grid-connected electro-mechanical power generation systems are shown in Fig. 1-5. A wind turbine is used in the figures to represent the prime mover.

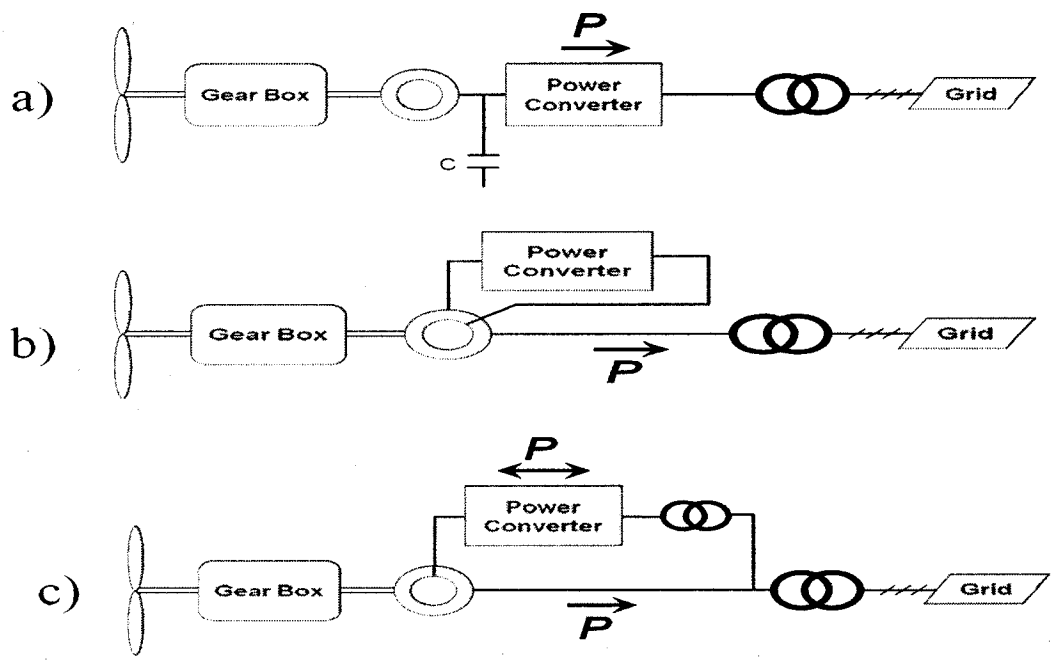

Fig. 1-5 Common generator and power electronic converter configurations [12, 13]

Type (a) configuration is typical of uncontrolled generators such as squirrel-cage induction generators (SCIGs) or permanent magnet synchronous generators (PMSGs). A

gear box is included when the generator presents a low number of poles and the turbine speed is low. The generator can be connected directly to the grid in which case the wind turbine will operate with constant speed. The power converter can be either a simple soft-starter or a more elaborate converter that allows the shaft speed to be varied, feature that can be used for operating the turbine at the point of maximum power. Such a converter would be of the ac-ac type (frequency converter), requiring either a matrix converter or an ac-dc-ac converter for the job. It is worth mention that it should be rated at the full generator power. A capacitor is often included in the system to provide reactive power to a direct-coupled SCIG.

Type (b) is commonly used with wound rotor induction generators (WRIGs). A variable resistance is connected to the rotor circuit in a configuration known as optislip that allows a limited variation of the shaft speed. It has been used by the Danish manufacturer Vestas since the mid-1990s. The major disadvantage of this system is the reduced efficiency due to the losses in the variable resistance.

Type (c) configuration also employs a WRIG. However in such a case, the variable resistance of type (b) configuration is replaced by a frequency converter. It provides a wider range of dynamic speed control compared with the optislip, depending on the size of frequency converter. Typically, the shaft speed range is from -40% to +30% of synchronous speed for a converter rated at approximately 30% of nominal generator power. The converter can also perform the reactive power compensation and minimize the grid-connection transient i.e. smoother grid connection. The variable speed concept is used by this configuration and it basically maintains the power quality characteristics of the pitch-regulated system [12].

1.3 THESIS SCOPE AND CONTRIBUTION

The focus of this research work is on simple and economical electro-mechanical energy conversion systems for stand-alone applications. It considers the use of an unregulated prime movers and squirrel-cage induction generators that present low cost, robustness and high power density (W/kg). The major challenge in this case is the regulation of the magnitude and frequency of the generated voltage. Instead of using the conventional ac-dc-ac frequency converter that is rated at 2 p.u power, a small (0.5-1 p.u power) power electronic converter with an energy storage device (battery) in the dc side is placed at the stator side of the generator. A suitable strategy needs to be devised for controlling the real and reactive power components so as to achieve good power quality. The main contributions of this thesis are:

1. Analysis and design of a low cost stand-alone electro-mechanical energy conversion system suitable for unregulated prime movers.
2. Modeling of the system and calculation of key components such as filters, for reduced harmonic content, and linear controllers for the regulation of the magnitude and frequency of the output voltage.
3. Implementation of a 2-hp prototype and extensive testing with different types of unregulated prime movers, considering variations in the input mechanical power and variations in the electrical load.

1.4 THESIS OUTLINE

The contents of this thesis are organized in five Chapters.

The first Chapter introduces the topic of renewable energy and electro-mechanical energy conversion schemes. Two types of prime movers are considered in the study. Different power electronic converter topologies that are commonly used in conjunction with renewable energy sources are also discussed here.

The second Chapter discusses the relevant theory and modelling of the proposed system. DQ model of the VSI are presented and then linear PI controllers are designed. A control scheme is proposed for the overall system voltage and frequency regulation based on the independent P and Q control. The control scheme is tested by implementing PI controllers and the simulation results are presented to validate the design for the proposed control scheme.

The third Chapter explains the design of the main components of the proposed system. Induction generator parameters are identified based on conventional laboratory tests and then a procedure for the Steady-state analysis of induction generator is presented. Excitation requirement for the induction generator to maintain 1 p.u terminal voltage at no-load and at full-load are determined. Frequency and voltage loops are also designed here.

The fourth Chapter presents experimental results based on a 2-hp prototype system. Two types of prime movers are considered for the experimental tests, a hydro turbine and the wind turbine. Extensive laboratory tests are performed to see the effect of voltage and frequency regulation of stand-alone generating system with variations in load as well as variations in wind speed. Experimental results verify the effectiveness of the proposed control scheme.

The fifth Chapter summarizes the work carried out in this thesis and the final conclusion. Suggestions for future work on this topic are also presented here.

CHAPTER 2
MODELING OF THE PROPOSED SYSTEM

2.1 INTRODUCTION

The overall system under consideration is shown in Fig. 2-1. There one can see an unregulated turbine (prime mover) that supplies mechanical power to the induction generator. In the stator of the induction generator one can also see a dump load and one capacitor bank for the excitation of the generator during startup. These are separated from the ac load, a VSI and another capacitor bank by a breaker so that some power can be supplied to the load by the VSI, when the prime mover cannot supply any mechanical power to the generator. The second capacitor bank, in the load side of the breaker, is used for filtering the switching harmonics of the VSI [14].

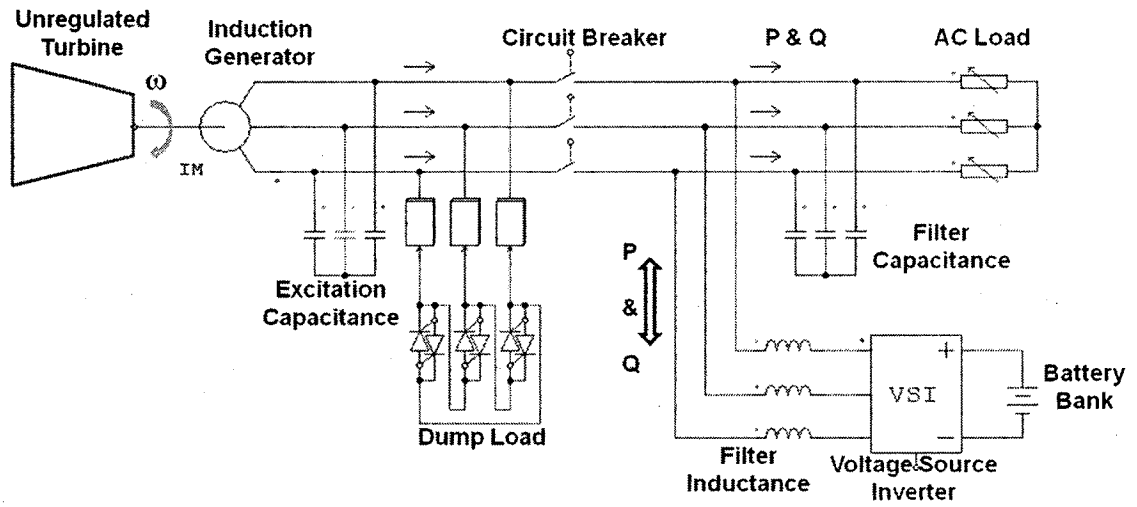

Fig. 2-1 Schematic diagram of the proposed regulated stand-alone SEIG system

The focus of the Thesis is on the control of the VSI under normal conditions. That is, when the circuit breaker is closed, the generator supplies active power to the system and the state of charge of the battery is such that it can absorb or supply active power to the ac system. The start-up of the generator and control of the dump load are out of the scope of this Thesis.

The aim of the modeling of a system is to obtain in mathematical form a description of the dynamical behavior of the system in terms of some physically significant variables. As the nature of the system changes, the system variables also changes. Despite the differences in the physical variables used to characterized systems in various disciplines, certain fundamental similarities exist. It is therefore necessary to analyze the relationships between the system variables and to obtain a mathematical model. So to represent a physical system by using computer simulation, a suitable mathematical model representing the physical variables is necessary. In the proposed scheme, there are three main systems that need to be modeled for the purpose of the computer simulation as shown in the schematic diagram of the system in Fig. 2-1. They are the induction generator, the voltage source inverter (VSI) and the unregulated prime mover. For the purpose of computer simulations the modeling of all the three main systems are necessary.

In the following section, first we will discuss the per-phase steady-state model of induction generator to carry out its steady-state analysis and then the DQ based model of the VSI with the necessary formulation of equations and their derivations that are necessary to model the system will be presented. The model of the prime mover was already discussed in Chapter 1 under the characteristics of the prime mover. Based on the

DQ model of the VSI, linear current controllers are designed. A control scheme is proposed for the regulation of stand-alone self-excited induction generator voltage and frequency, based on the independent control of active and reactive power. Finally to verify the proposed control scheme, some preliminary simulation results are presented.

2.2 MODEL OF THE SQUIRREL-CAGE INDUCTION GENERATOR

To understand the steady-state behavior of shunt capacitor SEIG in stand-alone schemes, one needs to investigate the based configuration of SEIG i.e. the regular shunt SEIG that is driven by an unregulated turbine supplying power to an isolated load. Steady-state analysis plays a vital role in designing phase of the system and is also essential for understanding the operation of the system. The schematic diagram of such an application is shown in Fig. 2-3. In this section, the procedure of calculating the steady-state performance of SEIG supplying power to an isolated community, at given speed for different values of capacitance will be discussed. All the equations will be derived that are necessary for the steady-state analysis of SEIG.

2.2.1 SELF-EXCITATION OF THE INDUCTION GENERATOR

The phenomenon of self-excitation of an induction machine is well established. An induction machine with capacitors connected to its terminals and driven by a prime mover can build up voltage in a manner similar to the dc shunt machine. Residual magnetism in the core of the induction machine sets up a small alternating voltage in the stator, this voltage applied to the capacitor causes a lagging magnetizing current to flow

in the stator windings. If the capacitance is of the proper value, the excitation current that can flow will cause the air gap flux to increase, resulting in a higher voltage, larger excitation current drawn by the capacitor, more air gap flux, and so on until the terminal voltage reaches its final value. The final or steady-state value of the voltage is determined by the saturation curve and the capacitive reactance per phase. The criterion being that the lagging volt-amperes of excitation equal the leading volt-amperes of the capacitors [15, 16]. Under no-load, the steady-state value of the air-gap voltage V_g (same as the phase voltage) is given by the intersection of the magnetization curve and capacitor load line as shown in Fig. 2-2.

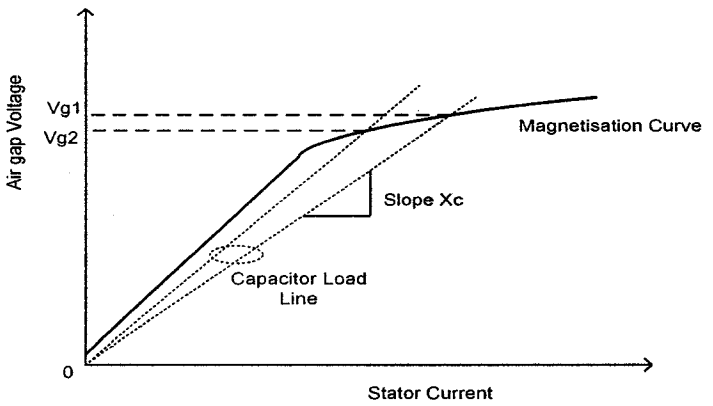

Fig. 2-2 Magnetization curve and capacitor load line

2.2.2 STEADY-STATE ANALYSIS OF SEIG [17]

Various analytical models have been developed to predict the steady-state performance as well as the transient performance of SEIG operating with either regulated or unregulated prime movers. The most commonly used models in the literature are, impedance-based model, DQ reference frame model, admittance-based model and

operational circuit-based model. In [18], the induction generator performance was studied using the stand-alone self-excited generating system shown in Fig. 2-3 and the analytical model based on the conventional single-phase equivalent circuit with per-unit parameters is shown in Fig. 2-4 for balanced steady-state condition. In this thesis the same steady-state equivalent circuit of induction generator is used to get the performance of the machine under different operating conditions by using Matlab simulations.

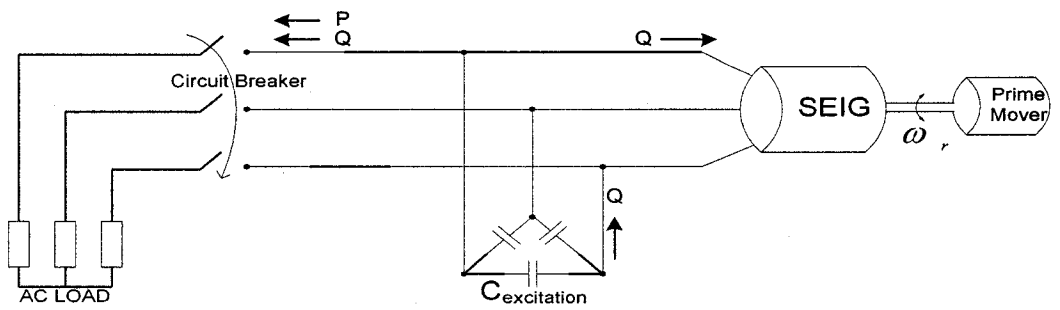

Fig. 2-3 Stand-alone self-excited induction generator (SEIG)

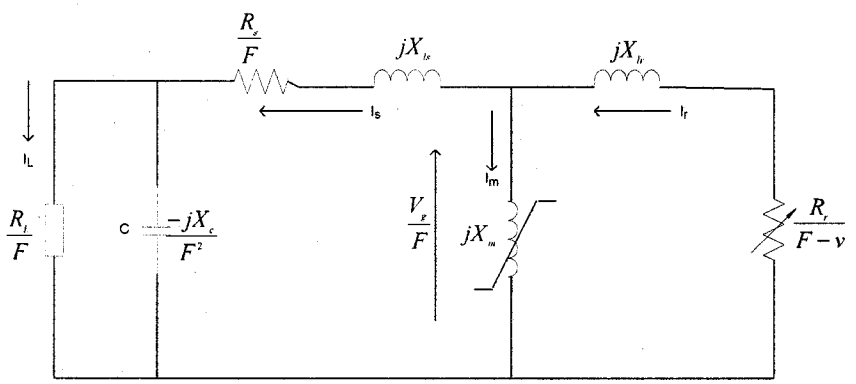

Fig. 2-4 The per-phase steady-state equivalent circuit of stand-alone induction generator

As one can see from Fig. 2-3, the induction generator operates with a three-phase capacitor bank, Δ-connected across its stator terminals and supplying power to the ac load. By using the equivalent circuit of Fig. 2-4, the per-unit frequency F and the magnetizing reactance X_m of the nonlinear magnetizing characteristics of the generator

are obtained as a function of terminal capacitance C and per-unit shaft speed v for a given machine parameters by setting the stator loop impedance term to zero.

$$I_s.Z_s = 0 \tag{2-1}$$

Where,

$$Z_s = (\frac{R_s}{F} + jX_{ls}) + (\frac{\frac{-jX_c}{F}R_L}{-jX_c + FR_L}) + \frac{(\frac{R_r}{F-v} + jX_{lr})jX_m}{(\frac{R_r}{F-v} + jX_{lr} + jX_m)} \tag{2-2}$$

Since under steady-state conditions, I_s cannot be equal to zero, $Z_s = 0$. This implies that both the real and imaginary parts of the characteristic impedance, Z_s are equal to zero. The real and the imaginary parts are non-linear functions with X_m and F as the two unknown variables, and they can be written in a compact form as follows:

$\mathrm{Re}\{Z_s\}=$

$$f(X_m, F) = (A_1X_m + A_2)F^2 + (A_3X_m + A_4)F + A_5 \tag{2-3}$$

$\mathrm{Im}\{Z_s\}=$

$$g(X_m, F) = (B_1X_m + B_2)F^3 + (B_3X_m + B_4)F^2 + (B_5X_m + B_6)F + (B_7X_m + B_8) \tag{2-4}$$

Where, the coefficients A and B in (2-3) and (2-4) contains machine parameters, per-unit speed and load impedance and are defined in the appendix (A-2).

The Newton-Raphson method is used to solve the above two nonlinear equations with two unknown parameters i.e. the magnetizing reactance (X_m) and the per unit frequency (F) for a given machine parameters, excitation capacitance, magnetizing curve, load impedance and the per-unit speed. In the model, load power factor is assumed to be unity and the core loss parameter is neglected. The model used in Fig. 2-4 has been extended for the evaluation of various steady-state performance characteristics of stand-

alone induction generator. The implementation of the Newton-Raphson algorithm in Matlab program to carry out the steady-state analysis of SEIG is as follows,

Newton-Raphson iteration equation is,

$$\begin{bmatrix} X_m \\ F \end{bmatrix}_{i+1} = \begin{bmatrix} X_m \\ F \end{bmatrix}_i = J^{-1} \begin{bmatrix} f \\ g \end{bmatrix} \tag{2-5}$$

Where i is the number of iteration and J is the Jacobian matrix and is given by,

$$J = \begin{bmatrix} \frac{\partial f}{\partial X_m}(X_m, f) & \frac{\partial f}{\partial F}(X_m, f) \\ \frac{\partial g}{\partial X_m}(X_m, f) & \frac{\partial g}{\partial F}(X_m, f) \end{bmatrix} \tag{2-6}$$

The iteration process starts by using the initial conditions as, $\begin{bmatrix} X_m \\ F \end{bmatrix} = \begin{bmatrix} X_{mo} \\ v \end{bmatrix}$ where X_{mo} is the unsaturated magnetizing reactance and v is the per-unit speed. When the iteration stops at a preset error, the right values of the magnetizing reactance X_m and the per-unit frequency F which satisfy both (2-3) and (2-4) can be obtained.

To find the steady-state performance of SEIG under specified conditions, one needs the value of the air gap voltage V_g at the calculated value of X_m and F. The air gap voltage can be computed by using the machine magnetization curve. The magnetization curve shown in Fig. 3-6 and Fig. 3-7 is obtained experimentally, by running the machine at synchronous speed that corresponds to a per-unit frequency F at 1-p.u.

The magnetization curve obtained experimentally showing the air gap voltage V_g and the magnetization reactance X_m will be discuss in chapter 3, where all the data are presented in p.u systems. The V_g versus X_m curve is non-linear and need to be linearized at the

saturation region. Excel program can be used to get the piecewise linearized equations of the saturation part as shown in Fig. 3-7.

By knowing X_m and F, the air gap voltage V_g can be computed from the linearized equations obtained in (3-11) from the experimental plot of V_g versus X_m characteristics. Since all the parameters (X_m, F, v *and* X_c) are known, the steady-state performance of the induction generator using the equivalent circuit shown in Fig. 2-4 can be easily calculated as follows,

$$I_s = \frac{V_g}{F(Z_1 + Z_{LC})}, \quad I_L = \frac{I_s Z_C}{(R_L + Z_C)}, \quad V_T = I_L R_L, \quad P_{o(w)} = 3 V_T I_L$$

$$I_r = \frac{I_s Z_m}{(Z_2 + Z_m)}, \quad Q_{(var)} = 3 V_T^2 \frac{F}{X_C}, \quad P_{IN(w)} = 3 I_r^2 R_r \frac{F}{(F - v)}, \tag{2-7}$$

$$Z_1 = R_s + jFX_{ls}, \quad Z_2 = \frac{R_r F}{F - v} + jFX_{lr}, \quad Z_c = \frac{-jX_c}{F}, \quad Z_{LC} = \frac{Z_C R_L}{(Z_C + R_L)}$$

One can also include the unregulated prime mover characteristics in the steady-state model of three-phase balanced induction generator described above. Here the speed of the unregulated prime mover in terms of angular frequency of the generator is obtained by equating the real power delivered by the prime mover and the input power of the generator. From the reactive power balance between the VAR supplied by the excitation capacitor and consumed by the machine and load, single equation in terms of angular frequency is obtained, which is solved numerically to obtain frequency and hence the steady-state performance of SEIG is computed [8].

2.3 D-Q MODEL OF THE VSI AND DESIGN OF INNER CURRENT CONTROL LOOPS [19, 20]

The schematic diagram of stand-alone self-excited induction generator (SEIG) with excitation capacitor, voltage and frequency controller (current controlled VSI + battery bank) and consumer load is shown in Fig. 2-5.

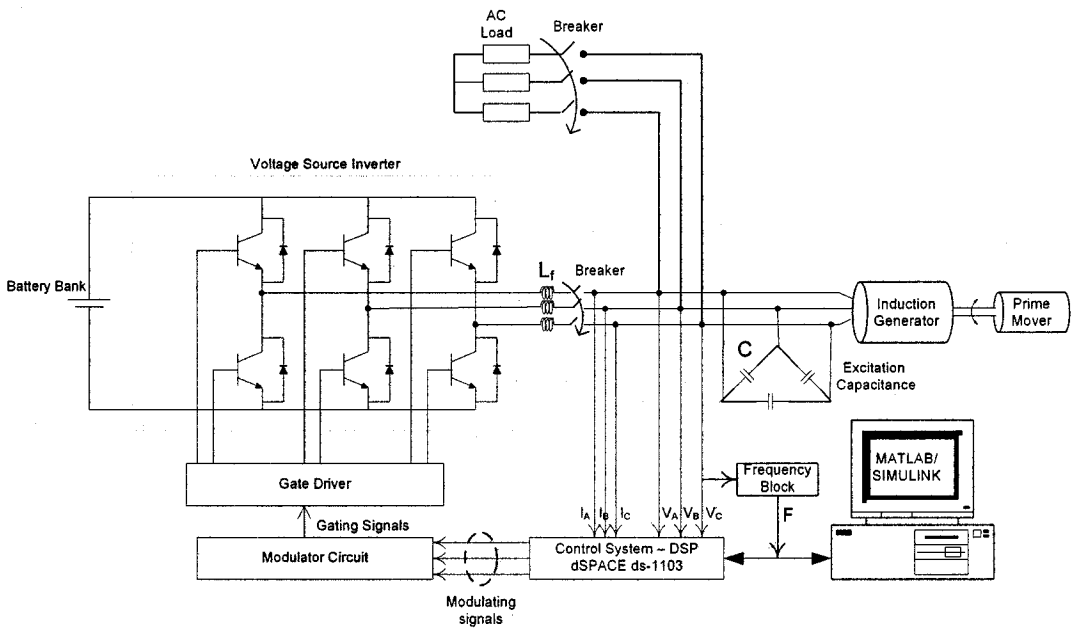

Fig. 2-5 Schematic diagram of SEIG controller system

The controller consists of a three-phase insulated gate bipolar transistor (IGBT) based current controlled voltage source inverter (CC-VSI), a battery bank on the dc-side and an inductor on the ac-side. The output of the inverter is connected through the ac filtering inductor to the stator of the induction generator. A battery bank is used to supply or absorb active power *P*. The current controller is implemented in the DQ synchronous reference frame. A suitable model can be developed from the VSI model alone as shown in Fig. 2-6, where a battery bank is placed at the dc side of the VSI. Thus the self

supporting dc bus is supplied by a battery bank therefore the dc bus voltage would not change significantly. Besides, P will not be used to regulate V_{dc} but F of the generator.

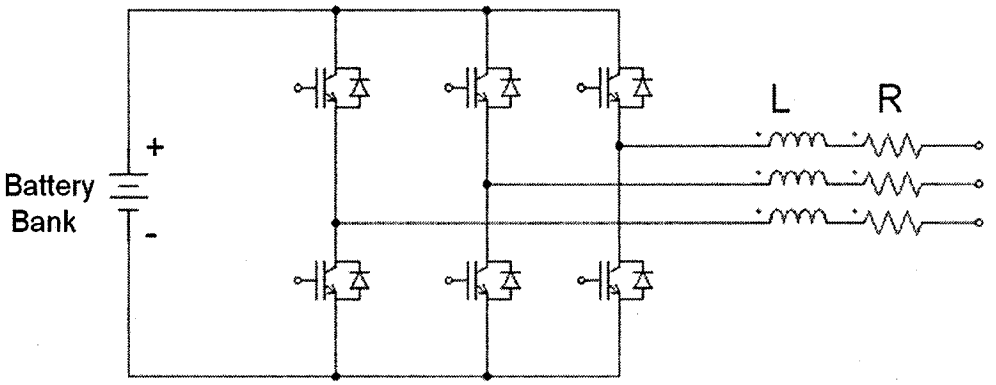

Fig. 2-6 Model of the CC-VSI

The DQ reference frame equivalent circuit model of VSI is shown in Fig. 2-7. This figure focuses only in the portion involving the filter inductance on the ac side of the inverter, i.e. only active and reactive power flow between the machine terminal bus with voltages V_d and V_q and the inverter output bus with voltages E_d and E_q.

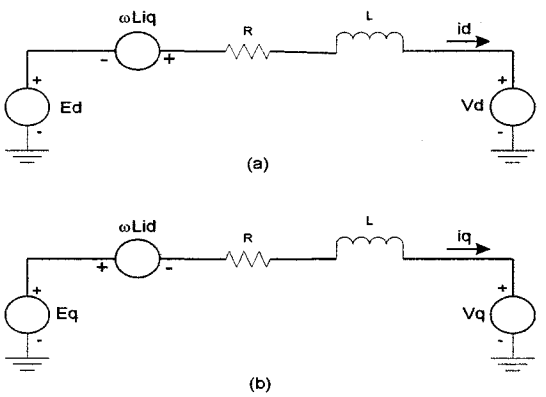

Fig. 2-7 DQ reference frame power circuit representation of filter inductor of VSI with an equivalent series resistor

The system behaviour can be better described by the following loop equations for both d-axes and q-axes circuits as shown in Fig. 2.7 (a) and (b). By applying KVL to the circuit one gets,

$$E_d = -\omega L i_q + R i_d + L\frac{di_d}{dt} + V_d \tag{2-8}$$

$$E_q = \omega L i_d + R i_q + L\frac{di_q}{dt} + V_q \tag{2-9}$$

The terms $\omega L i_q$ in (2-8) and $\omega L i_d$ in (2-9) represent a coupling between the two circuits. That is, a variation in the current in the d-axis circuit (i_d) will create a variation in the current in the q-axis circuit (i_q), and vice-versa. Thus when one wants to vary either i_d or i_q both E_d and E_q would have to be varied. Besides, if V_d and V_q vary, the currents will have to vary and then the feedback control loop will define a corrective action with E_d and E_q. These problems can be solved by including feed-forward loops based on

$$E_{d\_ff} = -\omega L i_q + V_d \tag{2-10}$$

$$E_{q\_ff} = \omega L i_d + V_q \tag{2-11}$$

In this way, one can simplify the relationships between i_d and E_d as well as i_q and E_q, resulting equations are,

$$E_d = R i_d + L\frac{\partial i_d}{\partial t} \tag{2-12}$$

By using Laplace transformation, one gets the following transfer function:

$$E_d(s) = R I_d(s) + sL I_d(s) \tag{2-13}$$

$$\frac{I_d(s)}{E_d(s)} = \frac{1}{R + sL} \tag{2-14}$$

The same transfer function will also apply to the q-axes circuit i.e. for the i_q and E_q transfer function. Once we know the transfer function, a linear PI controller can be designed to eliminate the steady-state error. To determine the parameters of the inner PI current controller i.e. the k_p and k_i, the following block diagram in closed loop form can be used:

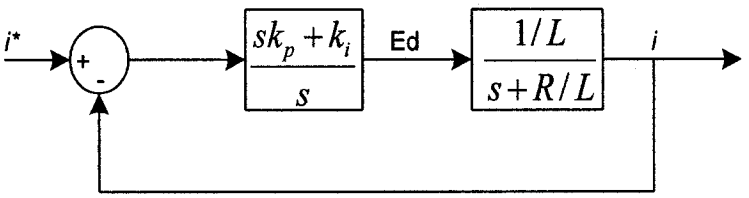

Fig. 2-8 Block diagram for the PI current controller

From the block diagram, the closed loop transfer function can be obtained as follows:

$$\frac{i}{i^*} = \frac{k_p}{L} \frac{s + k_i / k_p}{s^2 + \frac{R + k_p}{L} s + \frac{k_i}{L}} \tag{2-15}$$

From the control system theory, we can solve for the damping ratio and the natural oscillating frequency by equating the characteristics equation in (2-15) with that of the general second order characteristics equation. Doing so yields the following results:

$$\xi = \frac{(R + k_p)/L}{2\sqrt{\frac{k_i}{L}}} \qquad \text{and} \qquad \omega_n^2 = k_i / L$$

With this knowledge in hand, the parameters of the inner current regulator can be designed as follows:

$$k_p = 2\xi\omega_n L - R \tag{2-16}$$

$$k_i = L\omega_n^2 \tag{2-17}$$

According to the technical optimum theory, $\xi = \frac{\sqrt{2}}{2}$ and ω_n relies on the specified time response. Generally the natural frequency is selected as, $\omega_n = \omega_s/50$.

2.4 PROPOSED CONTROL SCHEME FOR THE SYSTEM VOLTAGE AND FREQUENCY REGULATION

The proposed control scheme for the voltage and frequency regulation of SEIG driven by an unregulated turbine is shown in Fig. 2-9. The scheme consists of a voltage source inverter with a battery bank on the dc side. Since a 500 V battery bank was not available in the laboratory, one was emulated by using a full bridge diode rectifier, a filter capacitor and a variable resistor as a dump load. In this way, the VSI can supply and absorb active and reactive power to compensate for shortages and surpluses between the other elements connected to its ac side.

If the input power of the prime mover is constant as in the case of unregulated hydro turbine with a constant head, then the speed of the prime mover and SEIG remains constant therefore the generated frequency will be constant. In the proposed control scheme the magnitude of the SEIG terminal voltage as well as its frequency are measured, and corrective measures are taken according to the control diagram shown in Fig. 2-9. Errors in voltage magnitude affect the reactive power of the VSI ($Q = 1.5\ V_q\ I_d$) while errors in frequency are corrected by means of active power control ($P = 1.5\ V_q\ I_q$).

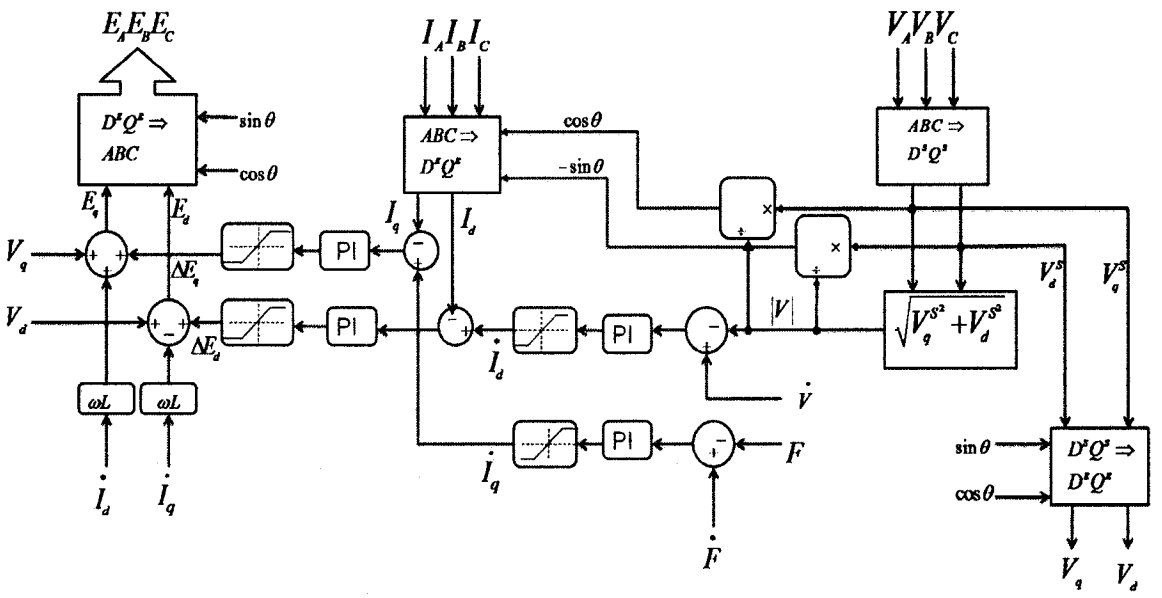

Fig. 2-9 Proposed control scheme for the regulation of voltage and frequency of SEIG

The output of this control system will be a set of three phase sinusoidal signals which will be used as the PWM modulating signals for the gating of the six inverter switches. The control scheme of the VSI is based on the principles of real and reactive power flow between the two buses in a given power system. With the implementation of the above control scheme there is the possibility of decoupling the real power and reactive power so as to ensure the independent regulation of the voltage and frequency at the ac load by reactive and real power respectively.

The regulation of the real and reactive power can be accomplished by controlling the quadrature and direct axes currents I_q and I_d, which can readily be obtained from the abc to dq0 transformation of the three measured inverter line currents. Based on the reference frame selection it is clear that the current I_d exerts control over the reactive power while the current I_q exerts control over the real power with the following relationships,

$$P = \frac{3}{2} . V_q . I_q \tag{2-18}$$

$$Q = \frac{3}{2} . V_q . I_d \tag{2-19}$$

The implementation of the proposed control scheme in Simulink is accomplished by measuring the generator terminal voltage (line-neutral) and the inverter output currents. The voltages V_q and V_d are obtained from the measured three-phase voltages (V_A, V_B, V_C) and then converted it into the stationary dq0 frame first and then in the rotating dq0 frame. By converting the voltages to the rotating frame, we see that the DQ values in the rotating frame are dc values, which yield zero error to step inputs when using the PI controllers. Furthermore, based on the reference frame selection it is clear that the magnitude of V_d has a zero value while V_q has the same magnitude as the peak of the line-neutral generator voltage. From the V_d and V_q components, the voltage magnitude is computed and then the unit vector is generated. The unit vector is used for the transformation between the abc and the dqo frame. Similarly the currents I_d and I_q are obtained from the measurement of the three-phase inverter currents and then converted directly into the rotating dqo frame.

The regulation of the load voltage is accomplished by comparing the actual terminal voltage to a desired reference value. The error between the two goes through the PI controller. By the action of the PI controller, the reference I_d current is generated, which has control over the reactive power, as was mentioned earlier. The reference I_d current is then compared to the actual I_d current and the error between these two by the action of another inner PI current controller defines the direct axis component of the modulating signal E_d of the PWM voltage source inverter.

As for the regulation of the frequency, it is accomplished in a similar manner. Here we compare the actual terminal voltage frequency to a desired reference frequency. The error between the two goes through a PI controller. By the action of the PI controller, the reference I_q current is generated, which has control over the real power. The reference I_q current is then compared to the actual I_q current, and the error signal between these two passed by another inner PI current controller that defines the quadrature axis of the modulating signal E_q of the PWM voltage source inverter. In the control scheme limiters are used to avoid exceeding the rated current and voltage of the inverter. The active and reactive power injected or absorbed by the VSI depends on I_d and I_q currents which can be controlled by varying E_d and E_q components of VSI with SPWM. These signals are added to the feed-forward signals and then converted back to abc to be used as the modulating signals of the PWM. The proposed control scheme will be first tested in a simpler application, where the inverter is connected to the power grid that exchanges controllable amounts of active and reactive power.

2.5 PRELIMINARY SIMULATIONS

Various tests were performed on the implemented control scheme in Simulink to verify the validity of inner current control loop design. This section discusses the various simulation tests and their results.

Based on the selected parameters of L=32mH, R=0.1Ω and the switching frequency of the inverter is selected to be f_{sw}=10kHz, the gains of the PI controllers from (2-16) and (2-17) can be found as, k_p = 56.769 and k_i = 50532 and Fig. 2-10 shows the step response of the inner current control loop tested with simple transfer functions in Matlab.

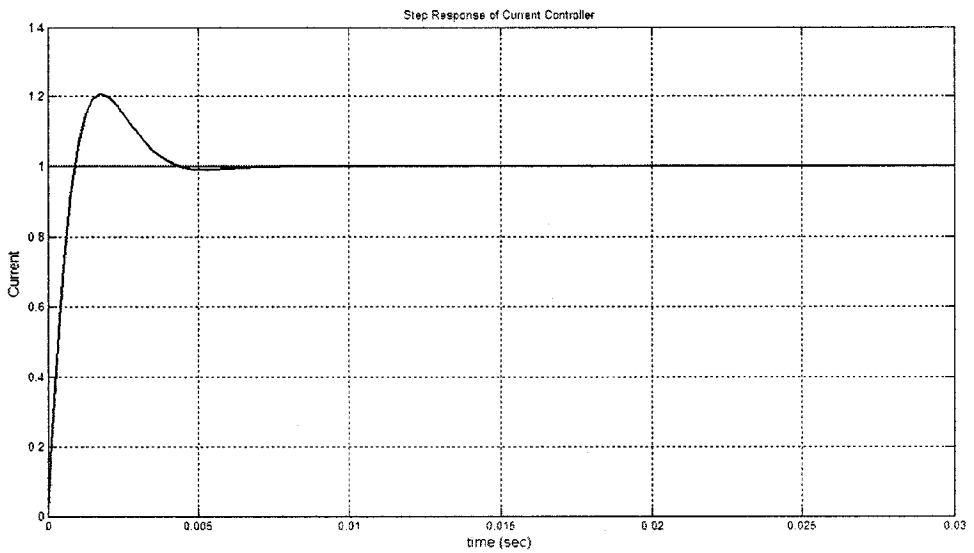

Fig. 2-10 Step response of the inner current control loop

From the trace shown above, the overshoot is approximately 19.5 %. The rise time is approximately 1.5 ms and the transient process is a bit less than 5.5 ms, which is an acceptable response. Once the current control loop design is verified, then the whole scheme can be implemented in Simulink and various tests were performed to further verify the inner current control loop and its validity and performance. The results obtained from these simulations are presented in the following sections.

2.5.1 ID AND IQ REGULATION

The first simulation test that was performed on the implemented scheme with Simulink was the I_d and I_q regulation by imposing the reference currents as the result of step inputs directly in Simulink and see the system response. This test actually tells us that how effectively the inner current control loops are designed and how the designed controllers for the proposed system, reacts for such a step input. The Simulink

implementation of this test is shown in Fig. 2-11. For the simulations, the VSI was connected directly to a three phase voltage source with a magnitude of $208V_{rms}$ line-line with a 1mH inductor in series with each voltage source.

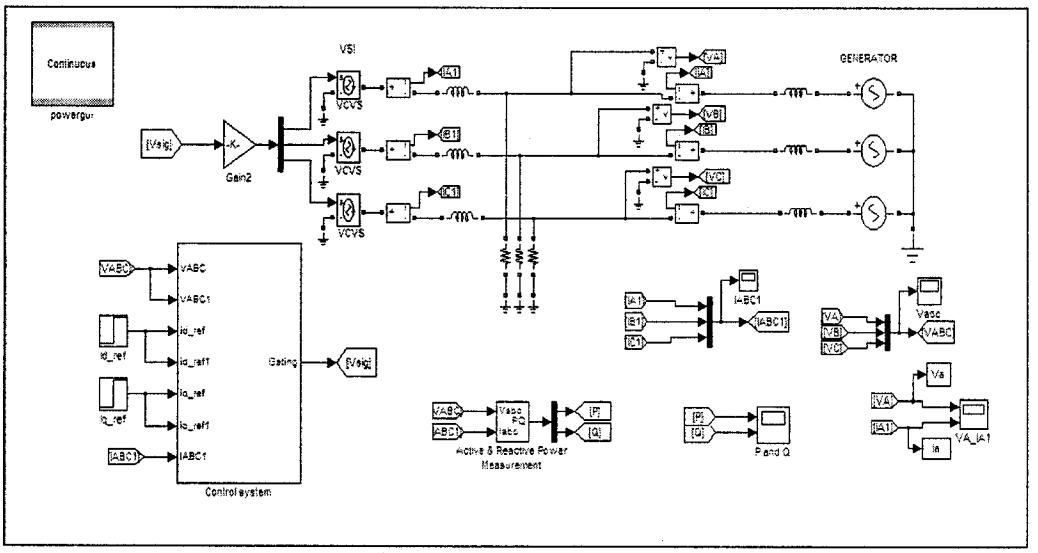

Fig. 2-11 Simulink implementation for the Id and Iq regulation test

In addition to avoid the introduction of current harmonics and to simplify the analysis, the voltage source inverter was modeled by three voltage-controlled voltage sources (VCVS). The magnitude and the phase of the input signals for the VCVS are generated by the control system itself. So the VCVS is actually taking the three modulating signals generated from the control system and convert them into appropriate voltage signals. A 32mH inductor is placed between the VCVS and the voltage source.

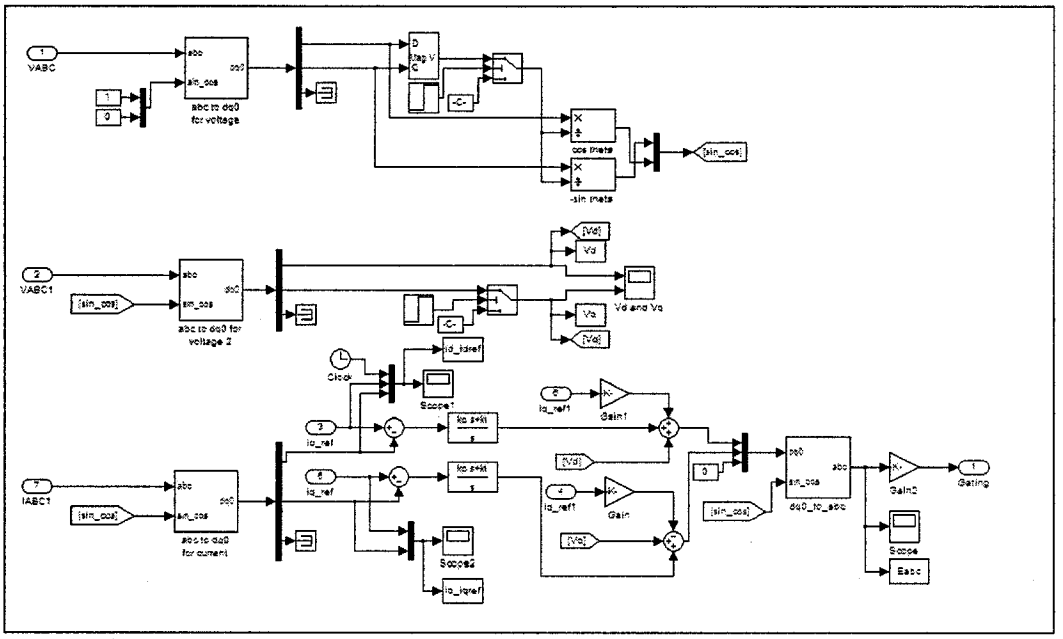

Fig. 2-12 Sub-system inside the main control system

First a step input of magnitude one for the reference current I_{dref} is applied while I_{qref} =0, and then a step input for I_{qref} is applied while keeping I_{dref} =0. This way one can easily analyzed the coupling effect between both the axes currents. As we can see in Fig. 2-13 and Fig. 2-14 that the system reacts very well for such a step input. Also one can notice that there is a relatively small coupling between both the axes currents.

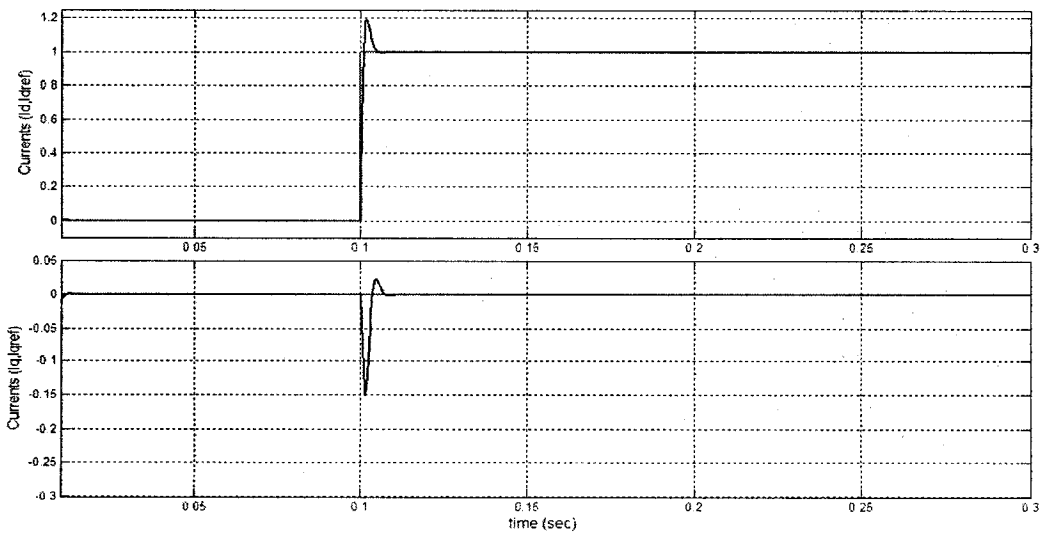

Fig. 2-13 Step change in the reference current Id_{ref} including feed-forward

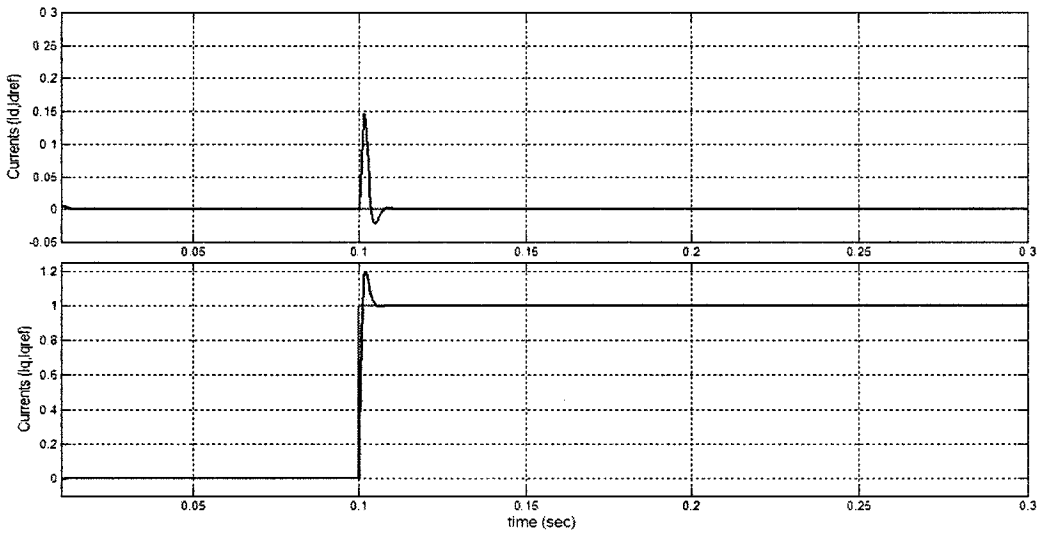

Fig. 2-14 Step change in the reference current Iq_{ref} with feed-forward

To verify the effectiveness of the feed-forward terms in minimizing the coupling effect between both the axes currents, a simulation was run without the feed-forward terms. As one can see in Fig. 2-15 and Fig. 2-16, without the feed-forward terms the coupling effect between both the axes current is greater than with feed-forward terms. This shows that the feed-forward term does reduce the coupling effect and hence making the system more stable by independent control of both the axes currents.

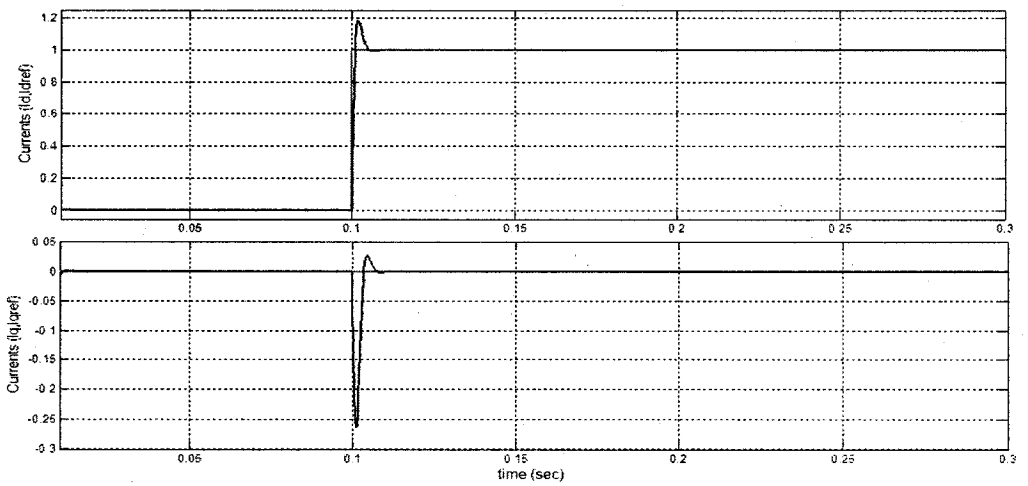

Fig. 2-15 Step change in the reference current Id_{ref} without feed-forward

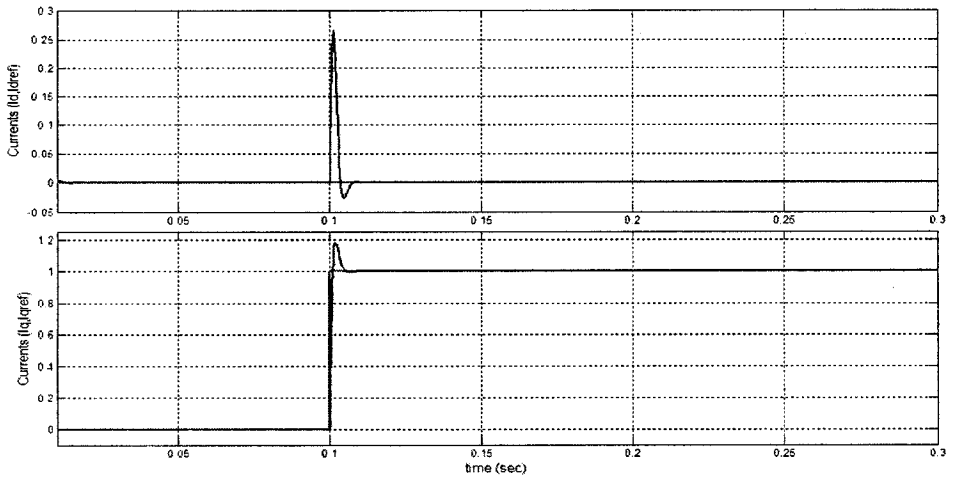

Fig. 2-16 Step change in the reference current Iq_{ref} without feed-forward

2.5.2 REAL AND REACTIVE POWER REGULATIONS

For this test, the reference current I_{dref} and I_{qref} are generated using (2-18) and (2-19) and applying a step input for P and Q. The simulink model for the power equations are shown in Fig. 2-17. Thus the model is generating the reference currents by imposing the required active and reactive power. Since the active power P is responsible for the regulation of quadrature axes current component, I_{qref} and reactive power Q is responsible for direct axes current component, I_{dref}. A simulation was run first by setting active power $P > 0$ and then $P < 0$, and another simulation was run for the reactive power by imposing $Q > 0$ as well as $Q < 0$. In fact for $P > 0$, the VSI should supply active power P to the system, and for $P < 0$ the VSI should absorb P. In the first case the VSI current should be in-phase with the voltage while in the second case it should be out of phase by 180°. Similarly for the reactive power, if $Q > 0$, then the VSI must absorb Q and if $Q < 0$ it should supply Q into the system. Here in the first case the current should lag the voltage by 90° while in the second case it is leading by 90°.

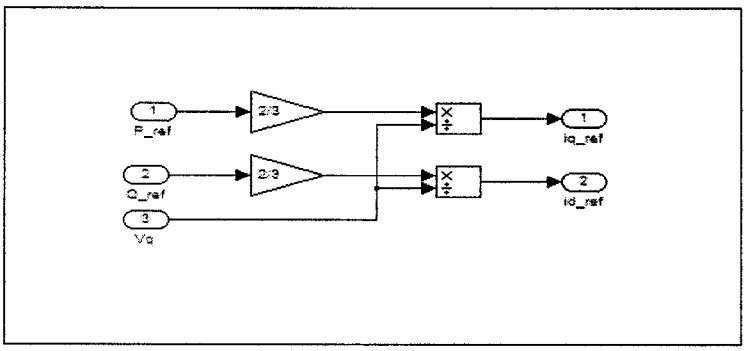

Fig. 2-17 Modeling of equations (2-18) and (2-19)

This is verified by the simulation results shown in Fig. 2-19 to Fig. 2-22. The Simulink implementation for this test is shown in Fig. 2-18

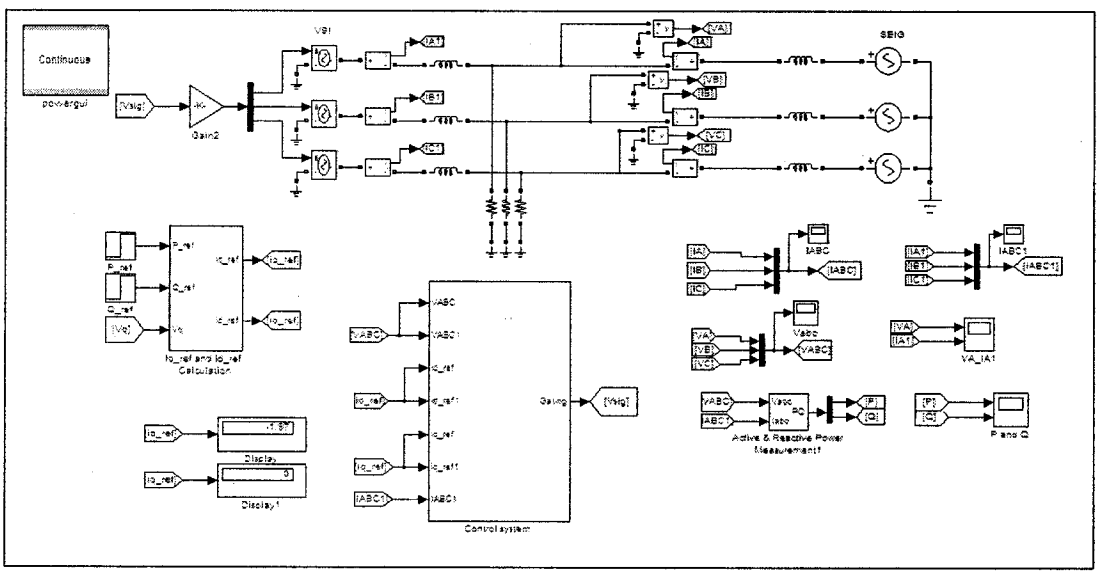

Fig. 2-18 The Simulink implementation for the regulation of (P) and (Q)

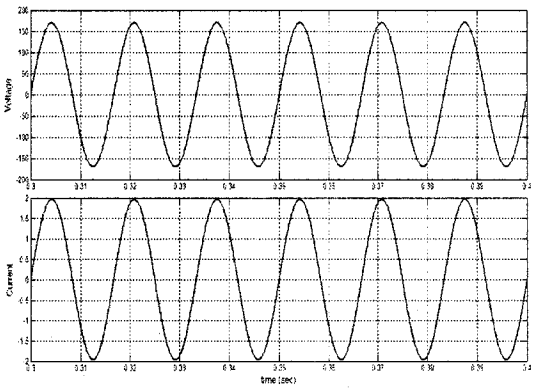

Fig. 2-19 P = 500 and Q = 0

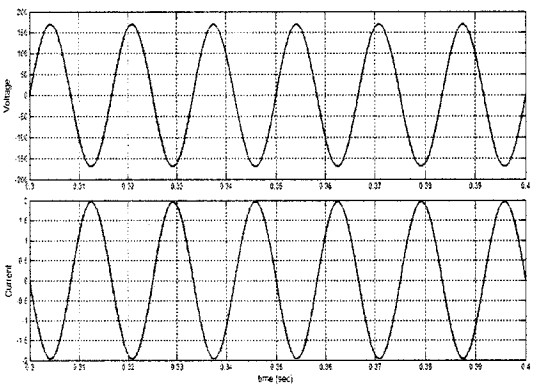

Fig. 2-20 P = -500 and Q = 0

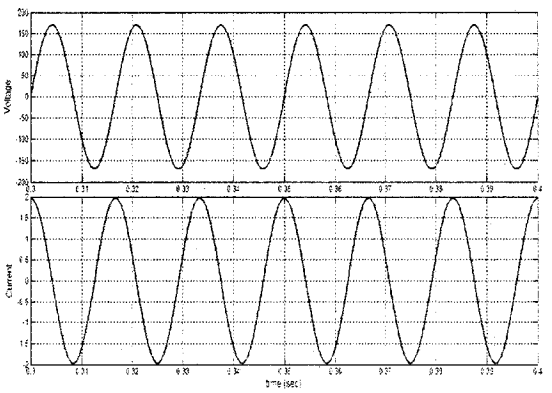

Fig. 2-21 P = 0 and Q = -500

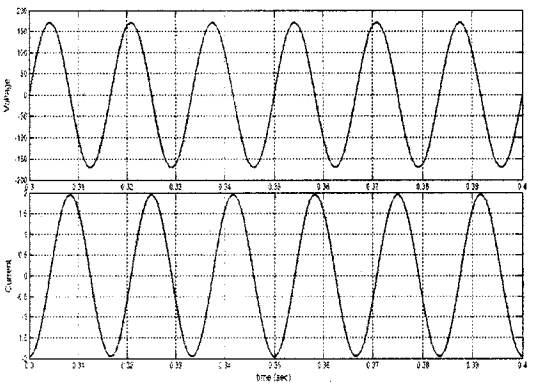

Fig. 2-22 P= 0 and Q = 500

2.6 CONCLUSIONS

This chapter has focused on the modeling of the proposed system. There are three main systems that need to be modeled as shown in the proposed schematic diagram in Fig. 2-1. They are the prime mover, the induction generator (SEIG) and the voltage source inverter (VSI). It started with the introduction about the proposed system, its main components and then the importance of system modeling is presented. The steady-state analysis of SEIG is carried out and the related equations are derived that is necessary to analyze the steady-state model of SEIG. Newton-Raphson algorithm is used to solve the

two non-linear equations for the two unknown parameters i.e. the magnetizing reactance X_m and the per-unit frequency F.

Then, the DQ modeling of the VSI is presented. Based on the DQ model, a transfer function is derived for the plant and then a linear PI controller is designed. The proposed control scheme for the overall system to regulate the system voltage and frequency is discussed and then the control scheme is implemented in Simulink and tested to verify the current control loops. Finally with the implemented control scheme some simulation results were presented and the results validate the current control loop design.

CHAPTER 3

SYSTEM DESIGN AND IMPLEMENTATIONS

3.1 INTRODUCTION

The main schematic of the overall system that need to be designed based on a 2-hp induction generator with an excitation capacitance, a 2-hp dc machine as a prime mover and a current controlled voltage source inverter (VSI) with dSPACE control system is shown in Fig. 3-1.

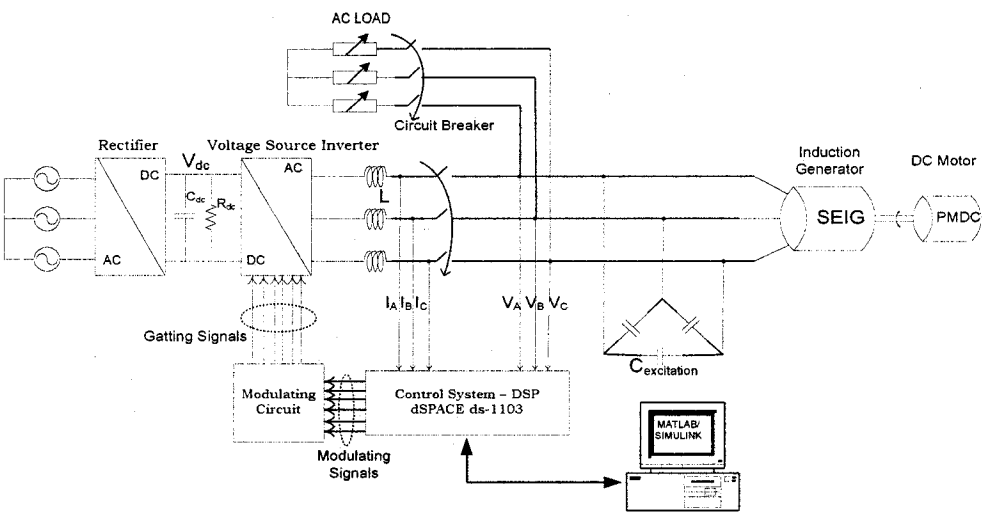

Fig. 3-1 Main schematic of the overall system

As one can see in the schematic diagram, a permanent magnet dc machine emulates the prime mover and a squirrel-cage induction machine is used as the generator. An excitation capacitor is connected at the stator of induction generator to supply the required reactive power needed by the generator. A consumer load and a VSI are connected in parallel with the induction generator. Furthermore, the VSI is connected to a

dc bus capacitor and a resistor on the dc side. The dc bus of the VSI is supplying by a full bridge diode rectifier that configures a battery bank and hence a VSI based controller. The VSI is to supply and absorb active power. For that, a battery bank should be placed at its dc side. Since a 500 V battery bank was not available in the laboratory, one was emulated using a three-phase diode rectifier to supply active power, a variable resistor to consume active power and a capacitor for filtering. It should be noted that the variable resistor allows the dc bus voltage to be manually regulated in the steady-state but not during transient conditions.

An excitation capacitor is connected at the stator of the induction generator to supply the required reactive power needed by the induction generator during start-up and it is calculated based on the rated voltage at 1p.u for a given speed and load impedance. A technique will be used based on the Newton-Raphson algorithm to calculate the no-load as well as full-load capacitance requirement for the induction generator. In the following section, we will discuss how to design the various parameters of the main components in the proposed system and then based on the design the proposed system will be implemented/modeled in Simulink and finally some simulation results will be presented.

3.2 CHARACTERISTICS OF A DC MACHINE [21]

Permanent magnet dc machines PMDC are widely found in a wide variety of low-power applications. In the PMDC machines the field winding is replaced by a permanent magnet, resulting in a simpler construction. Permanent magnets offer a number of useful benefits in low power applications. Chief among these is that they do not require external

excitation and its associated power dissipation to create magnetic fields in the machine. The space required for the permanent magnets may be less than that required for the field winding, and thus permanent-magnet machines may be smaller, and in some cases cheaper, than their externally-excited counterparts. Since there is no field control for the PMDC motor, the torque control is generally based on the control of the armature current. Therefore, there is no magnetic saturation when overload torque is needed. A permanent magnet dc machine is used to emulate different type of prime movers in this study. When a dc voltage source, implemented with another variable transformer and three-phase diode rectifier, is applied to its armature, it presents the same torque versus speed characteristics as of impulse type hydro turbine. For the emulation of a wind turbine, an additional dc-dc converter is placed between the dc voltage source and the motor's armature to control the armature current and thus realize the same torque versus speed characteristics as of a wind turbine.

The torque versus speed characteristics and the related theory about the impulse type hydro turbine was already discussed in chapter 1 under the prime mover characteristics. The equivalent circuit of a permanent magnet dc motor is shown in Fig. 3-2 and its nameplate data is given in Table 3-1.

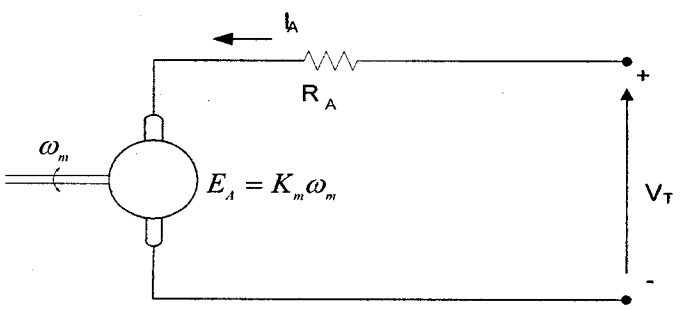

Fig. 3-2 Equivalent circuit of a permanent magnet dc motor

Table 3-1 Nameplate data of permanent magnet dc machine

Baldor-manufacturer Permanent magnet dc machine	
Power (hp)	2
Rated speed (rpm)	1750
Voltage (volt)	180
Current (A)	8.5

The dc machine supplies the real power to the induction generator. To represent the impulse type hydro turbine, an assumption is made that the river has a constant head of water and the turbine gate is opened to a fixed desired position. The torque versus speed characteristics of the impulse type hydro turbine is a straight line as defined by (1-2) and was shown in Fig. 1-1.

The internal generated voltage by the dc machine is given by,

$$E_A = K\phi\omega_m = K_m\omega_m$$
$$K_m = K\phi \tag{3-1}$$

The induced torque developed by the machine is given by,

$$\tau_{ind} = K\phi I_A = K_m I_A \tag{3-2}$$

The KVL equation for the permanent magnet dc motor is,

$$V_T = E_A + I_A R_A \tag{3-3}$$

By using equations (3-1) and (3-2) the machine torque versus speed characteristic can be derived from (3-3) as,

$$\omega_m = \frac{V_T}{K_m} - \frac{R_A}{K_m^2}\tau_{ind} \tag{3-4}$$

This equation is just a straight line with a negative slope. A typical torque versus speed characteristics of a dc machine is shown in Fig. 3-3 and the resulting experimental torque versus speed characteristics is shown in Fig. 3-4, which is a typical of an impulse type hydro turbine shown in Fig. 1-1. In the experimental result shown in Fig. 3-4, the thin line represents the linearized curve of the original characteristics of the dc machine. This characteristic can be obtained in laboratory by running the dc machine as a prime mover with the induction generator that is supplying power to a variable load. This way, we can measure the input armature current, armature voltage and speed of a dc machine.

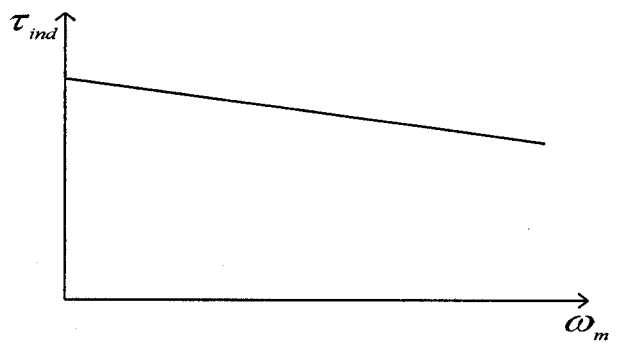

Fig. 3-3 Typical torque versus speed characteristics of a dc machine

The shaft speed at zero torque can be adjusted by varying the dc voltage applied at the armature of the PMDC motor.

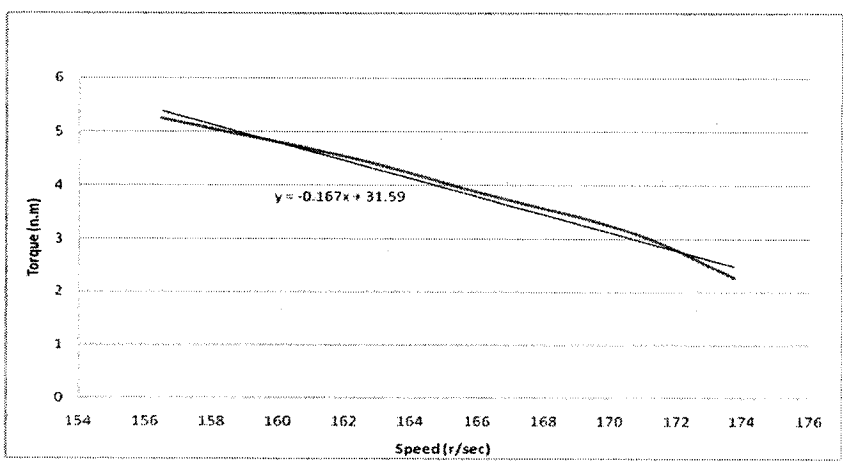

Fig. 3-4 Experimental torque versus speed characteristics of a dc machine

3.3 PARAMETERS IDENTIFICATION OF THE INDUCTION GENERATOR, [21, 22]

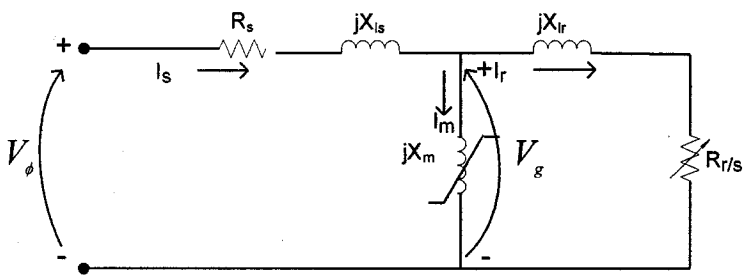

Fig. 3-5 Per-phase equivalent circuit of induction motor

The equivalent circuit of an induction machine is a very useful tool for determining the motor response to change in loads. The name plate data of the squirrel-cage induction machine is tabulated in Table 3-2

Table 3-2 Nameplate data of induction machine

Baldor-manufacturer Squirrel-cage induction machine nameplate data	
Power (hp)	2
Rated speed (rpm)	1725
Voltage (volt)	208
Current (A)	6.1
Frequency (Hz)	60
Poles	4
Stator connection and Phase	Y-connected and 3

However if a model is to be used for the induction generator, it is necessary to determine what the element values are that go into the induction motor model . Then the

same model parameters of induction motor will be used to model the induction generator. The exact details of how each induction motor test must be performed in order to achieve accurate results are described in *IEEE* standard-112. However the conventional tests that are performed in the laboratory to get the parameters of induction machine are as follows:-

Stator dc resistance test:

This test gives us the stator resistance R_s of the machine. The test is conducted by using a dc voltmeter and a dc ammeter, a dc voltage is applied across each two phase. Since the current flows through two of the three star-connected stator windings, the total resistance in the current path is $2R_s$. Therefore,

$R_s = \frac{V_{dc}}{2I_{dc}}$, these values have to be further corrected by a factor of 1.05 to 1.25 to account for the skin effect.

Blocked rotor test:

This test is essentially equivalent to the short circuit test of a transformer. In this test the rotor of the motor is blocked, so that it cannot rotate. Then a reduced magnitude of the voltage is applied to the stator terminals until the rated current is obtained. By using the two wattmeter method, voltmeters and ammeters the resulting power, voltage and current are measured in each phase. Since in blocked rotor test, the slip (s) is equal to 1 therefore the rotor circuit impedance is relatively small and the magnetization reactance X_m is large, the stator current has a numerical value similar to that of the rotor circuit. Therefore the excitation current is also neglected. This test gives us the stator and the rotor leakage reactance X_{ls} and X_{lr}. The following equations can be used in block rotor test to get stator and the rotor leakage reactance.

$$P = \sqrt{3} V_T I_L \cos\theta \Rightarrow \cos\theta = \frac{P}{\sqrt{3} V_T I_L}$$

$$|Z_{LR}| = \frac{V_T}{\sqrt{3} I_L}$$

$$R_{LR} = R_s + R_r = Z_{LR} \cos\theta \qquad (3\text{-}5)$$

$$X_{LR} = Z_{LR} \sin\theta$$

$$0.5 X_{LR} = X_{ls} = X_{lr}$$

No load test:

This test is similar to the open circuit test of a transformer. The purpose of this test is to provide information about the rotational losses of the motor and its magnetization current. In this case, a full rated voltage is applied across the stator terminals. The motor is not loaded, so the only load seen by the motor is the friction and the windage losses. Here the slip (s) is equal to zero and this causes the rotor resistance becomes high, therefore the power is dissipated only as losses. In this test two wattmeter method, voltmeter and ammeters are used to measure the total power, voltage and the current across each phase of the Y-connected stator windings. This test will give us the information about the magnetizing reactance X_m. The equations used in the no-load test to get the magnetization reactance are given as,

$$P_{SCL} = 3I^2 R_S, \quad P_{IN} = P_{losses} = W_1 + W_2$$

$$P_{IN} = P_{SCL} + P_{ROT}$$

$$Z_{NL} = \frac{V_\phi}{I}, \qquad R_{NL} = \frac{P_{IN}}{3I^2} \qquad (3\text{-}6)$$

$$X_{NL} = X_{ls} + X_m = \sqrt{Z^2_{NL} - R^2_{NL}} \quad OR$$

$$\cos\theta_{oc} = \frac{P_{IN}}{VI} \Rightarrow X_m = \frac{V}{I \sin\theta_{oc}}$$

Thus after performing all the above tests in the laboratory, the parameters of the induction machine obtained are tabulated in Table 3-3. The per-unit values are defined in the appendix (A-1)

Table 3-3 Parameters of the induction generator

R_s (Ω)	R_r (Ω)	X_{ls} (Ω)	X_{lr} (Ω)	X_m (Ω)
1.33	0.891	1.44	1.44	37.9

3.3.1 MAGNETIZATION CHARACTERISTICS OF INDUCTION MACHINE

In order to determine experimentally the magnetization reactance X_m at different air gap voltages V_g, the machine were driven at synchronous speed corresponding to supply frequency by the dc motor and the input impedance per phase at different input voltages is measured. Since we need the variation of X_m with the air gap flux proportional to $V_{g/F}$ therefore it is necessary to calculate the air gap voltage by subtracting the voltage drop in the stator leakage impedance from the input voltage. Hence the magnetization reactance X_m at each voltage is obtained by subtracting the stator leakage impedance from the measured input impedance. To obtain the magnetization curve, the following equations were used [23]:

$$P = \sqrt{3}VI\cos\phi \tag{3-7}$$

$$V_g = V - I(\cos\phi - j\sin\phi)(R_s + jX_{ls}) \tag{3-8}$$

$$P_C = \frac{P}{3} - I^2 R_s$$

$$R_c = \frac{V_g^2}{P_c} \tag{3-9}$$

$$I_c = \frac{V_g}{R_c}$$

$$\mathrm{I_m} = \sqrt{I^2 - I_C^2}$$

$$X_m = \frac{V_g}{\mathrm{I_m}} \tag{3-10}$$

Fig. 3-6 shows the experimental result of the magnetization characteristics and Fig. 3-7 shows the variation between the air gap voltage $V_{g/F}$ and the magnetization reactance X_m.

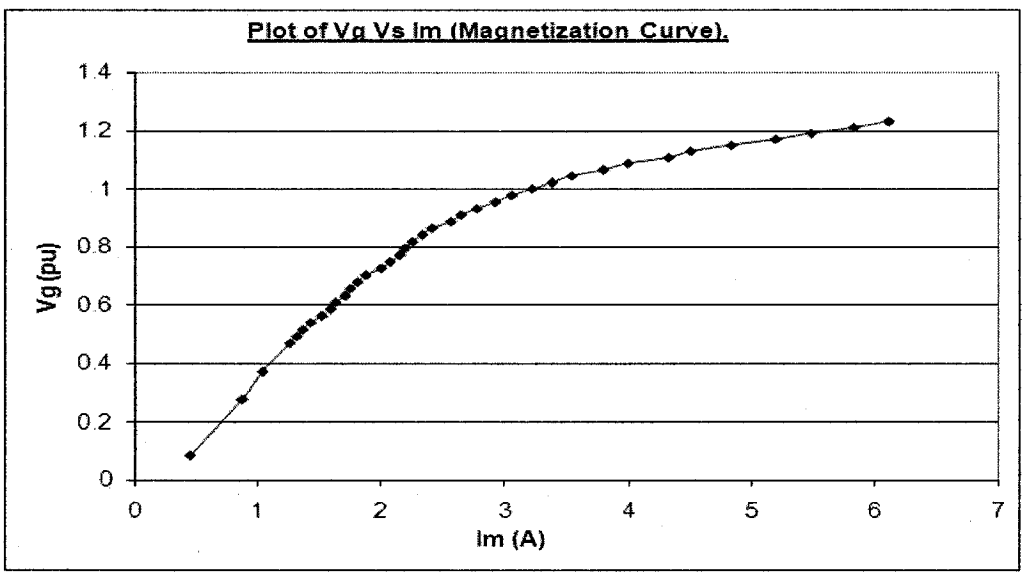

Fig. 3-6 Induction machine magnetization characteristics

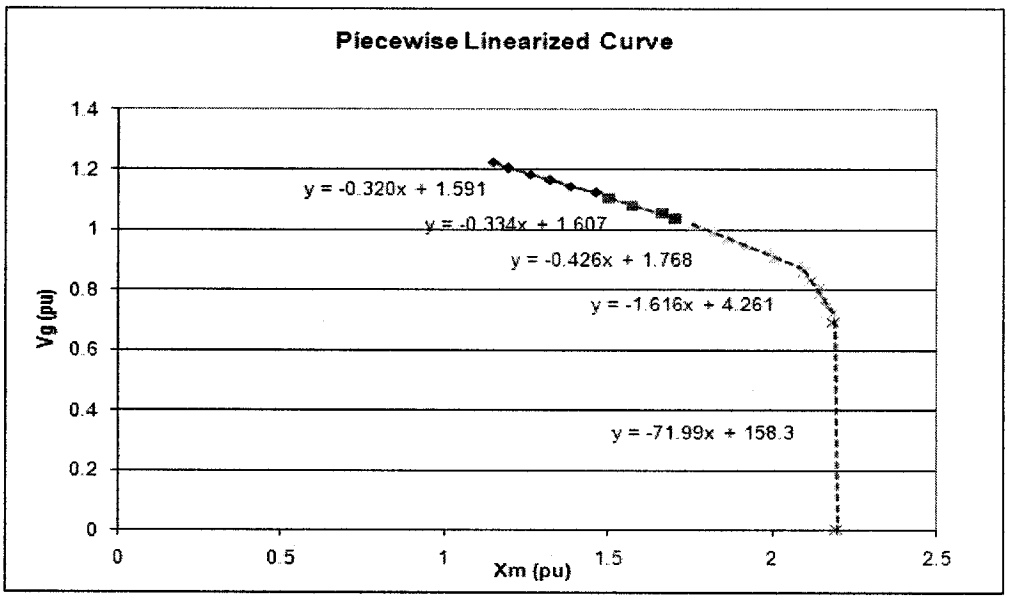

Fig. 3-7 Plot of Air gap voltage versus magnetization reactance

As one can see in Fig. 3-7, the variation between $V_{g/F}$ and X_m presents a non-linear characteristic due to the magnetic saturation of the iron core. So to simplify the analysis the variation under the saturated region was piecewise linearized by using Microsoft excel program. Thus from Fig. 3-7, the piecewise linearized equations are,

$$\frac{V_g}{F} = 1.591 - 0.320X_m \qquad (X_m \geq 1.462)$$

$$\frac{V_g}{F} = 1.607 - 0.334X_m \qquad (1.462 \leq X_m \leq 1.706)$$

$$\frac{V_g}{F} = 1.768 - 0.426X_m \qquad (1.706 \leq X_m \leq 2.088) \qquad (3\text{-}11)$$

$$\frac{V_g}{F} = 4.261 - 1.616X_m \qquad (2.088 \leq X_m \leq 2.190)$$

$$\frac{V_g}{F} = 158.39 - 71.99X_m \qquad (2.190 \leq X_m \leq 2.2)$$

These equations along with the machine parameters are feed into the Matlab program by using Newton-Raphson algorithm to get the performance and steady-state

analysis of induction generator. The steady-state analysis using the equivalent circuit to solve the non-linear equations by Newton-Raphson algorithm was already explained in chapter 2.

3.4 CALCULATION OF THE EXCITATION CAPACITANCE FOR CONSTANT SHAFT SPEED AT NO LOAD AND FULL LOAD [14]

It is well known that a capacitor bank is required for the operation of squirrel-cage induction generator in the stand-alone mode. Also, that the capacitance required for producing a regulated voltage varies with the power demanded by the load and with the shaft speed. This problem is more critical in systems that employ unregulated turbines, as is considered in this thesis. The capacitance required exciting the squirrel-cage induction generator for operation at a certain voltage level, rotor speed, load impedance and power factor can be calculated as shown in [24]. It must lie within certain limits for an induction generator to self-excite and to secure safe operation. The limiting conditions are obtained when the magnetizing reactance X_m is equal to the unsaturated value X_{mo}. The variation of no-load as well as full-load terminal voltage with excitation capacitance is shown in Fig. 3-8. It shows that V_g increases with excitation capacitance. Appropriate value of shunt capacitance can be chosen for a given terminal voltage. This value is selected by solving the steady-state equivalent circuit of induction generator shown in Fig. 2-4.

Generally magnetizing reactance X_m and per-unit frequency F are computed to estimate the performance of the machine for a given capacitance, load and speed as was discussed in chapter 2. But for a desired level of voltage and a given load and speed corresponding to minimum and maximum active power, the excitation requirement in

terms of capacitance can be computed. An algorithm is developed to compute the capacitance required for obtaining constant terminal voltage at a given speed and load. For this purpose two equations are solved by using the Newton-Raphson method to compute X_c and F for a given speed and load corresponding to minimum (no-load) and maximum (rated) power. The method used here is almost same as was discussed in chapter 2 for the steady-state analysis of induction generator to solve the equivalent circuit for the two unknown parameters X_m and F. From Fig. 2-4, the same loop equation for the stator current I_s can be written as,

$$I_s Z_s = 0 \tag{3-12}$$

Under steady-state self-excitation $I_s \neq 0$, therefore from equation 3.12, $Z_s = 0$. This means that the real and imaginary parts of Z_s would be zero. By solving the real and imaginary parts of Z_s separately the following two non-linear equations are obtained with X_c and F are the two unknown variables.

$$f(X_c, F) = C_1 F^3 + C_2 F^2 + (C_3 X_c + C_4) F + C_5 X_c = 0 \tag{3-13}$$

$$g(X_c, F) = (D_1 X_c + D_2) F^2 + (D_3 X_c + D_4) F + D_5 X_c = 0 \tag{3-14}$$

Where, the constants C and D are defined in the appendix (A-2).

In (3-13) and (3-14), the constants C and D contain machine parameters, load resistance R_L and the per-unit speed v are independent but the magnetizing reactance X_m depends on magnetization characteristics of the machine. Since magnetization characteristics is non-linear in nature as shown in the previous section. We have to linearized it and then used in the Matlab program. For maintaining the desired terminal voltage, the air gap voltage V_g has to vary with load resistance. Thus for a given value of load and terminal voltage, the value of air gap voltage can be calculated as below,

$$V_g = \frac{V_T}{(1 - \frac{Z_1}{Z_{LSC}})} \tag{3-15}$$

Where,

$$Z_{LSC} = Z_1 + Z_{LC}, \qquad Z_{LC} = \frac{Z_C R_L}{(Z_C + R_L)}$$

$$Z_1 = R_s + jFX_{ls} \qquad Z_C = \frac{-jX_C}{F^2}$$

Equations (3-13) and (3-14) are non-linear algebraic equations and can be solved for X_c and F for a given load and speed. The same Newton-Raphson method is employed as was discussed in chapter 2, for the steady-state analysis of SEIG to solve these equations but here for the unknown parameters X_c and F is used to calculate the excitation capacitance. The initial conditions used here is $X_{co} = X_{mo}$ and $F = v$, where X_{mo} is the maximum unsaturated magnetization reactance.

Fig. 3-8 shows how the terminal voltage of the induction generator varies with the excitation capacitance when the generator operates at no-load and at rated load when the shaft speed is kept at rated value. There one sees that the excitation capacitance should vary between 22.66 μF and 30.66 μF. The flow chart for the computation of the excitation capacitance at constant terminal voltage and given speed is shown in Fig. 3-9.

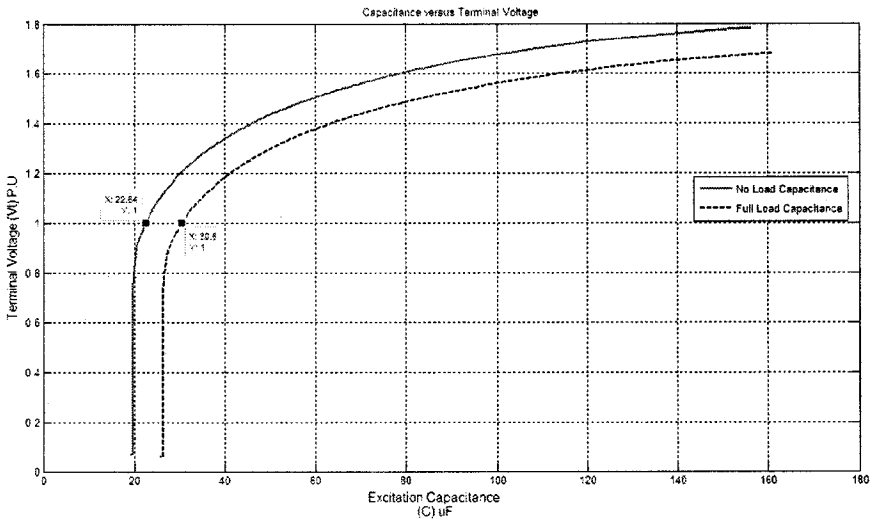

Fig. 3-8 Computation of excitation capacitance at rated voltage and fixed speed

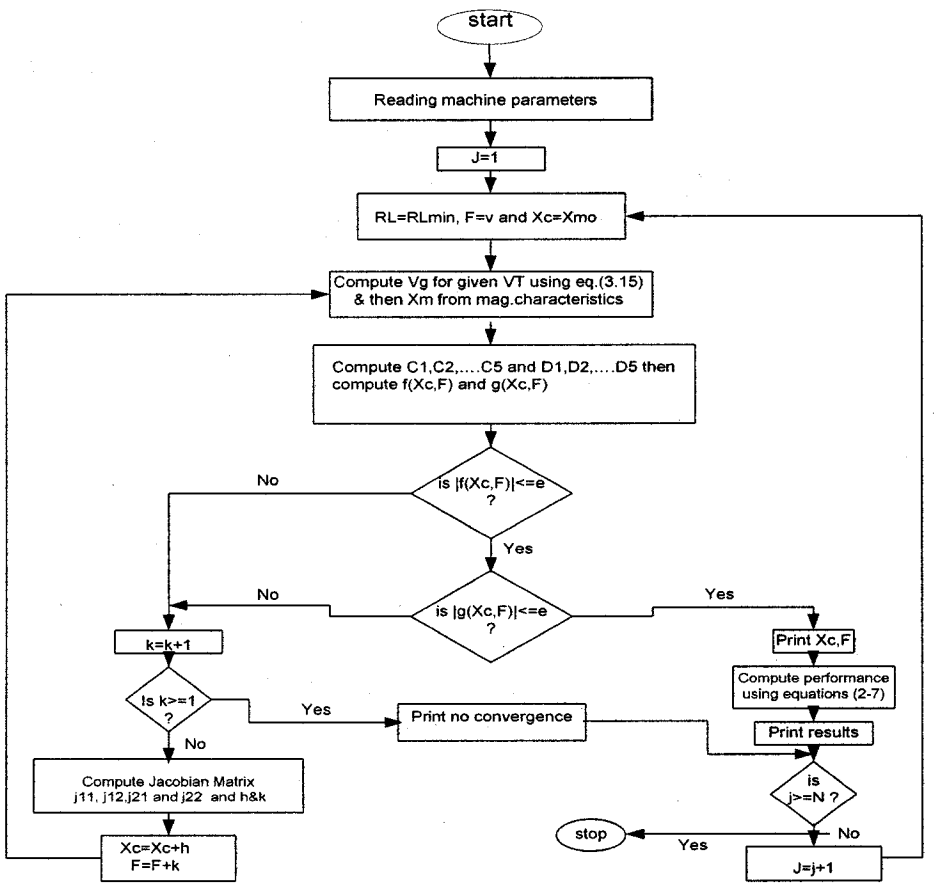

Fig. 3-9 Flow chart for computation of excitation capacitance at constant terminal voltage and at given speed [24]

3.5 DESIGN OF THE VOLTAGE SOURCE INVERTER (VSI)

The voltage source inverter VSI consists of switching devices with a battery bank that is emulated by a full bridge diode rectifier on the dc side and a filtering inductor on the ac side. The switches are insulated gate bipolar transistors ($IGBT_S$). The amount of reactive power and active power to be supplied by the VSI to the generating system from no-load to full-load is the main deciding factor for designing the components of the VSI. When the terminal voltage of the generator is higher than the reference voltage, the VSI should absorb excess reactive power to regulate the terminal voltage. When the terminal voltage is less than the reference voltage, the VSI should supply additional reactive power to regulate the terminal voltage.

From Fig. 3-8, the capacitance required to maintain 1-p.u of terminal voltage at no-load is $C_o = 22.66\mu F$ and the capacitance required to maintain 1-p.u of terminal voltage at rated resistive load is $C_L = 30.66\mu F$. So the amount of reactive power the generator requires at no-load is Q_o=1107 *VAR* and the rated resistive load is Q_L=1500 *VAR*. Assuming that the fixed excitation capacitor will provide the reactive power required for no-load operation then the VSI should be able to supply the additional reactive power required at full-load to maintain constant terminal voltage: $Q_A = (Q_L - Q_O)$ = 393 *VAR* and the corresponding current rating is $I_A = Q_A/\sqrt{3}V$ = 1.09 *A*. However, the VSI should also be able to inject/absorb active power to regulate the frequency. This has to be calculated for given ranges of wind speed and for load variation. In [10] the size of the VSI was selected as 0.5-p.u of the generator's rated power, the wind speed range was assumed to be from 3 to 9 m/s and a computation was carried out to see what would be the range of load, for which voltage and current could be regulated. Alternatively, one

could design the VSI so that it can supply rated load when there is no wind. This aspect, however, is beyond the scope of this thesis. The overall current rating of the VSI available in the laboratory is I_s = 30 A rms. At no-load the voltage across the generator terminals is the rated voltage of 208 V. For satisfactory PWM operation the dc bus voltage of the VSI must be greater than the peak of the generator voltage, as

$$V_{dc} = \frac{2\sqrt{2}(\frac{V}{\sqrt{3}})}{m_a} \tag{3-16}$$

Where, m_a is the modulation index and V is the line-line rms voltage of the induction generator. To make it sure that the inverter should always operate in the linear region, the selected value of $m_a = 0.68$. From (3-16), V_{dc} = 500 V. If current ripple $I_{cr(p-p)}$ through the ac inductor is allowed to be 6.5% , then the inductance can be calculated as [23],

$$L = \frac{\frac{\sqrt{3}}{2} m_a . V_{dc}}{6.a.f_s.I_{cr(p-p)}} \tag{3-17}$$

Where f_s = switching frequency (10 kHz), a = changes in current during transient (typically 120-190%, in this work a =1.9). Thus from (3-17) L= 39.7 mH, available inductance in the laboratory is L= 32 mH. Since the battery bank on the dc side of the VSI was emulated by a full bridge diode rectifier with a variable resistor and a filter capacitor. The filter capacitor selected here is C_{dc} = 1100 μF, just to minimize the voltage ripples. Although it is reported in the literature that the value of C_{dc} should be between (0.5-0.7-p.u) or above 0.9-p.u to minimize the voltage ripple and to avoid any possibility

of resonance [23]. The selected value is above 0.9-p.u. The value of maximum R_{dc} is selected based on the rated power of the generator and dc bus voltage. Thus, $R_{dc} = V^2_{dc}/P_{rated} = 167.5\ \Omega$. The maximum voltage rating for IGBT switches can be calculated by considering a 10% change in the generator terminal voltage as follows [23],

$$V_m = \sqrt{2}\,(V_s + V_L + V_d) \tag{3-18}$$

Where, V_L = voltage drop across the inductor and it can be calculated as, $V_L = 2\pi.f.L.I_A = 13.14$ V and V_d = 10% change in the generator voltage and V_s=208 V. So from (3.18), V_m= 342 V. The rated current of the generator is 6.1 A, considering the safety factor, the maximum line current for the VSI can be calculated as,

$$\mathrm{I_m} = 1.25(I_{cr(P-P)} + \sqrt{2}I_s) \tag{3-19}$$

So I_m = 10.86 A. The commercially available voltage and current ratings of the VSI in the laboratory are 440 V and 50 A. Therefore the maximum voltage and current ratings of IGBT switches is considered to be 440 V and 50 A. Thus the design values of the different components of VSI is shown in Table 3-4,

Table 3-4 Designed parameter values for the VSI

V_{dc}	C_{dc}	R_{dc}	L	m_a	f_{sw}	V_m	I_m
500 V	1100 μF	167.5 Ω	32 mH	0.68	10 kHz	440 V	50 A

3.5.1 VOLTAGE AND FREQUENCY CONTROL LOOP DESIGN

In chapter 2, Fig. 2-9, we proposed four control loops for voltage and frequency regulation of overall system. Two inner current control loops (I_d and I_q), one outer loop for an ac voltage regulation and one for outer frequency regulation. The inner current control loops were designed in section 2.3 for the DQ model of VSI. This section will

present and explain the designing of the two outer loops. The approximate Thevenin equivalent circuit showing only the magnetization reactance (X_m), the only parameter which is effected by the magnetic saturation of machine in stand-alone applications is shown in Fig. 3-10. Since from the magnetization curve in Fig. 3-7, the maximum saturated magnetizing reactance is X_{mo} = 2.2-p.u. We will select the value of X_m corresponding to 1-p.u of voltage from Fig. 3-7, to make sure that the machine operates in the saturation region. So X_m = 30.4 Ω is selected. From the equivalent circuit shown in Fig. 3-10, one can write the KVL as,

$$V_s = jX_m I_d + V_L \tag{3-20}$$

Using small signal analysis one gets,

$$\frac{\Delta V_s}{\Delta I_d} = jX_m \tag{3-21}$$

Thus, the plant transfer function for the voltage loop will be,

$$\frac{\Delta V_s}{\Delta I_d} = 30.4 \tag{3-22}$$

Since the above transfer function is simply a gain, so we will design a simple integrator controller with a gain K that will produce the reference current I_d. The inner current control loop is represented by a unity gain and the block diagram is shown in Fig. 3-11. The crossover frequency for the controller is selected 10% of the switching frequency. For the simulation results, the switching frequency of the VSI is selected 2 kHz, so the crossover frequency will be $f_x = 0.1 f_{sw} \Rightarrow \omega_x = 2\pi f_x = 1256 rad/s$

$$G_c V(s) = \frac{K}{s}, \quad s = j\omega_x \tag{3-23}$$

$|G_c V(s)|\left|\frac{\Delta V_s}{\Delta I_d}\right| = 1 \Rightarrow (\frac{K}{1256})(30.4) = 1$. So the designed gain for the integral controller is

$$K = 41 \Rightarrow G_c V(s) = \frac{41}{s}$$

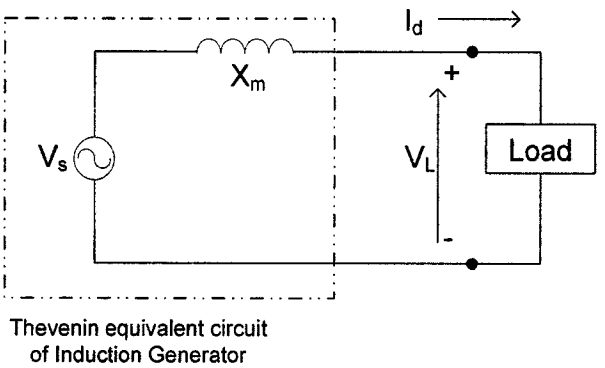

Fig. 3-10 Thevenin equivalent circuit

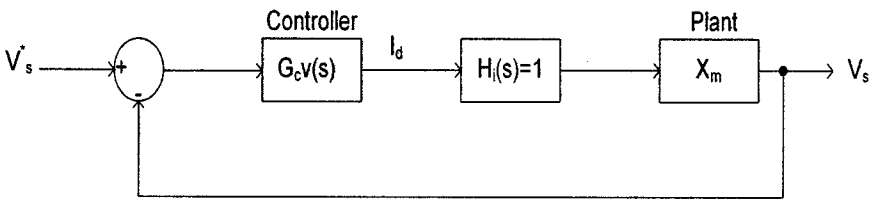

Fig. 3-11 Voltage control loop block diagram

The step response for the voltage controller is shown in Fig. 3-12.

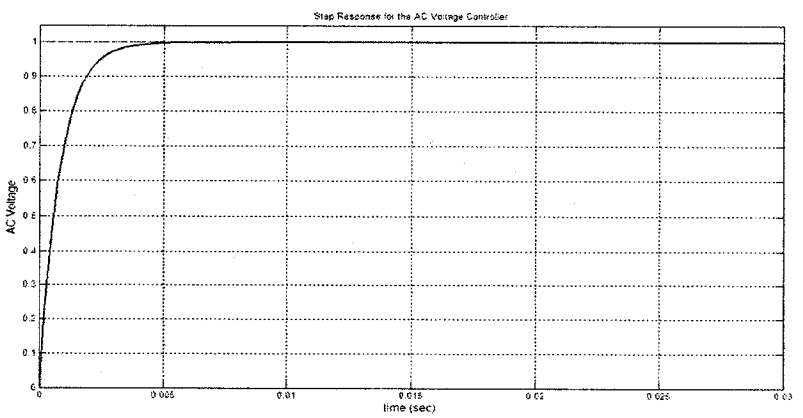

Fig. 3-12 Step response for the voltage control loop

The control block diagram for the frequency control loop is shown in Fig. 3-13. Here the plant is represented approximately by the equivalent inertia and the torque constant of the machine. Again the inner current control loop is represented by a unity gain. A PI controller is designed. Here we will select the bandwidth of the speed loop to be at least two orders smaller than that of the inner current loop to avoid any interference in the control loop from the switching frequency noise. Therefore, the closed loop transfer function will be,

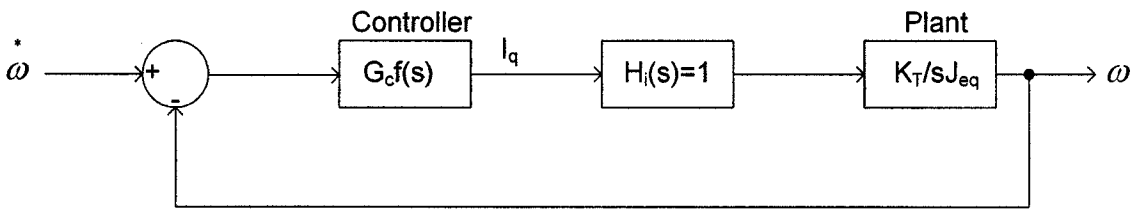

Fig. 3-13 Frequency control loop block diagram [25]

$$G_p(s) = \frac{K_T}{sJ_{eq}} \tag{3-24}$$

$$G_c f(s) = k_p \frac{(1+s\tau)}{s\tau} \tag{3-25}$$

$$\frac{\omega}{\omega^*} = \frac{G_c f(s) G_p(s)}{1 + G_c f(s) G_p(s)} = \frac{K_T k_p}{J_{eq}\tau} \frac{(1+s\tau)}{s^2 + \frac{K_T k_p}{J_{eq}} s + \frac{K_T k_p}{J_{eq}\tau}} \tag{3-26}$$

Comparing the closed loop characteristics equation with that of general second order equation, we get,

$$2\zeta\omega_n = \frac{K_T k_p}{J_{eq}} \tag{3-27}$$

$$\omega^2_n = \frac{K_T k_p}{J_{eq}\tau} \tag{3-28}$$

Where $\omega_n = \frac{\omega_S}{220}$, $\zeta = \frac{\sqrt{2}}{2}$, $K_T = 0.1 Nm/A$ *and* $J_{eq} = 0.01857 kgm^2$

From (3-27) and (3-28) the parameters of PI controller for the frequency loop can easily be found as, k_p =15 and τ = 0.0248.

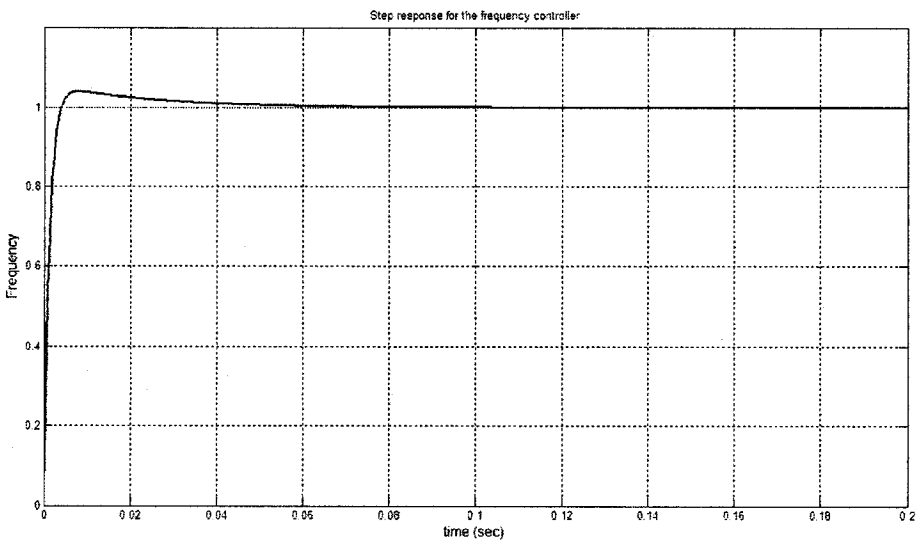

Fig. 3-14 Step response for the frequency control loop

The step response for the frequency loop is shown in Fig. 3-14. This completes the design of all the four control loops that we proposed for voltage and frequency regulation of stand-alone system.

3.6 CONCLUSIONS

In this chapter, we have discussed the design and the implementation of the overall system. The study started with the description of the various components in the main schematic diagram. The characteristics of a permanent magnet dc machine which is used as the prime mover for the induction generator is presented and then the parameter identifications for the induction generator based on conventional tests are described in detail. Synchronous speed test is performed to get the magnetization characteristics for the induction generator and then the steady-state analysis of induction generator is presented.

A procedure for the calculation of excitation capacitance requirement, for the induction generator is described based on the steady-state model for a given speed and the load impedance. The parameters of the VSI as well as the voltage and the frequency control loops are designed then the overall system is implemented in Simulink with the proposed control scheme to perform various experimental tests in the laboratory. The experimental results will be discussed in chapter 4.

CHAPTER 4

EXPERIMENTAL RESULTS

4.1 INTRODUCTION

Experiments are performed to study and verify the proposed control scheme for the regulation of the voltage and frequency of the overall generating system. Two types of prime movers are considered for the experimental test, a micro hydro turbine and a wind turbine. A small scale generating system using 2-hp, 6.1 *A* and 208 *V* induction generator, was assembled for experimental testing. A 2-hp, 8.5 *A* and 180 *V* permanent magnet dc motor is used as a prime mover to drive the generator. For a constant armature voltage applied through a full bridge diode rectifier with a *VARIAC*, the DC motor operates with constant power and its speed varies linearly with the load torque, similar to an impulse type hydro turbine with constant head. Similarly a dc machine can also be used to emulate the torque-speed characteristics of a wind turbine by varying its armature voltage what requires a dc-dc converter at the output of the diode rectifier to control its armature current. The schematic diagram of the implemented system is shown in Fig. 4.1. There one sees the stand-alone self-excited system with an excitation capacitor connected at the stator of the induction generator in parallel with a consumer load and a single voltage source inverter (VSI). The dc bus of the VSI is fed by another full bridge diode rectifier with a filtering capacitor and a dc resistance, and on the ac side of the VSI a filter inductance is connected.

The VSI is to supply and absorb active power besides reactive power control. For that, a battery bank should be placed at its dc side. Since a 500 V battery bank was not available in the laboratory, one was emulated using a three-phase diode bridge rectifier to supply active power, a variable resistor to consume active power and a capacitor for filtering. It should be noted that the variable resistor allows the dc bus voltage to be manually regulated in the steady-state but not during transient conditions. To monitor and control the stand-alone system, a dSPACE based controller is implemented in synchronously rotating DQ frame. By using LEM current and voltage sensors, the inverter three phase line currents and three phase line-to-neutral terminal voltages of the SEIG are sensed and acquired into a dSPACE DS-1103 controller board for processing. The gating signals generated by the dSPACE system that presents low voltage (0-5V), and need to be amplified to (0-15V) by passing through another analog circuit for the final gating signals of the VSI, as shown in the appendix A-3.

The Simulink implementation for the experimental setup is shown in Fig. 4-2 and the control circuit inside the main sub-system is shown in Fig. 4-3. The control structure with the VSI is implemented in Simulink with dSPACE by sensing the inverter line currents as well as the induction generator line-neutral voltages and then by using abc-dqo transformation blocks, the signals are converted into DQ reference frame. Since in the DQ reference frame, all the quantities appears as a dc value. One can easily design and implement linear controllers in DQ reference frame that yield zero steady-state errors. Since V_q is selected to be aligned with the induction generator terminal voltage, therefore the V_d component must be zero while the magnitude of V_q equals the peak value of the line-to-neutral generated voltage. So by sensing the induction generator terminal

voltage and comparing it with a reference voltage, the error signal is passed through a PI controller. The PI controller will generate the reference current component I_{dref} which is responsible for the reactive power Q regulation that is used for the induction generator voltage regulation.

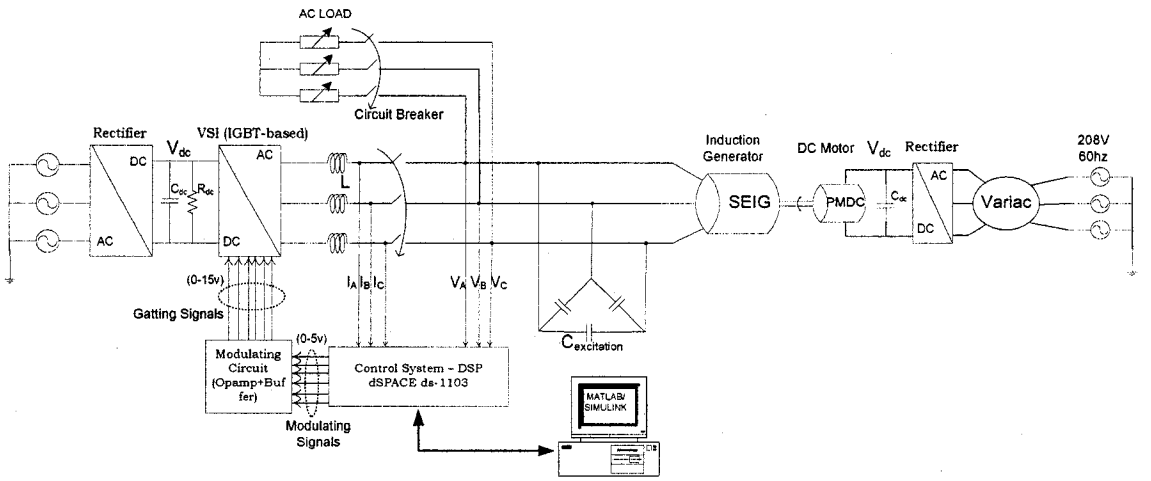

Fig. 4-1 The experimental setup for self-excited stand-alone generating system

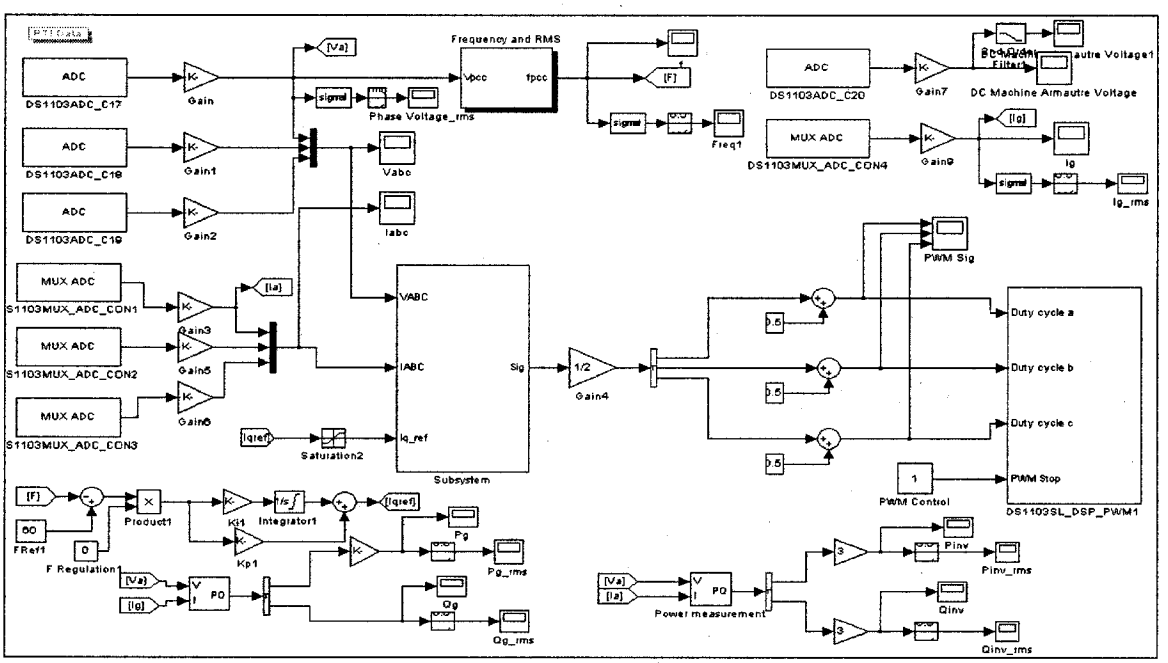

Fig. 4-2 Simulink implementation of the overall experimental setup

A similar controller is designed based on the frequency error which generates the reference current I_{qref}. The I_{qref} current component is responsible for the active power P regulation that is used for the frequency regulation. Another two inner PI controllers are designed based on the error signal between the VSI currents and the reference current. They generate the E_d and E_q components of the modulating signal of the VSI, which are required to regulate the magnitude and frequency of the voltage at the point of common coupling (output of the induction generator). The Simulink block that measures the frequency is shown in Fig. 4-4 and the PI controller implementation in Simulink is shown in Fig. 4-5.

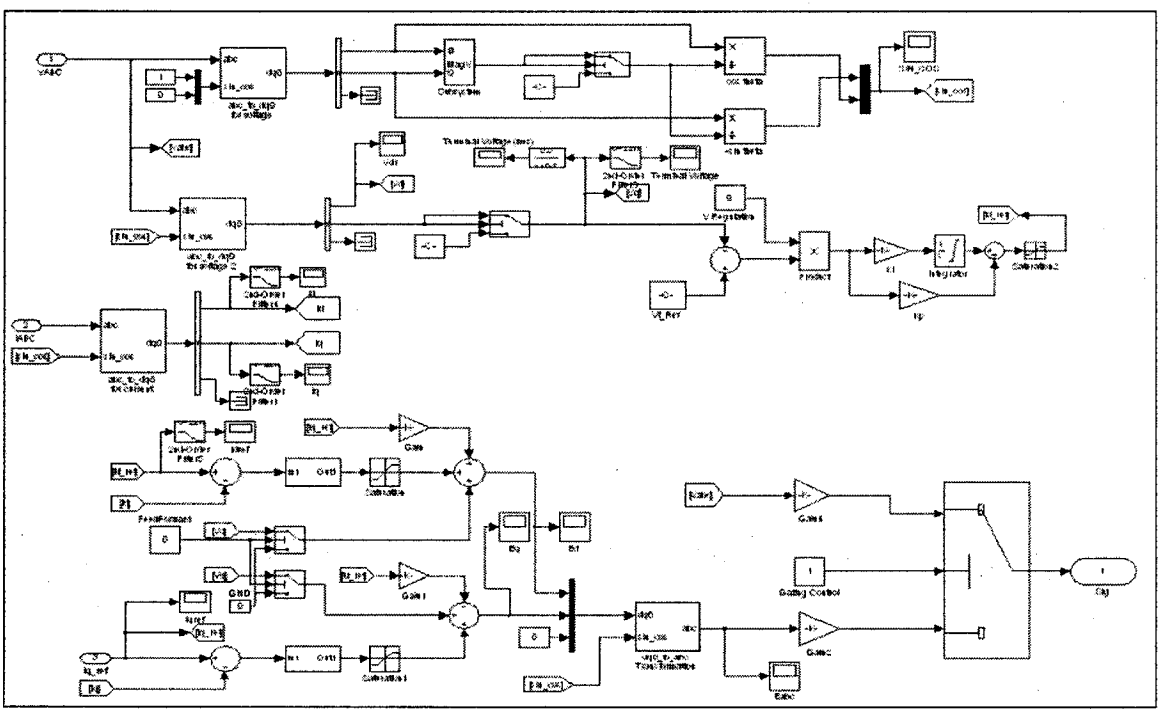

Fig. 4-3 Control circuit inside sub-system

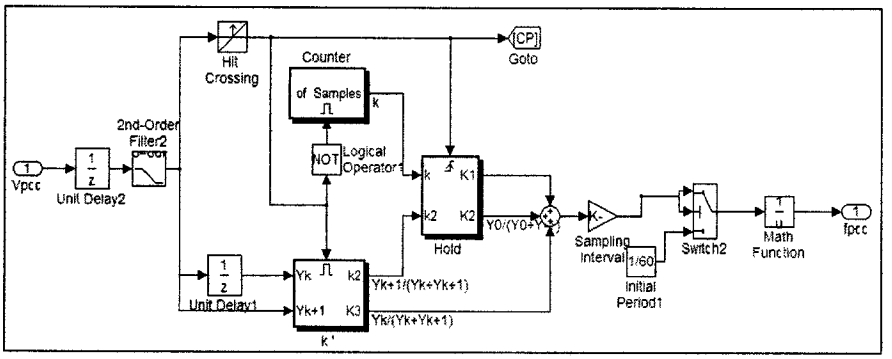

Fig. 4-4 Frequency measurement block inside sub-system (frequency and RMS) [26]

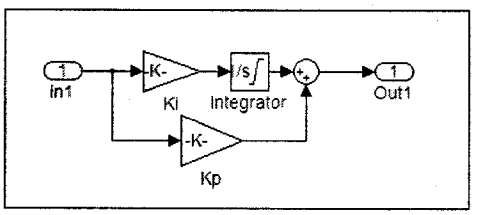

Fig. 4-5 Simulink implementation of PI Controller

4.2 THE DSP DEVELOPMENT SYSTEM [26]

Fig. 4-6 shows the DSP based instrumentation and the electronic circuits employed to monitor and control the self-excited stand-alone induction generator.

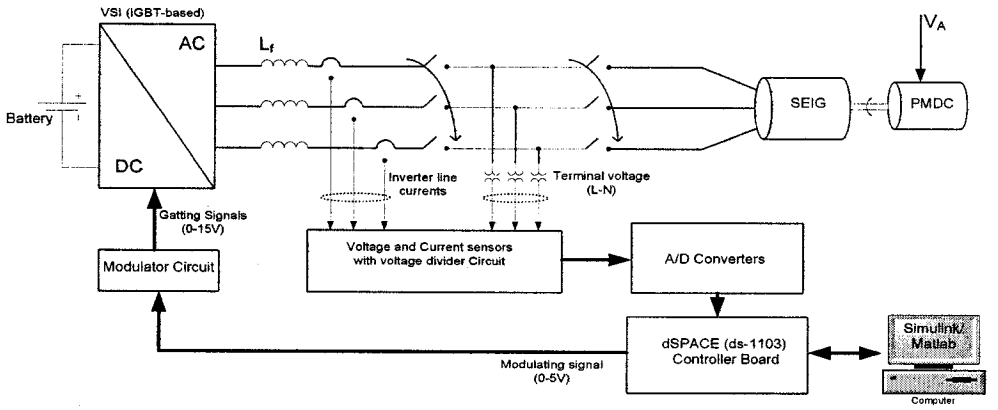

Fig. 4-6 The DSP based instrumentation for the experimental tests

The dSPACE system is commonly used for rapid prototyping of electrical control systems and is comprised of a DS-1103 PPC controller board. It is equipped with a Motorola PowerPC 604e processor, whose computing power allows for the simulation of large-scale floating-point control algorithms in real-time. A full range of I/O devices including a TMS320F240 slave DSP is available on-board. Using the Real-Time Interface to Simulink, automatic code generation from block diagrams is possible. I/O functions are specified graphically as part of the simulation model. Therefore, the migration from Matlab/Simulink to practical control of an external plant can be easily done by the inclusion of I/O blocks in the control circuits.

4.2.1 HARDWARE ARCHITECTURE

The DS-1103 PPC Controller Board is equipped with a Motorola PowerPC 604e processor for fast floating-point calculation at 333MHz. This high-performance superscalar microprocessor has three integer execution units, one floating-point arithmetic unit, and a separate load/store unit for fast memory access. The on-chip cache size is 32KByte for instruction and data. The processor's ability to execute instructions out-of-order leads to a performance improvement of about factor 2 for typical simulation models compared to strictly serial instruction flow.

A 2MByte local memory is used for program and data of the simulation model. The local memory is fully cached and cannot be accessed by the host PC in standard operation mode. For data buffering and exchange between PowerPC and the host, up to 128MByte of non-cached global memory is available. The host interface of the board is

used to perform board setups, program downloads, and runtime data transfer. It supports Plug & Play functionality for easy installation.

The board can be adapted to a wide range of closed-loop applications due to its large number of I/O devices. High-resolution A/D converters (16-bits and 12 bits) with a sampling time of 4us and 800 ns, respectively, are available, as well as D/A output channels with a resolution of 14-bit and a 5 us settling time. 32 digital I/O channels and a serial line interface complete the list of standard I/O units.

4.2.2 REAL-TIME INTERFACE TO SIMULINK

Using MATLAB and Simulink for modeling, analysis, design and offline simulation has become a de-facto standard for control system development. The Real-Time Interface enhances the Simulink block library with additional blocks, which provide the link between Simulink and the real-time hardware, as shown in Fig. 4-7. To graphically specify an I/O channel the corresponding block icon has to be picked up from the I/O block library and attached to the Simulink controller model. I/O parameters, such as voltage ranges or resolutions, can be set in appropriate dialog boxes. The Simulink model then is transferred into real-time code, using the Real-Time Workshop, state flow control, and the Real-Time Interface. Code generation includes the I/O channel specification and the multitasking setup, which are translated into appropriate function calls of the Real-Time Library. The library is a C function library providing a high-level programming interface to the hardware. The Real-Time Library also includes access functions for the slave DSP. These blocks cover the I/O functionality of the prototyping hardware.

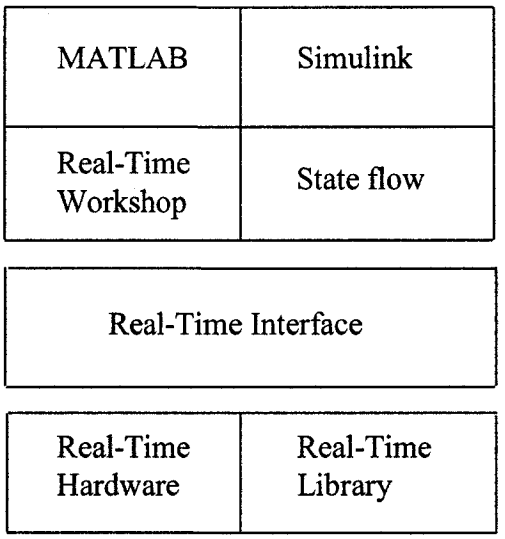

Fig. 4-7 The Real-Time Interface in the MATLAB/Simulink environment.

4.2.3 SIMULINK BLOCK LIBRARY FOR DS-1103

The block library for the DS-1103 PowerPC Controller Board is subdivided into two major parts according to the two microprocessor units on the board. The library shown in Fig. 4-8 comprises all I/O units that are directly served by the PowerPC master processor. Block icons for the standard I/O channels such as A/D, D/A converters, and digital I/O are included as well as the more complex incremental encoder blocks.

The slave DSP library, shown in Fig. 4-9, offers frequently used functions of the TMS320F240, such as single-phase and three-phase PWM signal generation, frequency measurement, A/D conversion, and digital I/O. Because the real-time simulation is executed in the master PPC board, it is wished to employ the functions provided by the slave DSP as much as possible to save the computation time on the Master PPC board.

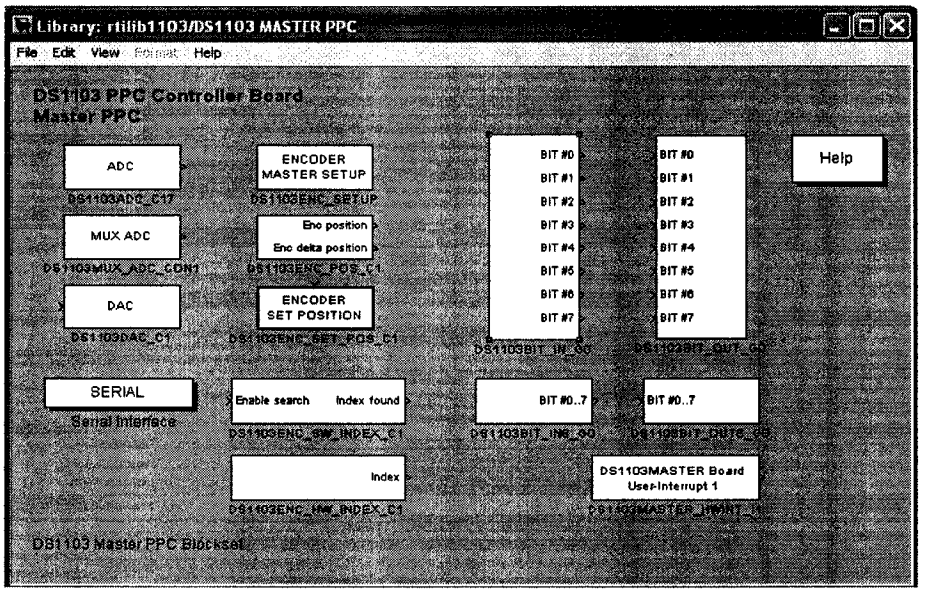

Fig. 4-8 Master Processor block library for Simulink.

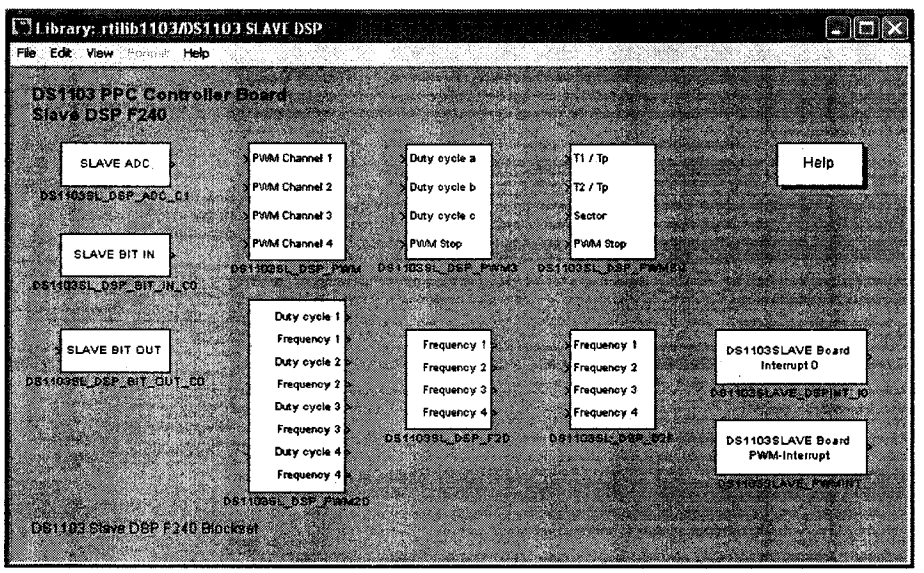

Fig. 4-9 Slave DSP block library for Simulink.

4.3 SYSTEM WITH AN IMPULSE TYPE HYDRO TURBINE

The schematic experimental block diagram for an impulse type hydro turbine is shown in Fig. 4-10.

The startup of the overall system is achieved by first imposing the inverter $P = 0$ and $Q = 0$. The initial excitation requirement for the induction generator to get rated voltage at rated load is provided by the excitation capacitor. The last step is to synchronize the VSI with the induction generator. An experimental setup has been implemented to verify the impact of the VSI with the proposed control scheme on the voltage and frequency regulation of a system based on the 2-hp induction generator. The prime mover of the system is 180V, 2-hp permanent magnet dc motor with a rated speed of 1750 rpm. It is controlled with a constant armature voltage, thus presenting a linear decrease of the shaft speed with the induced torque as shown in Fig. 3-3, obtained for rated armature voltage that is typical of an impulse type hydro turbine.

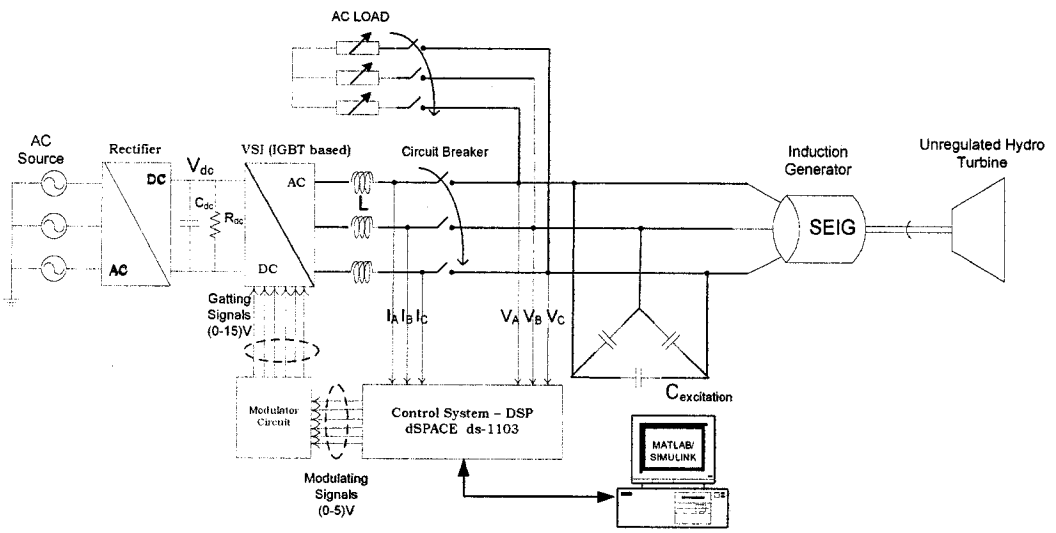

Fig. 4-10 System with an impulse type hydro turbine

To regulate the voltage and frequency of the induction generator, the VSI has to supply or absorb both the reactive power Q as well as active power P respectively.

For example if the voltage magnitude at the PCC is greater than the reference voltage, the VSI has to absorb some reactive power Q or if the voltage magnitude at the PCC is lower than the reference voltage, than the VSI must supply reactive power to bring the PCC

voltage equal to the reference voltage. The same will apply for the frequency regulation but here the VSI has to supply or absorb active power P to regulate the system frequency. In the following sections we will present different types of experimental tests to show that the VSI is regulating the induction generator voltage and frequency by implementing the proposed control scheme for various conditions.

4.3.1 EXPERIMENTAL RESULTS

The following tests were carried out under controlled conditions with relatively small variations of input mechanical power and electrical load around the rated operating condition. In this way, the dump load is not required for consuming excess of generated power instead the variable resistor present on the dc bus of the VSI is sufficient to consume excess power so the dump load has been omitted in the tests. The capacitance of the fixed Δ-connected capacitor bank is equal to 30.66μF that provides the total reactive power required by the induction generator when it supplies rated load (31.5Ω, Y-connected) at rated frequency 60Hz.

The dc bus voltage for the inverter was set at 500V. This voltage was selected to make sure that the inverter operation should be always in the linear region with m_a equals to around (0.68) to minimize the harmonics. Since a battery bank with this voltage was not available for the experiments in the laboratory, so it was emulated by a full bridge diode rectifier connected to the ac mains with a capacitive filter and a variable resistor as shown in Fig. 4-10. In this way, the dc bus can be made to supply and absorb active power without significant dc voltage magnitude variations. A 32-mH inductor was used

between the inverter and the ac bus. A 10-kHz triangular carrier was used for the SPWM operation.

The control scheme is implemented in the DSP (dSPACE DS-1103). LEM sensors are used at the PCC for sensing the line to neutral voltages of the SEIG and inverter output currents. Another analog circuit board is used to convert the PWM signals (0-5V) received from DS-1103 controller board (37-pin sub-D connector) to (0-15V) signals for proper inverter switching. One can also specify the proper dead time directly in the PWM3 block used to create the triangular signals in the real-time workshop library in Simulink/Matlab.

4.3.1.1 Load Variation Tests

The most serious problem with an induction generator in stand-alone system is its voltage and frequency variation with variation in load impedance. This happens because the fixed capacitor must supply all the reactive power needed by both the load and the generator. In order to regulate the voltage, the source of reactive power across the induction generator stator terminals has to vary. In this thesis, a voltage source inverter VSI is employed as a variable reactive power source to control its voltage and frequency.

The 1st test was conducted for the unregulated system (VSI disabled from the circuit). The load resistance is varied in steps and the magnitude and the frequency of the voltage at the PCC are measured. The results are as shown in Fig. 4-11 and in Fig. 4-12.

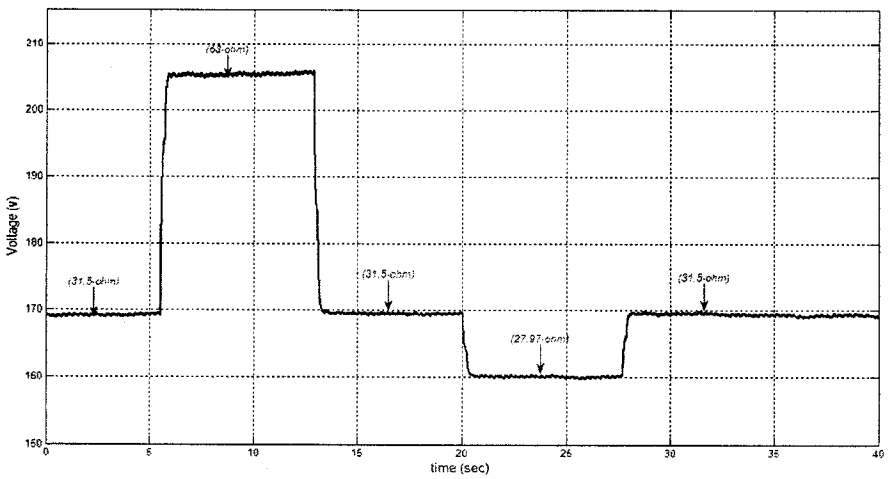

Fig. 4-11 Effect of load variation on the voltage for unregulated system

Here since the system is not regulated, therefore the load variation range should be small as compared with the regulated system to avoid the demagnetization of SEIG. The system operates initially with a rated load of 31.5Ω and maintaining the rated terminal voltage magnitude of 169.87 V (peak) line-neutral and the initial frequency is around the rated value as 60 Hz. Then a series of resistive load variations are conducted to see the behavior of the unregulated system. As both the Fig. 4-11 and Fig. 4-12 shows that the voltage and the frequency variations at the ac bus presents almost similar shapes. The magnitude of both the voltage and frequency increases as the load is reduced and decreases as the load is increased.

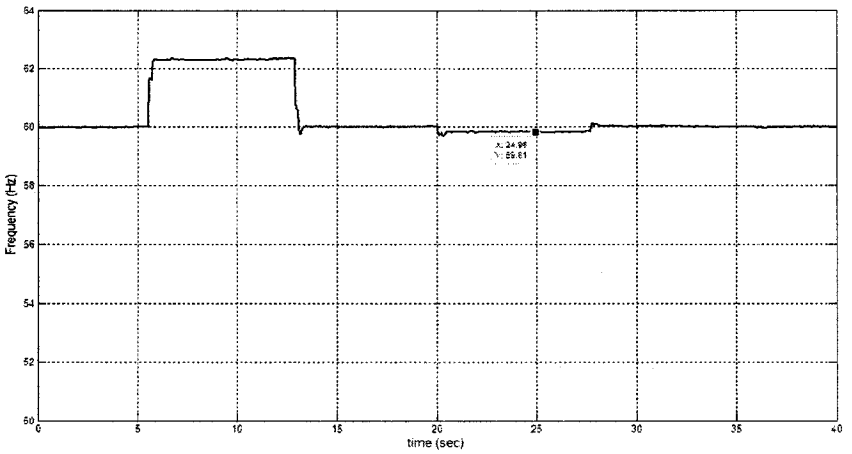

Fig. 4-12 Effect of load variation on the frequency for unregulated system

The 2nd test is conducted to see the effect of load variation on the regulation of voltage and frequency with the proposed control system regulating only the voltage. Now a wider range of resistive load variation can be employed for the VSI regulating only the ac voltage magnitude by means of reactive power control. Initially, the VSI operates as a STATCOM, no active power control, and the frequency is not regulated. Fig. 4-13 and Fig. 4-14 shows the voltage and frequency variations during variations in load respectively.

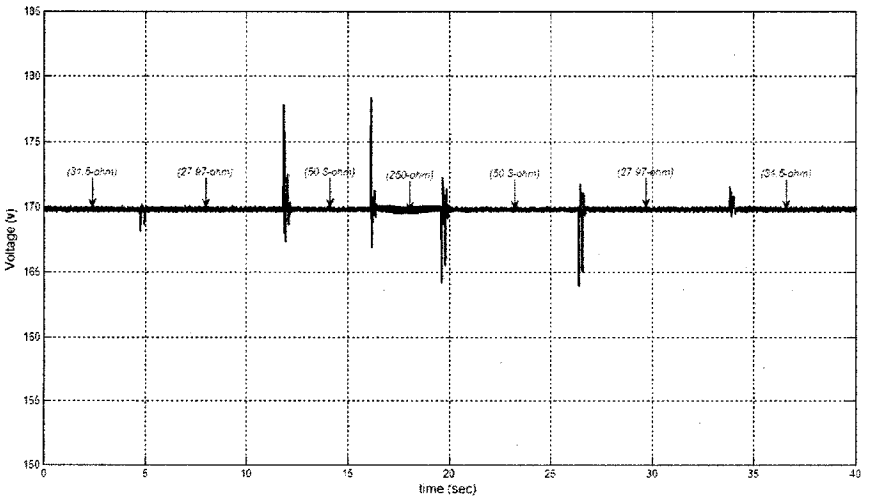

Fig. 4-13 Effect of load variation on the voltage when only voltage regulation

There one sees that the voltage is regulated properly in the steady-state and presents fast transient. The magnitude and duration of the transient depends on the magnitude of the load variation. In this case the frequency is not regulated and it presents larger variations as compared with the unregulated case for the same magnitude of resistive load variations. This can be explained by the fact that the magnitude of the speed variation of the unregulated turbine and frequency of the generated voltage depend on the magnitude of the variation of the active power demanded by the load. As in the unregulated case when the load resistance is increased or decreased, then the voltage magnitude also increases or decreases respectively, thus resulting in a smaller load power variation than when the voltage is regulated.

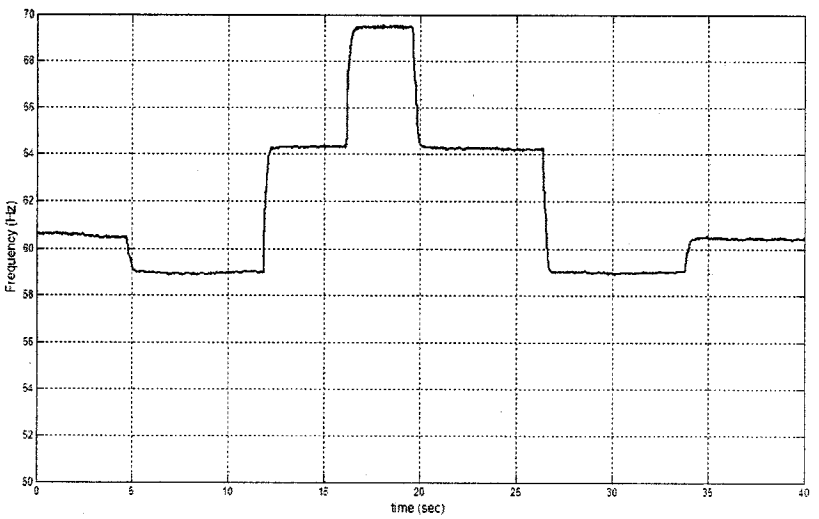

Fig. 4-14 The effect of load variation on the frequency, voltage regulated system

The variations in the reference and actual currents that are used in the control of VSI is also shown in Fig. 4-15 and Fig. 4-16. The effectiveness for the voltage control loop can be best visualized by inspecting the I_d and I_{dref} current waveforms. There one can see that the actual current follows perfectly with the reference current. The frequency is not regulated so the current I_q and I_{qref} have a zero value.

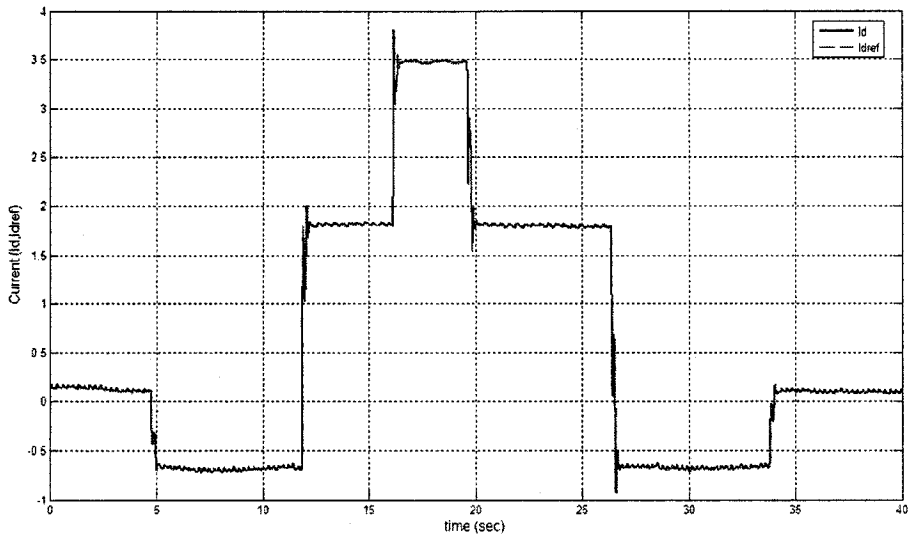

Fig. 4-15 Variations in the reference current I_{dref} and the actual current I_d

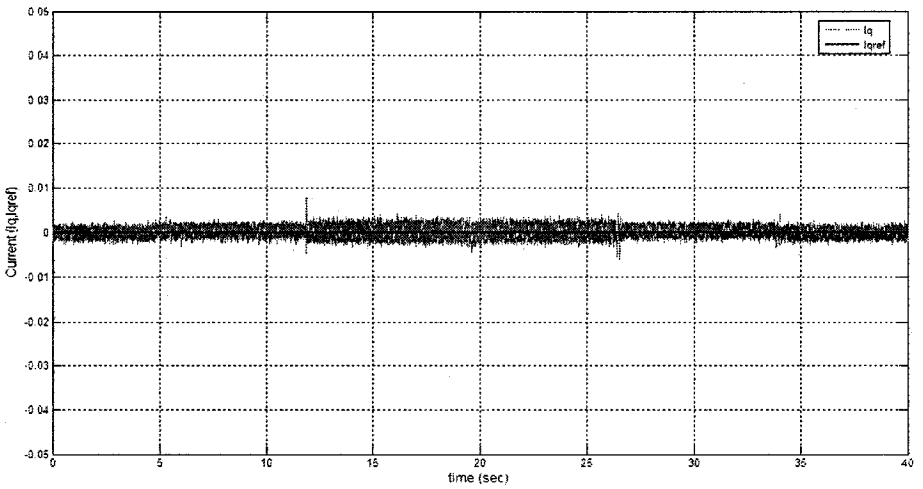

Fig. 4-16 Variations in the reference current I_{qref} and the actual current I_q

The 3rd test is conducted for the regulated system where both the system voltage and frequency are regulated by means of reactive and active power supplied or absorbed by the VSI respectively. As in Fig. 4-17 and Fig. 4-18, one can see that the voltage and the frequency are regulated perfectly and that the magnitude and the duration of the transients are proportional to the magnitude of the load variations. The actual and the reference currents of both axes follow each other as shown in Fig. 4-19.

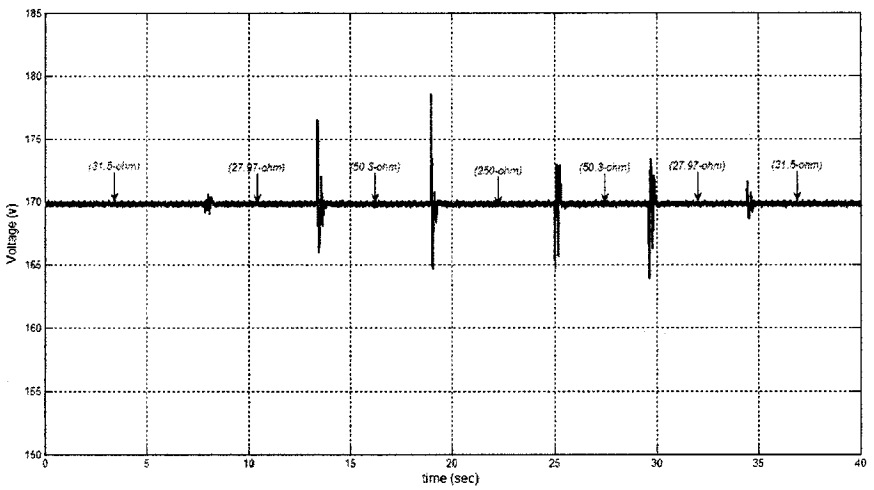

Fig. 4-17 The effect of load variation on the voltage with regulated system

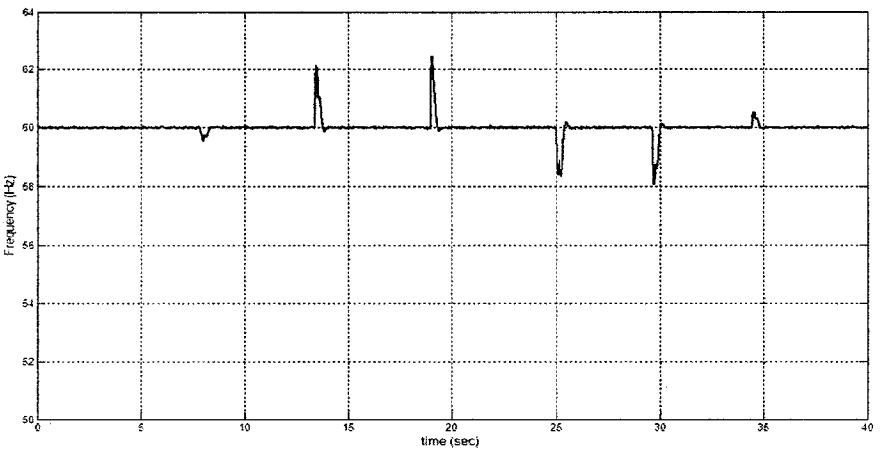

Fig. 4-18 The effect of load variation on the frequency with regulated system

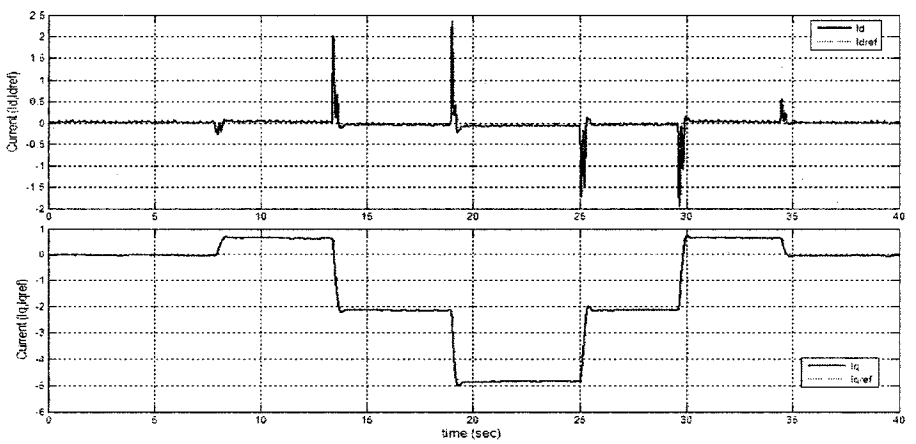

Fig. 4-19 Variations in the reference and actual current of both the axes

Fig. 4-20 shows the variation in the inverter current during system voltage and frequency regulations. As one can see from Fig. 4-20, the inverter current variation is also proportional to the load variations.

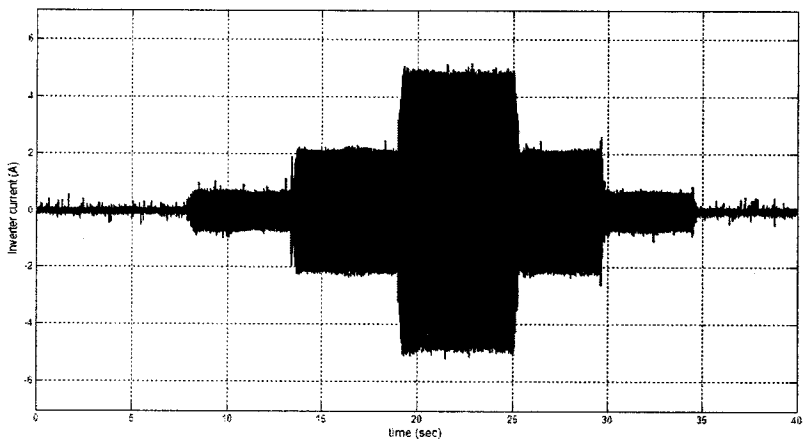

Fig. 4-20 Inverter current variations during voltage and frequency regulation

Fig. 4-21 shows the variation in P and Q of the inverter during system voltage and frequency regulation. It should be noted that variation in P is related to the frequency regulation and variation in Q is for the voltage regulation. One can notice in Fig. 4-21 that initially the system voltage and the frequency are at their rated values, the VSI P and Q should be zero, as there is no regulation required. If the frequency decreases the VSI should supply P and if it increases then the VSI should absorb P. Similarly if the voltage magnitude decreases the VSI should supply Q and vice versa.

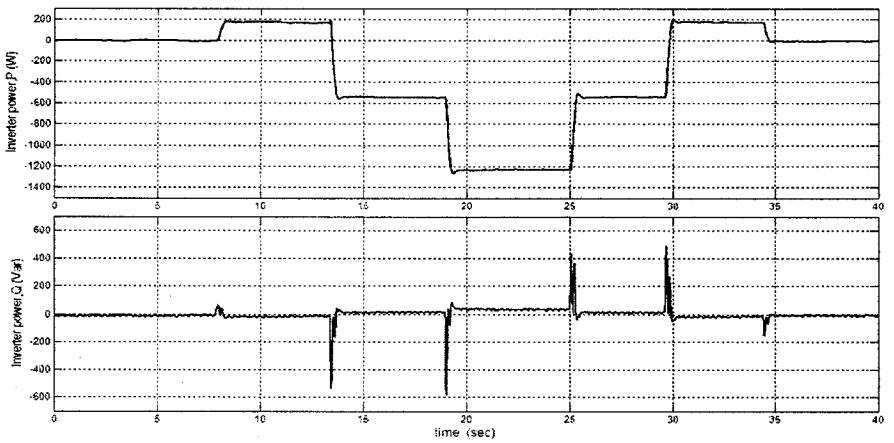

Fig. 4-21 Inverter P and Q variation during voltage and frequency regulation

The generator P and Q variations are shown in Fig. 4-22. The variations in the transient are proportional to the load variations and in the steady-state the generator always sees the constant load at its stator terminals, resulting a constant P and Q.

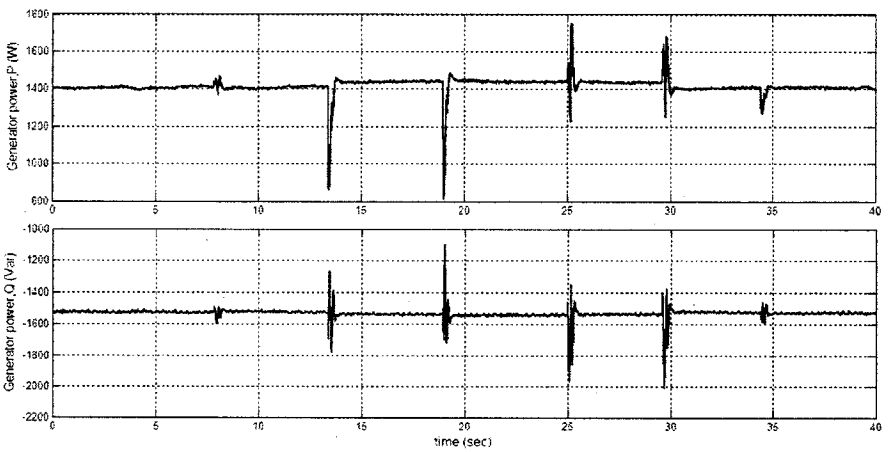

Fig. 4-22 Generator P and Q variation for both voltage and frequency regulated system

Fig. 4-23 shows the variation in the d and q components of the modulating signals of the VSI that are responsible for the overall system voltage and frequency regulations.

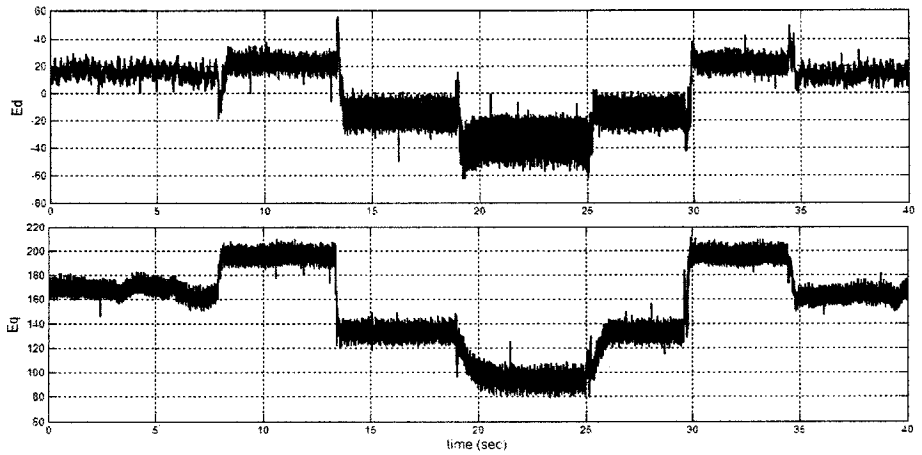

Fig. 4-23 E_d and E_q variation during voltage and frequency regulations

A summary of the steady-state values of the magnitude and frequency of the voltage at the PCC, when the load varies for the three cases discussed before are shown in Table 4-1. It is clear that if the VSI capabilities are limited to reactive power control only (STATCOM), it can regulate the voltage but the frequency variations are larger than for the unregulated case. Thus, the VSI should be equipped with an energy storage device in the dc side to be able to inject/absorb active power and regulate the frequency for better results.

Table 4-1 Steady-state values for the three cases

Three cases	R (Ω)	31.5	27.97
Unregulated System	Voltage (V)	169.5	160
	Frequency (Hz)	60	59.82
Only voltage regulation	Voltage (V)	169.83	169.83
	Frequency (Hz)	60.8	58.9
Both voltage & frequency regulation	Voltage (V)	169.83	169.83
	Frequency (Hz)	60	60

4.3.1.2 DC Machine Armature Voltage Variation Tests

It is well known that the induction generator voltage and frequency are dependent on the prime mover speed, the excitation capacitance and the impedance of the load (magnitude and power factor). The effect of ac load variation on the regulation of the generated voltage and the frequency has already been discussed with the detailed experimental results in the previous section.

In this section, we will discuss the effect of the prime mover input power variation on the regulation of voltage and the frequency of the induction generator. This was accomplished with a variation of the dc voltage applied to the armature of a dc motor to model a variation of the torque at zero speed of the unregulated hydro turbine. Here instead of applying full rated load, the induction generator is initially supplying power at a half rated load of 63Ω with corresponding reduced excitation capacitance found to be 25.66μF to allow more input armature voltage variations without any overloading of the machine. So initially the dc input armature voltage of dc motor is set at 206-V dc with the induction generator supplying power to a half rated resistive load with a terminal voltage of 171.5V (peak) line-neutral and with a frequency of 60.03Hz. For the armature voltage variation also, a similar comparison for the three cases is considered. Tests are carried out for the armature voltage variation to see the effect of prime mover input power variation on the regulation of voltage and frequency.

The 1st test is conducted for the unregulated system as shown in Fig. 4-24 to Fig. 4-26, as we increase or decrease the dc machine armature voltage to vary the prime mover speed then the induction generator terminal voltage and its frequency also proportionally increases or decreases respectively.

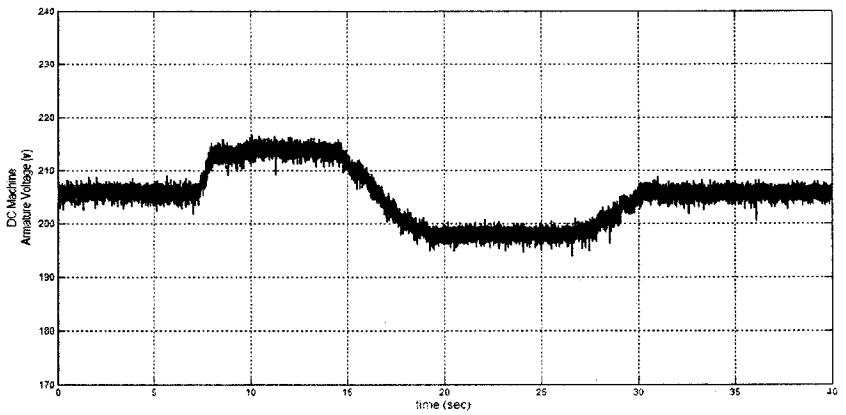

Fig. 4-24 Variation in armature voltage

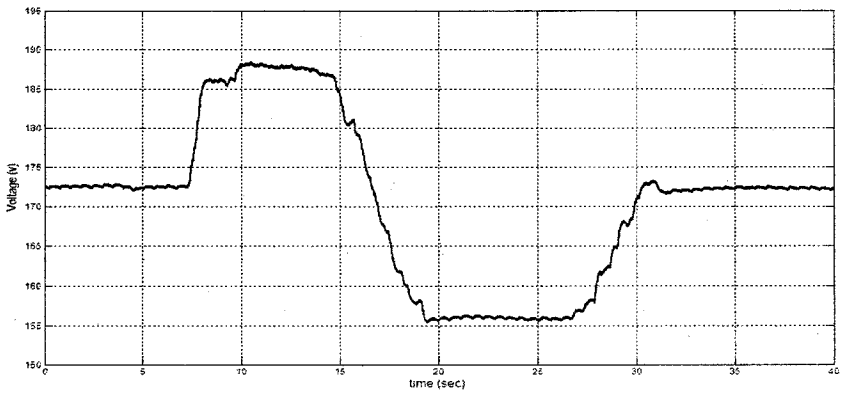

Fig. 4-25 Effect of armature voltage variation on the voltage for the unregulated system

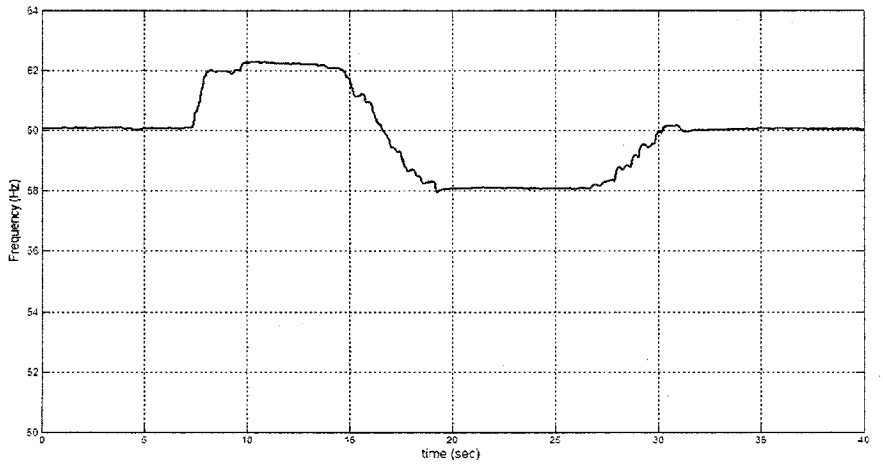

Fig. 4-26 Effect of armature voltage variation on the frequency for the unregulated system

The 2nd test is conducted by regulating only the induction generator terminal voltage and the frequency is not regulated in this case. At half rated load present, initially the induction generator terminal voltage and frequency is at their rated values. After some time, the armature voltage variation is carried out to see the variation on the voltage and on the frequency. As we can see from Fig. 4-27 to Fig. 4-30, that the terminal voltage is regulated perfectly irrespective of the variation in the armature voltage and the frequency is not regulated and it presents the linear increase or decrease with the prime mover speed variation. But the variation in the frequency is larger than with the unregulated case. The reason for larger frequency variation during only voltage regulation was already explained in the previous section. As one can see in Fig. 4-30, the actual and reference currents are also following each other. This shows the effectiveness of the proposed control scheme.

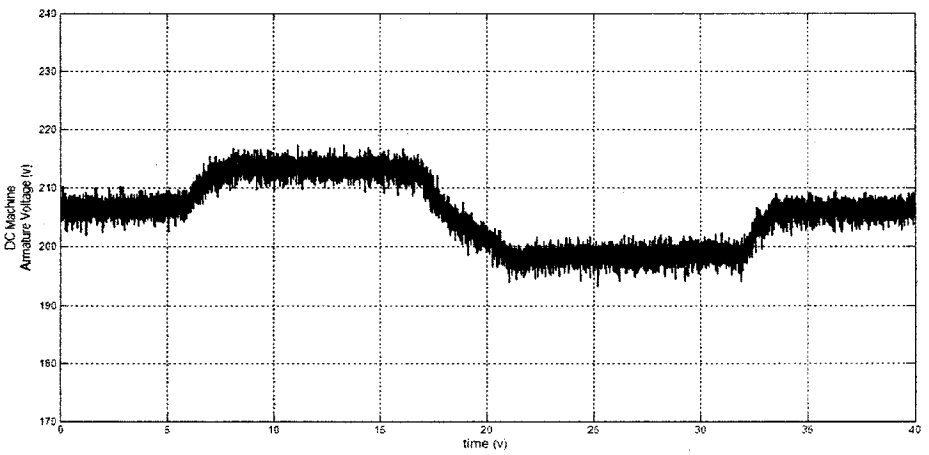

Fig. 4-27 Variation in armature voltage for voltage regulation only

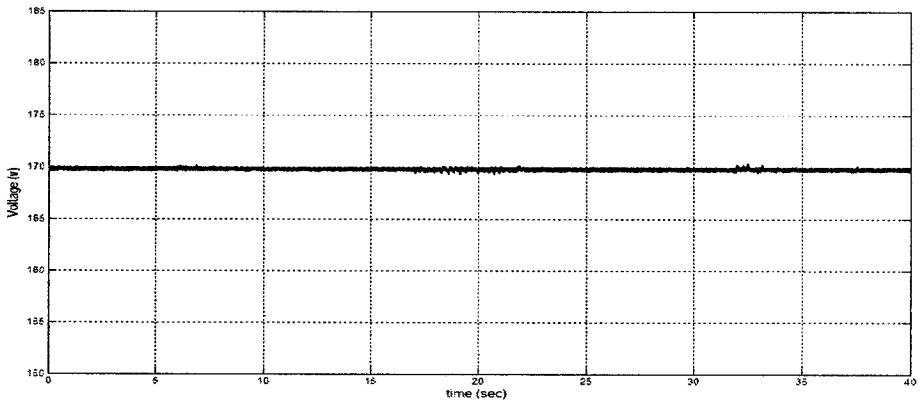

Fig. 4-28 Effect of armature voltage variation on the voltage for the voltage regulated system

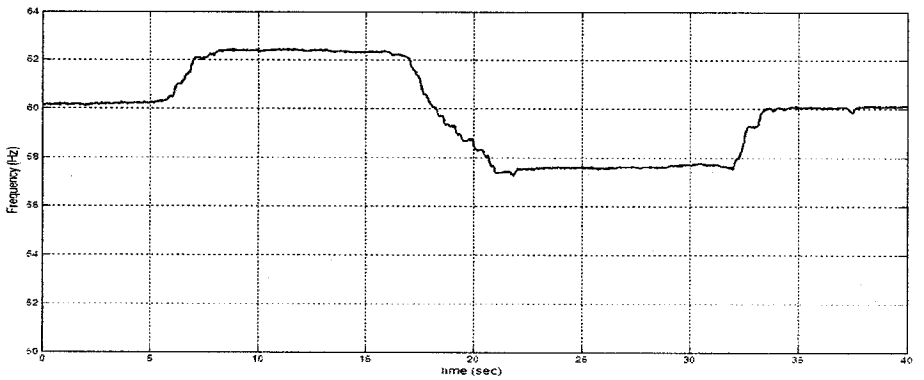

Fig. 4-29 Effect of armature voltage variation on the frequency for the voltage regulated system

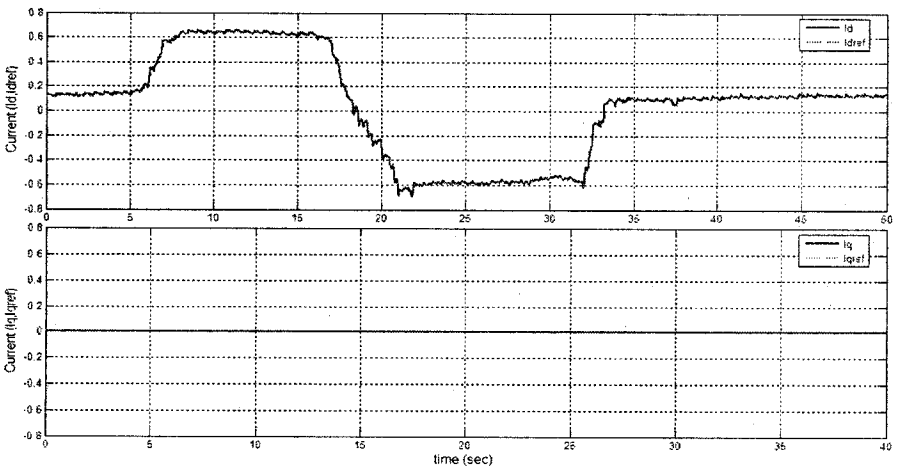

Fig. 4-30 Reference and actual current variations

Now the 3rd test is conducted to see the effect of armature voltage variation on the voltage and frequency, when the control system is regulating the overall system voltage and frequency. Experimental results show that the proposed control system is also effective in the regulation of the voltage and the frequency for variations in the torque of the unregulated turbine. We can see in Fig. 4-31 to Fig. 4-33 that the voltage and frequency are well regulated in the steady state. This result was obtained despite the fact that the variations in the armature voltage of the prime mover shown in Fig. 4-31 were carried out manually and it presents steeper transient than in the previous tests. In Fig. 4-34, one can also see the variation in the actual and the reference current and that they are following each other perfectly. The inverter current variations, during the voltage and frequency regulations are shown in Fig. 4-35.

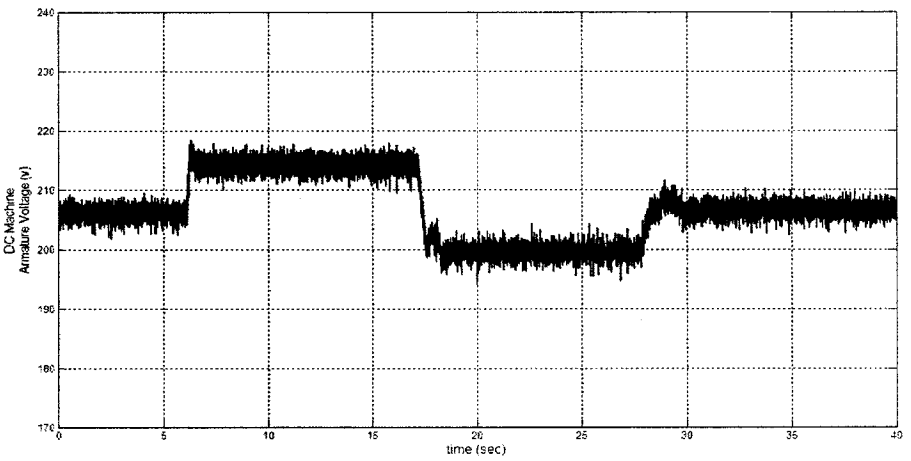

Fig. 4-31 Armature voltage variation of dc-machine

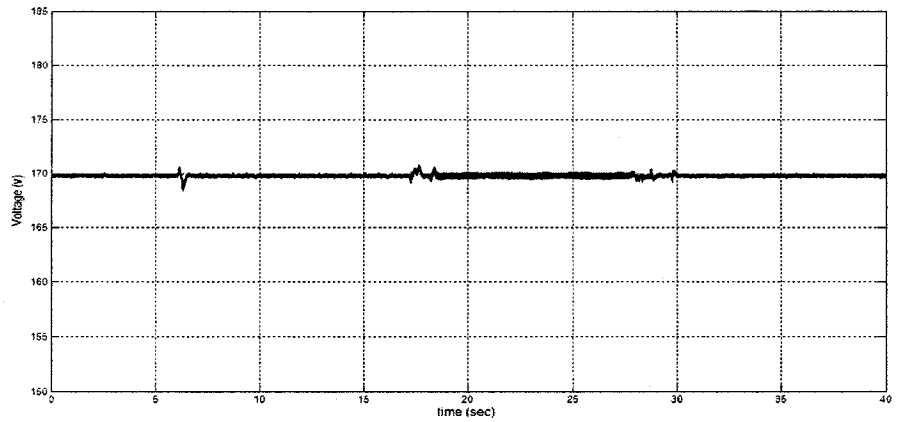

Fig. 4-32 Effect of armature voltage variation on the voltage for the regulated system

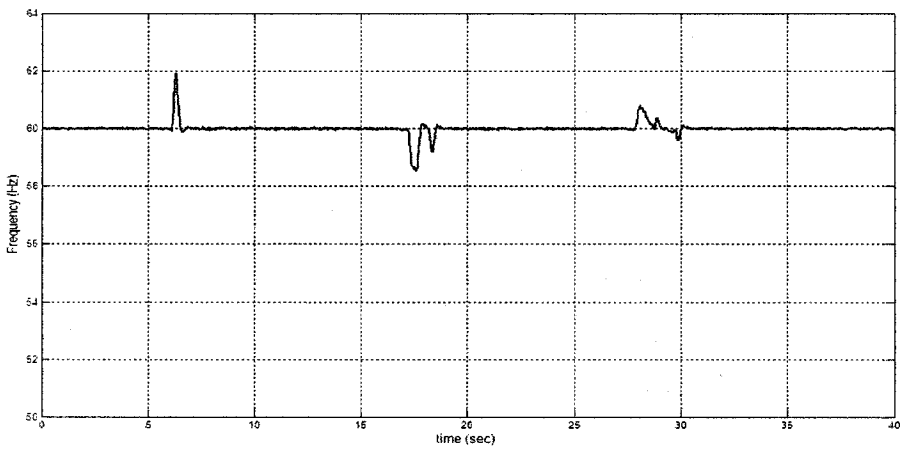

Fig. 4-33 Effect of armature voltage variation on the frequency for the regulated system

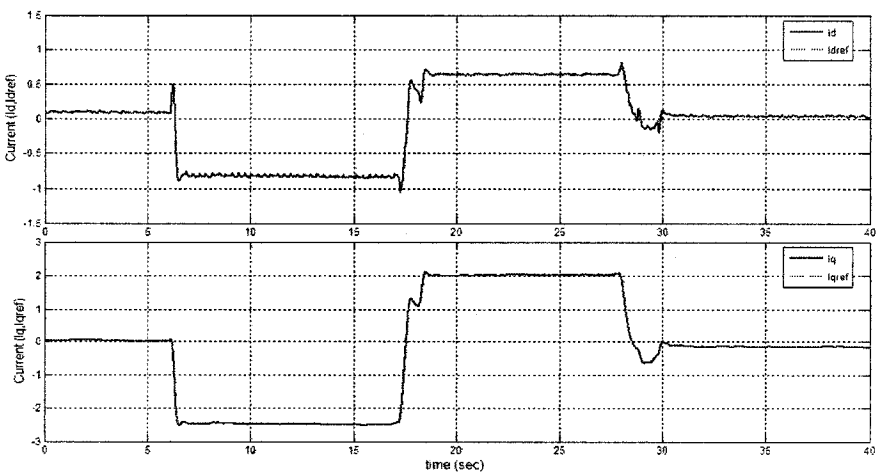

Fig. 4-34 Actual and reference current variations, Regulated system

The final steady-state values for the three cases are tabulated in Table 4-2. By comparing all the three cases, we can say that the variation in frequency for the unregulated case is smaller as compared with the voltage regulation case. The reason for that was already explained previously in the load variation test.

Table 4-2 Steady-state values for the three cases

Three cases	Armature Voltage - (V)	208	213
Unregulated system	Voltage (V)	172	188.5
	Frequency (Hz)	60.1	62.26
Only voltage regulation	Voltage (V)	169.83	169.83
	Frequency (Hz)	60.15	62.45
Both voltage & frequency regulation	Voltage (V)	169.83	169.83
	Frequency (Hz)	60	60

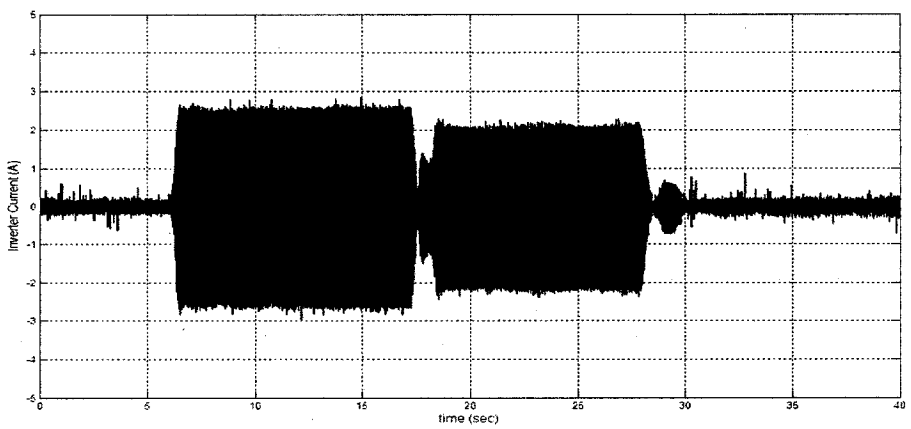

Fig. 4-35 Inverter current variations during voltage and frequency regulation

Fig. 4-36 presents the variation of inverter P and Q during voltage and frequency regulation. As one can see, when the system frequency increases, inverter should absorb

P and when it decreases then VSI should supply P. Similarly during voltage variations, the inverter should supply Q when the terminal voltage is reduced and if it increases then the VSI should absorb Q. Fig. 4-37 shows the generator P and Q variation. One can see there if the armature voltage increases, then the generator voltage should also increase and therefore supplies more power P to the ac load.

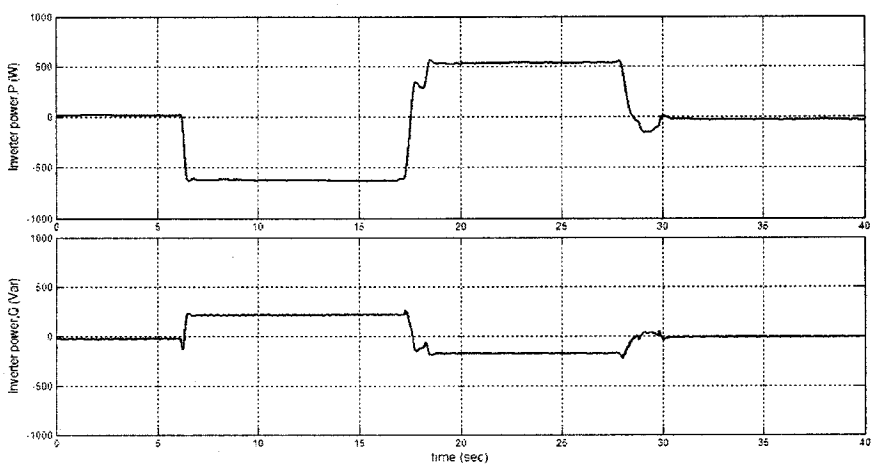

Fig. 4-36 Inverter P and Q variation during voltage and frequency regulation

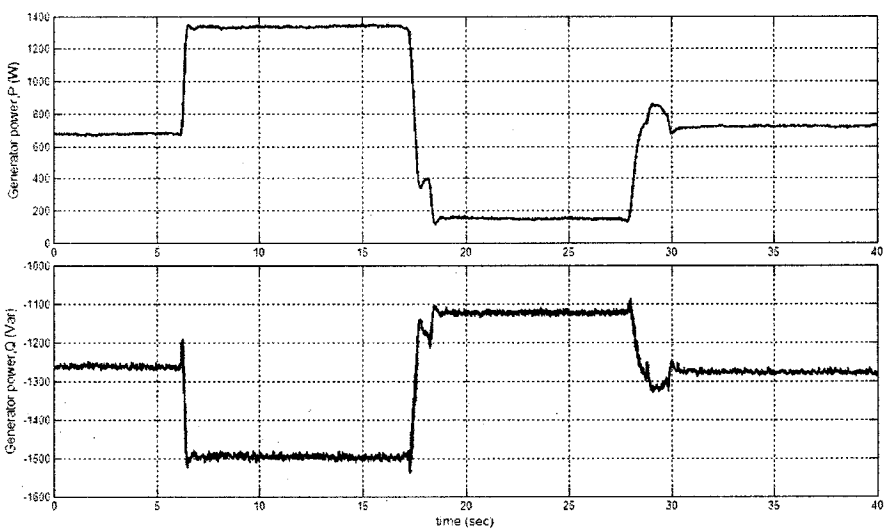

Fig. 4-37 Generator P and Q variation during voltage and frequency regulation

4.4 SYSTEM WITH WIND TURBINE

The schematic block diagram for the overall system considering the wind turbine is shown in Fig. 4-38. The wind turbine considered in this thesis has the following characteristics: three blade, fixed pitch, variable speed and horizontal axis wind turbine. The wind turbine is connected to the induction generator through a gear box with a ratio of 4:1. As in the case of stand-alone self-excited systems, the magnitude of the generated voltage and the frequency should be affected during variations in wind speed and load, if the system is unregulated. Since the wind speed is not constant at all times, so the induction generator voltage and frequency will vary depending upon the wind speed variations. In this section we will conduct experimental tests to show the impact of the VSI and the proposed control scheme on regulating the induction generator terminal voltage and frequency by considering the wind turbine during variation in the wind speed.

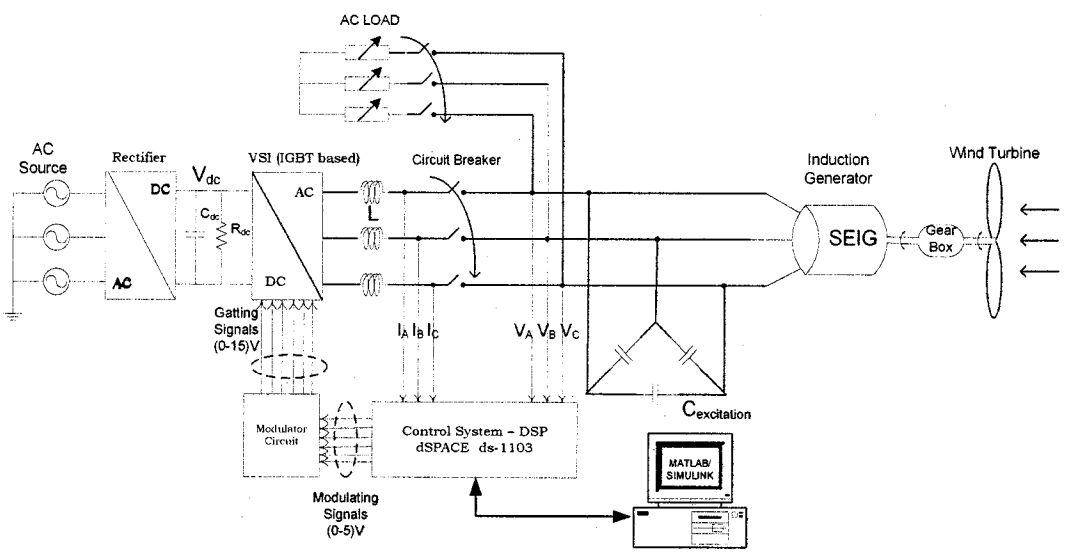

Fig. 4-38 System with a wind turbine

4.4.1 EXPERIMENTAL RESULTS

This work (wind turbine emulator) was done by another colleague (Mr. Saeed Khedri) in the P.D ZIOGAS power electronics laboratory, and I was using his set-up with my system to represent a wind turbine to run the induction generator. A permanent magnet dc machine drive is used to emulate the mechanical drive train of a wind power system with an induction generator under real conditions. The mechanical drive-train characteristics of the wind turbine are modeled through a two-mass system, representing the turbine, the gear box and generator moment of inertia connected by elastic shafts as shown in Fig. 4-39. This model is implemented within Simulink software environment and generates the reference values of torque that need to drive the dc machine.

The main parts of the wind turbine model includes blades, rotor and the hub which are contributing in major part of inertia and the mechanical drive-train which includes the low speed side shaft, the high speed side shaft (considered flexible) and the gearbox. Together with the wind speed as well as the generator speed feedback to the wind turbine and drive-train model, a reference turbine torque is generated from the torque-speed characteristics and then converted the reference torque to get the reference current that is used to control the dc machine.

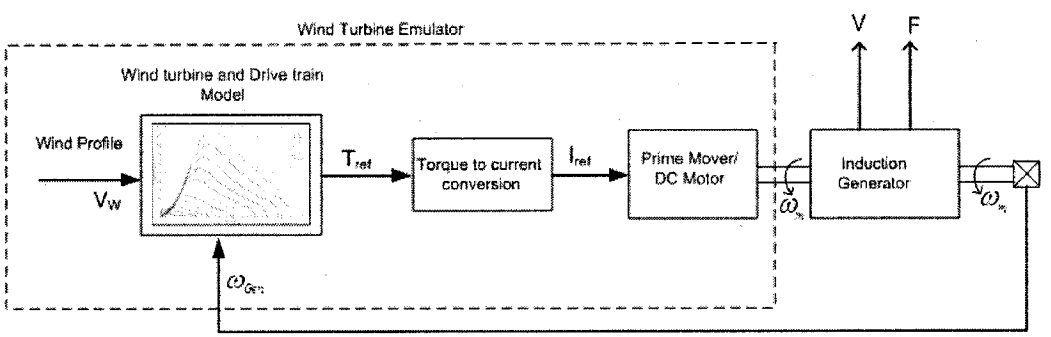

Fig. 4-39 Wind turbine emulator model

In the Fig. 4-39 above, the first part was implemented by Matlab/Simulink software. Its output, the reference current for the dc motor drive, is proportional to the torque at the high speed side of the gear box. The second part consists of the actual electric generator connected to the shaft of the dc motor that emulates the wind turbine and gear box. The only parameter of the actual hardware system that needs to be measured is the speed of the generator shaft (ω_{Gen}) that is used in the wind turbine emulator block.

The control logic of the wind turbine emulator was also implemented with a DSP (DS-1103 from dSPACE) system. Values for J_{WT}, B_{WT}, K and gear box ratio are implemented within the control desk software and can be modified at any time. A user interface was developed with the Control desk for varying some parameters such as wind speed (V), inertia of the wind turbine (J_{WT}), shaft damping constant (B_{sh}) and torsional coefficient of the shaft (K_{sh}). It also allows the visualization of other parameters such as the actual rotor speed, tip-speed ratio, torque coefficient and actual rotor torque.

To investigate if the proposed control system is also effective in regulating the voltage and frequency of the stand-alone self-excited induction generator by considering the input prime mover as the wind turbine, we will conduct a series of tests by varying the wind speed of the prime mover as well as some load variations on the stator side of the induction generator for different values of inertia (J) of the turbine. The following reference parameters were assumed in getting the experimental results for the wind turbine emulator: J_{WT} = (3, 7) $kg.m^2$, J_{gen} = 0.011 $kg.m^2$, B_{WT} = 0.193 *N.m.s/rad,* K = 1650.07 *N.m/rad* and the gearbox ratio = 4:1, with the oscillatory torque added to the model to make it close to the real model.

4.4.1.1 WIND SPEED VARIATION TESTS

In this section, we will analyze the effect of wind speed variation on the regulation of voltage and frequency of the stand-alone induction generator supplying power to a constant load. We will also compare the effect of regulation on the voltage and frequency for different values of inertia of wind turbine (J).

The first test is conducted for the unregulated system by setting the wind turbine parameters as, $J_{WT} = 3\ kg.m^2$ and $B_{WT} = 0.193\ N.m.s/rad$ and the wind speed is set to the rated value, V_w=7.85 *m/s*. One can see in Fig. 4-40 and Fig. 4-41, that at this rated wind speed the induction generator is supplying power to half rated load with rated voltage and frequency. Then after sometime, a step change in wind speed is applied i.e. the wind speed decreases to 7.35 *m/s* and then it increases back to the rated value. As in the unregulated case shown in Fig. 4-40 and Fig. 4-41, one can see that by changing the prime mover speed the induction generator voltage and frequency are also changes proportionally. They decrease if the wind speed decreases and increase if the wind speed increases.

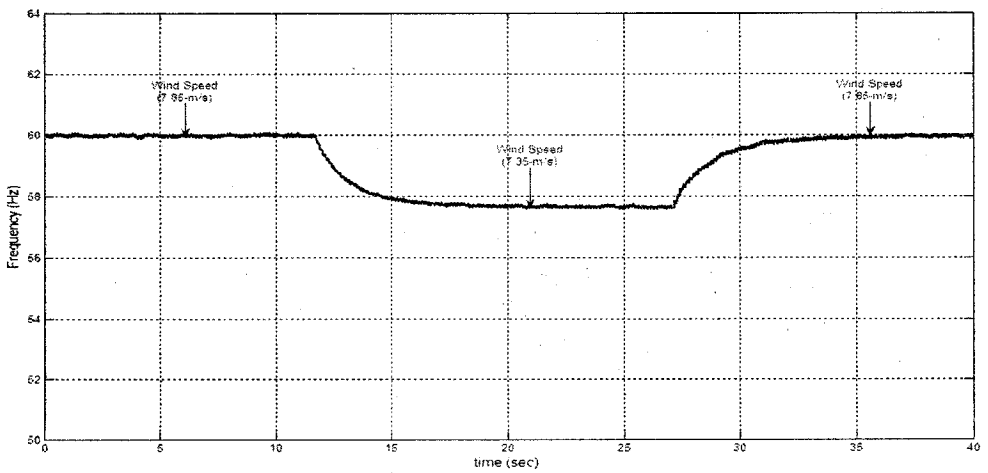

Fig. 4-40 Effect of wind speed variation on the frequency for the unregulated system

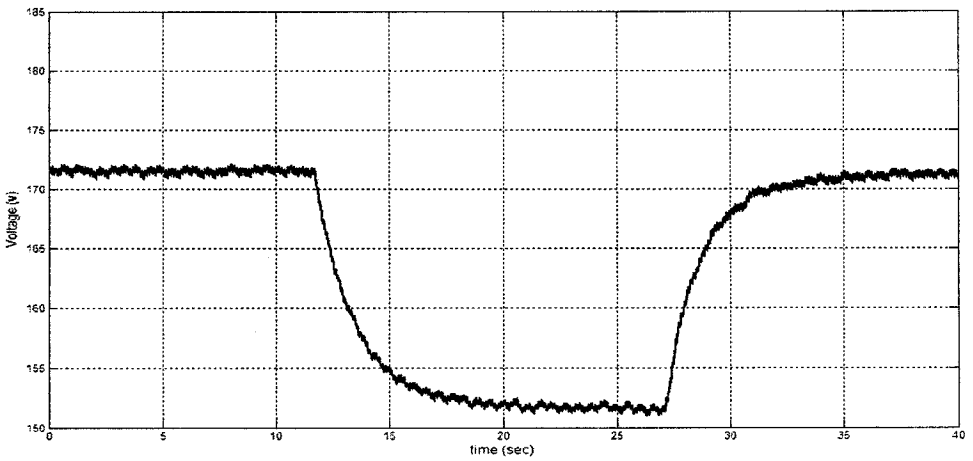

Fig. 4-41 Effect of wind speed variation on the voltage for the unregulated system

Now a 2nd test is conducted to see the effect of wind speed variation on the voltage and the frequency, while the control system is regulating both the voltage and the frequency. We can see in Fig. 4-42 and Fig. 4-43, that the control system is very effective in regulating both the system voltage and frequency whenever there is a step decrease in wind speed or a step increase. Thus, this justifies that the proposed control system is also very effective in regulating the generator terminal voltage and frequency when the input prime mover considered is a wind turbine. The reference and the actual currents that are responsible for the inverter P and Q regulation are shown in Fig. 4-44. They follow each other in the transient and in the steady-state. The inverter current, P and Q variations during the voltage and the frequency regulations are also shown in Fig. 4-45 and Fig. 4-46 respectively. The generator P and Q variations are also shown in Fig. 4-47 while the variations in the E_d and E_q components are displayed in Fig. 4-48.

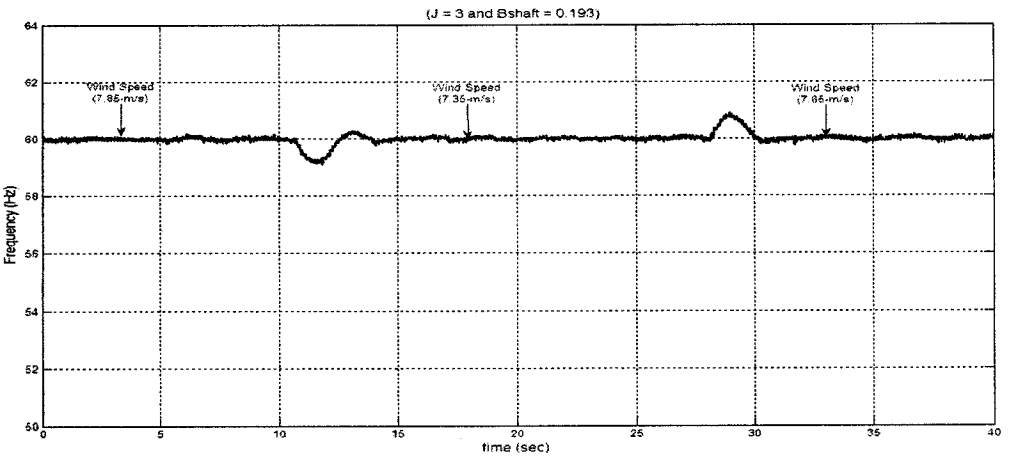

Fig. 4-42 The effect of wind speed variation on frequency, Regulated system

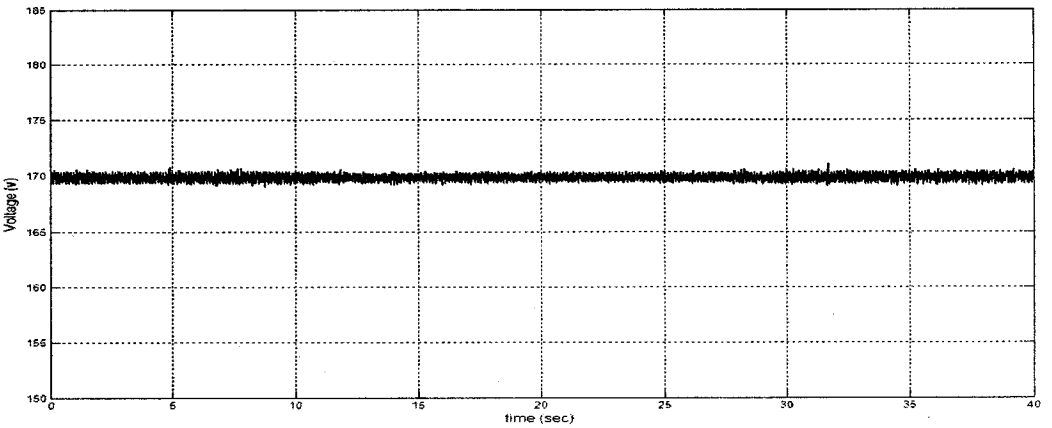

Fig. 4- 43 The effect of wind speed variation on voltage, Regulated system

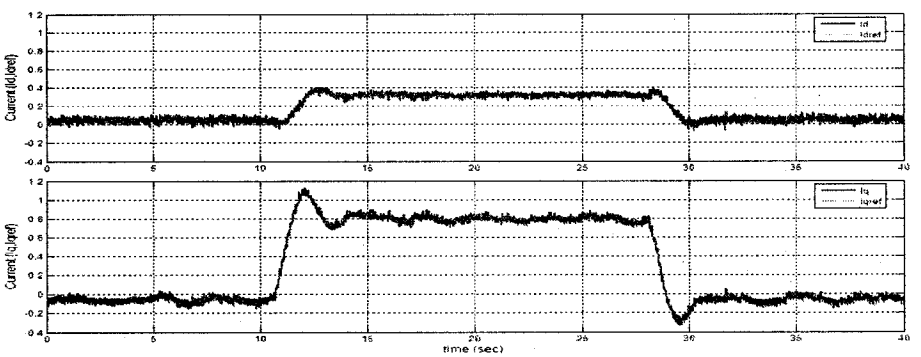

Fig. 4-44 Variations in reference and actual current, Regulated system

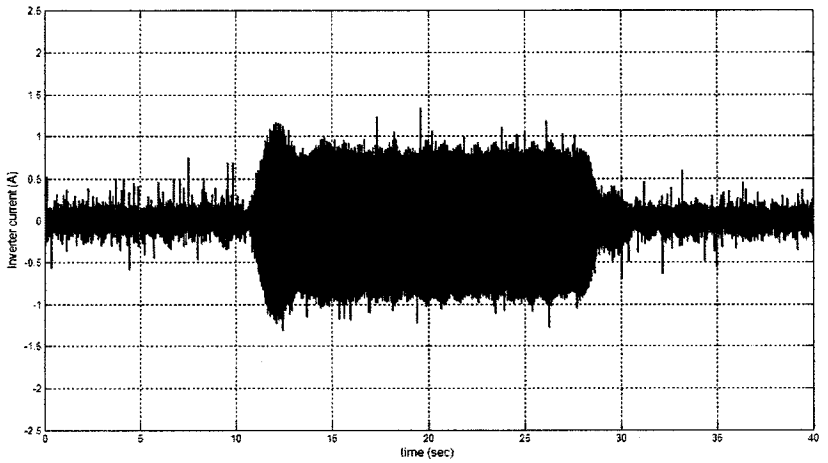

Fig. 4-45 Variation in inverter current at half rated-load (Regulated system)

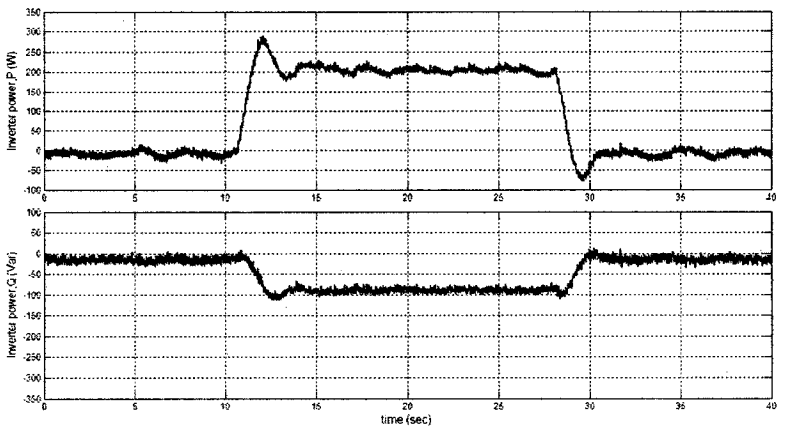

Fig. 4-46 Variation in inverter *P* and *Q* at half rated-load (Regulated system)

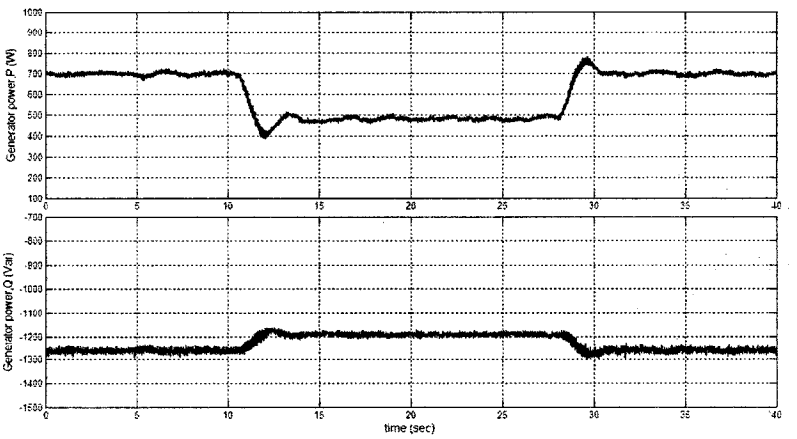

Fig. 4-47 Variation in generator *P* and *Q* at half rated-load (Regulated system)

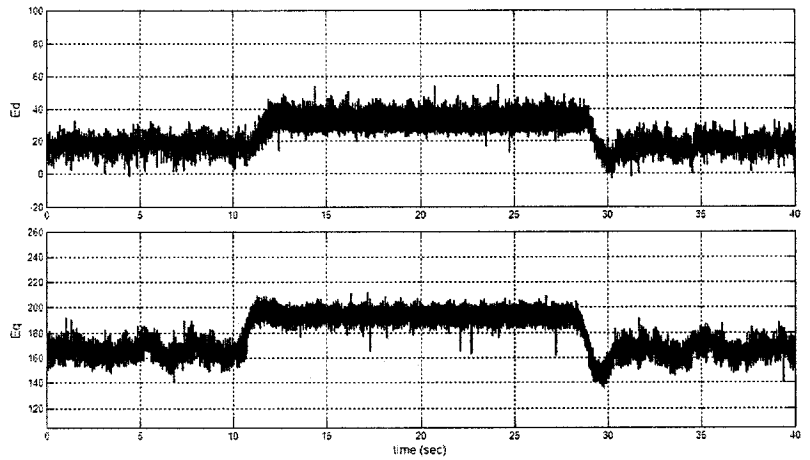

Fig. 4-48 Variation in E_d and E_q at half rated-load (Regulated system)

The next test is conducted, to see the effect of higher J of wind turbine on the regulation of voltage and frequency for the same wind speed variations. One can conclude from Fig. 4-49, Fig. 4-50 and Fig. 4-51, that the voltage and the frequency are regulated properly and that the reference and actual currents are also following each other. Thus the control system is also effective in regulating the voltage and the frequency, if the moment of inertia of wind turbine increases. But one has to say that by comparing the waveforms for both J in the case of wind speed variation, *as* J increases the speed of response of the system for the regulation of frequency should be slower and presents less oscillation.

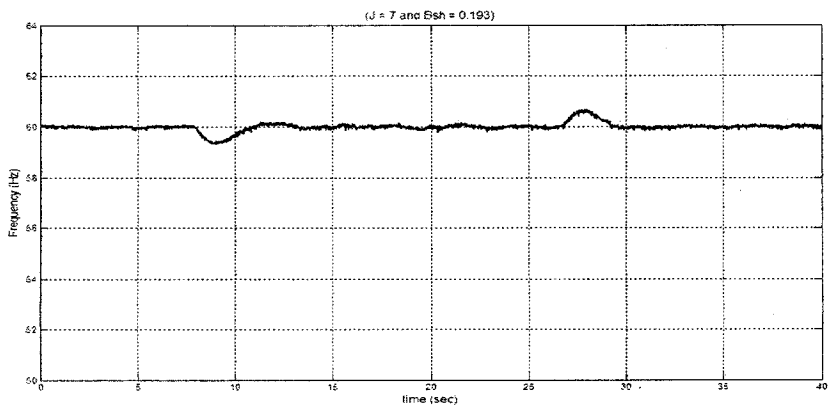

Fig. 4-49 Effect of wind speed variation on the frequency at half rated load

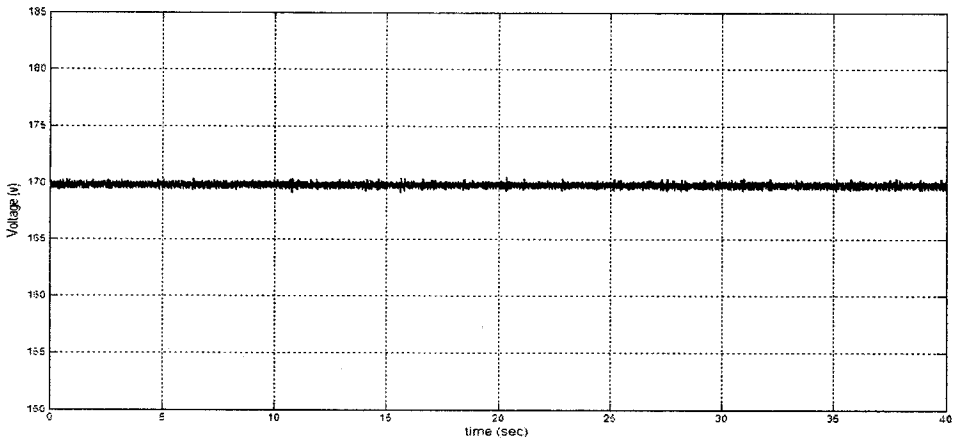

Fig. 4-50 Effect of wind speed variation on the voltage at half rated load

Table 4-3 Time response characteristics for different J during wind speed variations

Time response characteristics	J=3	J=7
	B_{sh} = 0.193	
Under shoot in the frequency waveform	59.02 Hz	59.25 Hz
Over shoot in the frequency waveform	60.94 Hz	60.67 Hz
Steady-state time	3.364 Sec	4.044 Sec
Oscillations in frequency waveforms	Greater	Smaller

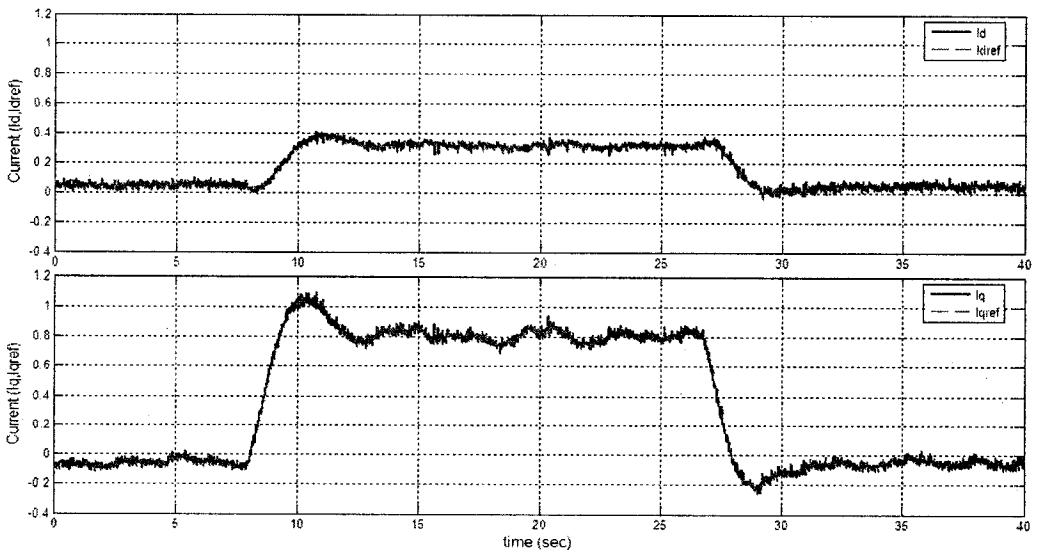

Fig. 4-51 Current variation at half rated-load (Regulated system)

Thus by inspecting the Table 4-3, one can conclude that if the wind turbine moment of inertia (J) increases, the dynamics of the system will be slower and the transient over-shoot and under-shoot in the frequency waveform will be lesser as compared to the lower value of J. So the controller parameters are dependent on the value of J selected, to get a faster response same as for lower value of J one needs to redesign the controller parameters based on the new value of J. Thus we can say that rotors with higher values of moment of inertia yield reduced oscillations in the shaft while presenting less over-shoot and slower dynamics.

4.4.1.2 LOAD VARIATION TESTS

In this section, for the same wind turbine setup operating at constant wind speed 7.85 m/s, now the effect of variations of the electrical load on the regulation of the voltage and frequency of the induction generator is investigated. A similar comparison can be made as in the previous case for different values of J. The induction generator is initially operating at rated half load of (63Ω) at a rated wind speed of 7.85 m/s that gives the rated line-line terminal voltage of 208 V at a frequency of 60 Hz. The same analysis is carried out for the load variation to compare the overall effect on the voltage and the frequency regulation with the variation of electrical load and J of wind turbine.

The first test is conducted for the unregulated system. The wind turbine parameters are set at $J = 3\ kg.m^2$ and $B_{WT} = 0.193\ N.m.s/rad$ and the system is initially operating at half rated load (63Ω) and the generator voltage and its frequency is also close to their rated values as shown in Fig. 4-52. After some time, the resistive load is changed to 50.32Ω and then it is changed again to return it to the rated half load conditions. As we can see from Fig. 4-52 and Fig. 4-53, that the variation in the voltage

and frequency are proportional to the load variations. The magnitude of induction generator terminal voltage and its frequency increases as the load power decreases and they decrease when the load power increases.

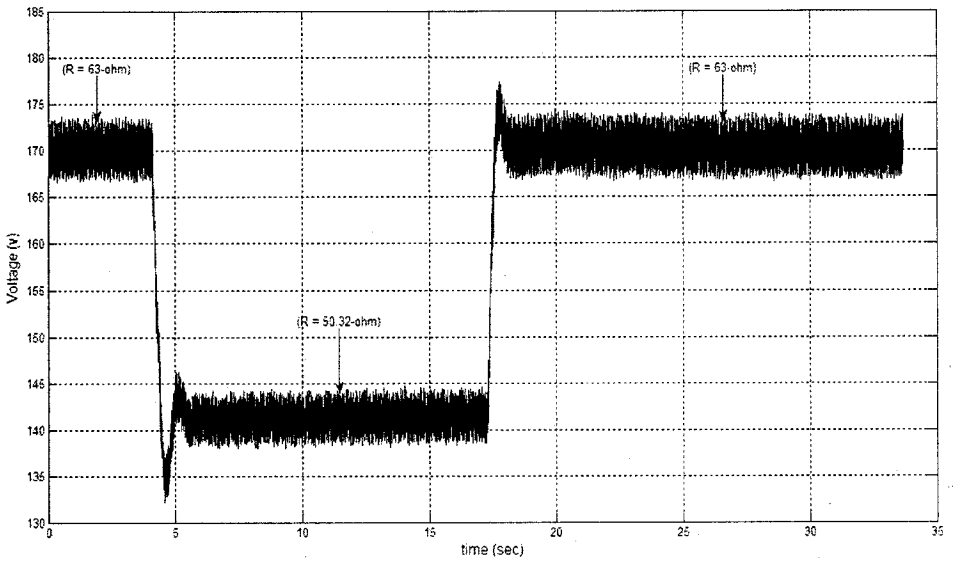

Fig. 4-52 Variation in voltage due to load variation for the unregulated system

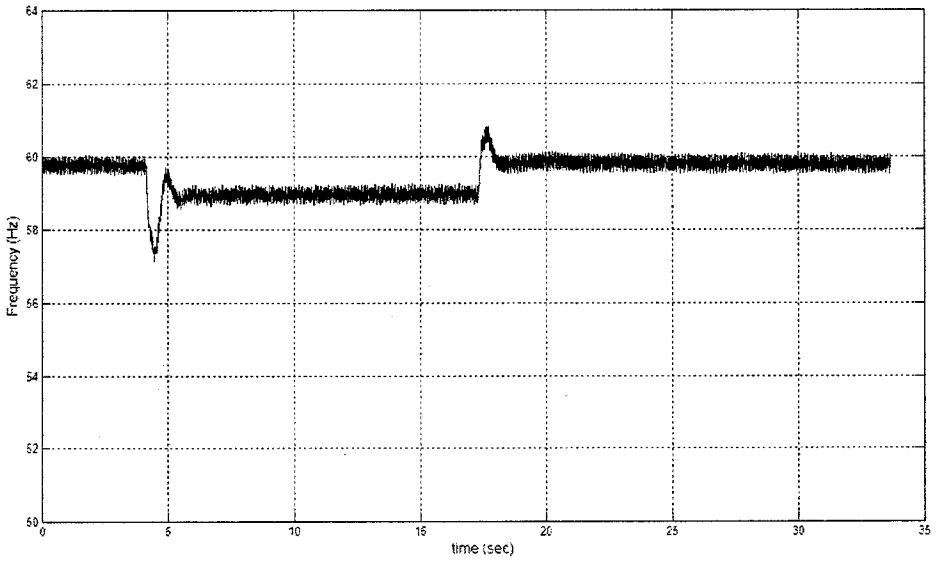

Fig. 4-53 Variation in frequency due to load variation for the unregulated system

The next two tests are carried out for two different values of wind turbine moment of inertia (J), to see the impact of the control system on the voltage and frequency regulation with varying loads. First test is conducted for $J = 3\ kg.m^2$ and wind speed is fixed at 7.85m/s. After sometime, a load variation is conducted to see the variation in the voltage and frequency. Fig. 4-54 and Fig. 4-55 shows the variation in voltage and frequency for the regulated system. One can see that both the quantities are regulated and that their respective currents are also following with the reference currents as shown in Fig. 4-56.

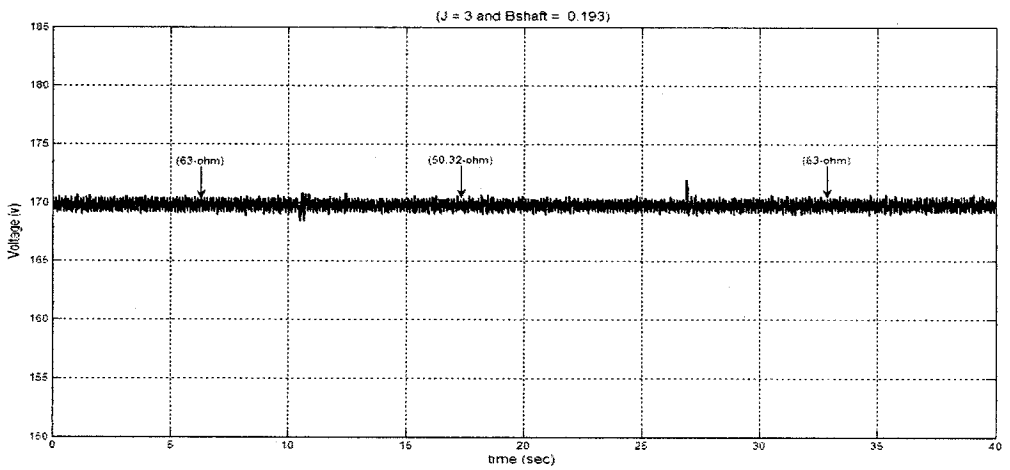

Fig. 4-54 Voltage variations for the regulated system

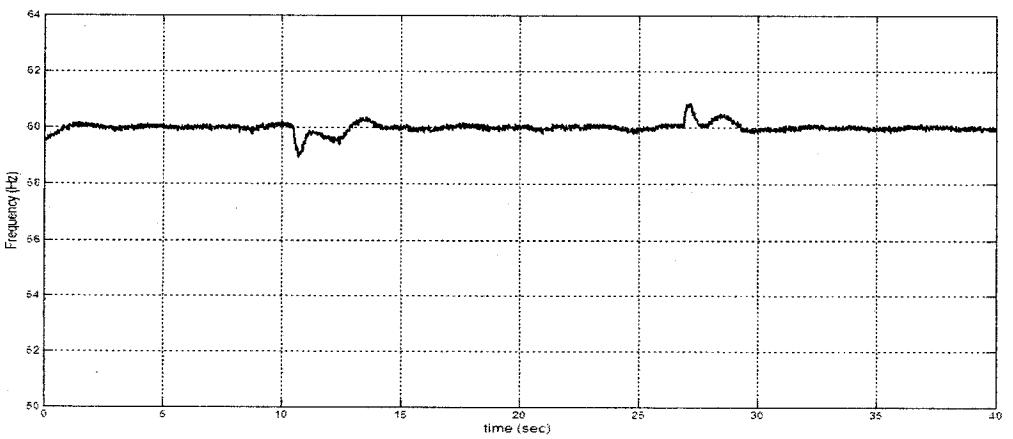

Fig. 4-55 Frequency variations for the regulated system

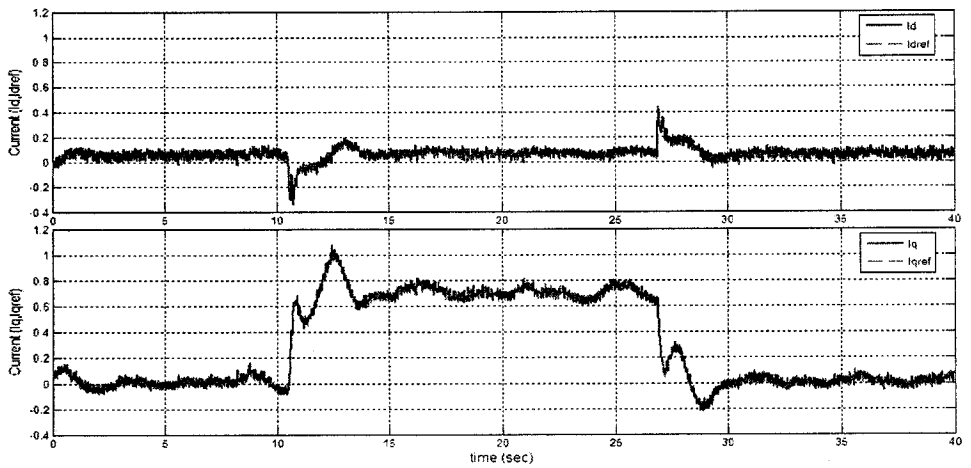

Fig. 4-56 Reference and actual current variations at half rated-load (Regulated system)

Fig. 4-57 to Fig. 4-60, show the variations in inverter current, inverter power, generator power and the (E_d, E_q) components of the VSI respectively during voltage and frequency regulations.

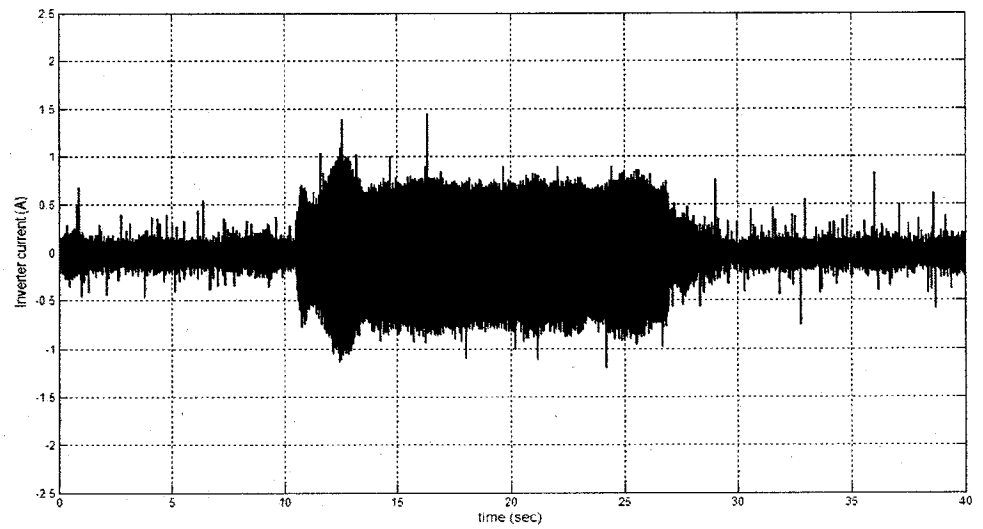

Fig. 4-57 Inverter current variations at half rated-load (Regulated system)

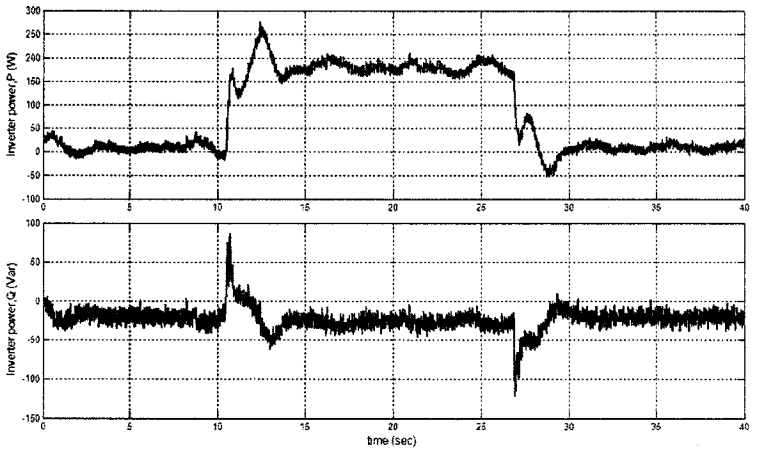

Fig. 4-58 Inverter P and Q variation at half rated-load (Regulated system)

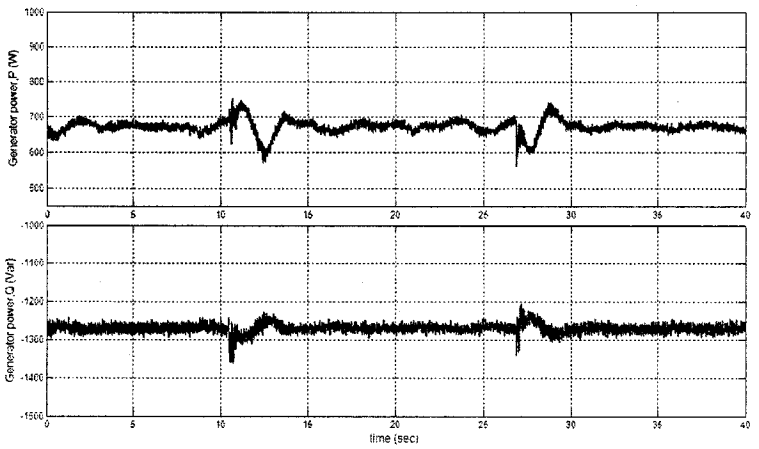

Fig. 4-59 Generator P and Q variation at half rated-load (Regulated system)

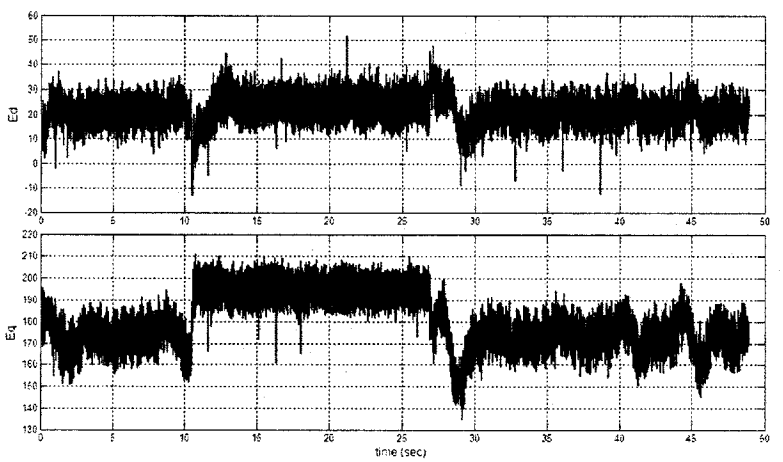

Fig. 4-60 E_d and E_q variation at half rated-load (Regulated system)

Now the last test is performed to see the effect on the voltage and frequency regulation by changing load and considering the wind turbine moment of inertia $J = 7$ $kg.m^2$, a larger value than before. A similar load variation is conducted at rated wind speed. From Fig. 4-61 to Fig. 4-62, one can see that the voltage and frequency are regulated and that their respective current variations are also shown in Fig. 4-63. Both the reference and actual currents are following each other. Hence the proposed control scheme is very effective in regulating the voltage and the frequency irrespective of any load variations. The same conclusion can be made based on the above results that higher values of J affect the dynamic response of the system, that causes a slower frequency response and also it presents rather a higher oscillations in the frequency waveform as compared with lower values of J during load variations.

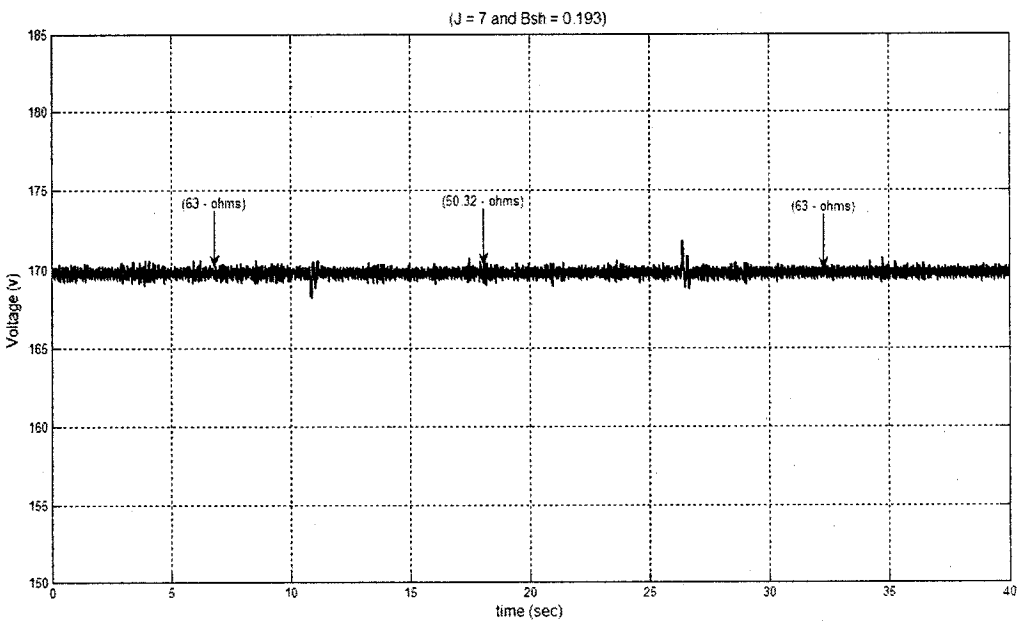

Fig. 4-61 Voltage variations at half rated-load (Regulated system)

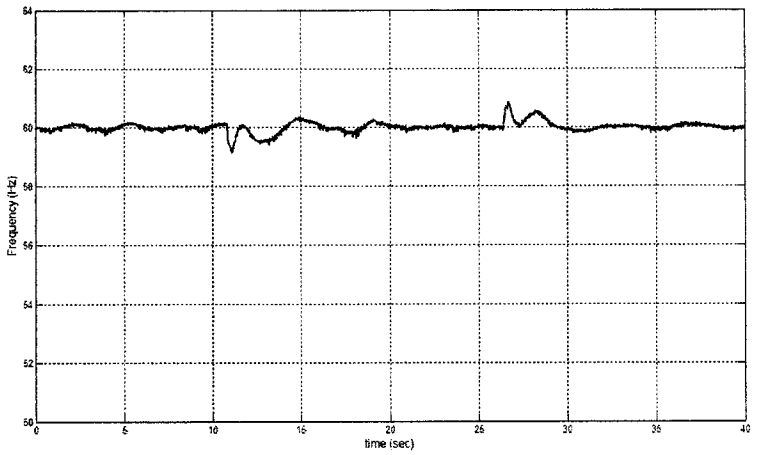

Fig. 4-62 Frequency variations at half rated-load (Regulated system)

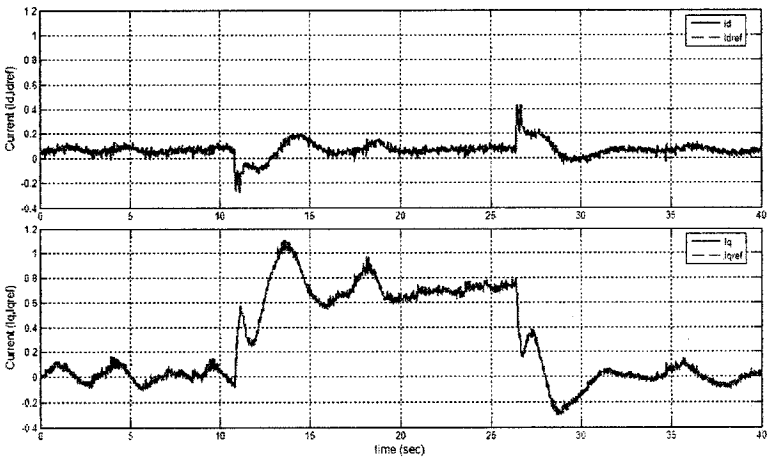

Fig. 4-63 Current variation at half rated-load (Regulated system)

4.5 CONCLUSIONS

This Chapter has presented the experimental results to validate the theoretical analysis and simulation results presented in previous Chapters. First, the hardware used to implement the set-up has been described in details. The control scheme for the inverter, with SPWM current control based on the DQ model of the VSI were implemented in a DSP development kit from dSPACE with user interface that allows monitoring and variation of the parameters of the system. A single voltage source inverter is used to

regulate the stand-alone induction generator terminal voltage and frequency. The proposed scheme for regulating voltage and frequency of an induction generator with an unregulated prime mover was tested for a hydro-type turbine and also for a wind turbine. The results show that by operating the VSI only as a STATCOM, no active power control, the voltage can be regulated but the frequency variation increases with respect to the unregulated system when constant impedance loads. This occurs because the magnitude of the speed variation of the unregulated turbine and frequency of the generated voltage depends on the magnitude of the variation of the active power demanded by the load. For the unregulated case, when the load resistance increases the voltage magnitude also increases, resulting in a smaller load power variation than when the voltage is regulated. For the induction generator operating in stand-alone with a wind turbine, the performance is also good but the speed of response depends on the inertia of the wind turbine. Finally experimental results verify that the proposed control system is very effective in the regulation of voltage and frequency of the stand-alone induction generator driven by unregulated turbines such a hydro turbine or a wind turbine.

CHAPTER 5

CONCLUSION

5.1 SUMMARY

Self-excited induction generators SEIGs are simple, rugged, maintenance free and inexpensive compared to the traditional synchronous generators in the low and medium power ranges. However, the regulation of the output voltage and frequency is an issue for stand-alone applications. Unlike synchronous machines, they require reactive power to generate active power and the output frequency varies with the load variation even if the shaft speed is regulated due to the slip factor. Therefore, instead of using a governor for the prime mover, which presents moving parts and requires maintenance, one can use a power electronic controller at the stator side of the SEIG. In order to reduce the size (rating) of the power electronic controller, the conventional 2 p.u ac-dc-ac converter is replaced by a smaller ac-dc converter with a battery bank in the dc side and a suitable control scheme in this thesis. The battery bank allows the VSI to compensate for the active power unbalance between an unregulated prime mover and a variable load. In this way, the shaft speed of the generator can be adjusted and the output frequency can be regulated. Researchers have shown that a STATCOM can be used to regulate the voltage magnitude of induction generators with regulated turbines by means of reactive power control. However, this work has shown that the regulation of the output voltage alone in SEIG based systems with unregulated prime movers increases the variation of the output frequency for input and load power variations. In the proposed system with the battery

bank, the VSI can operate as a UPS, supplying the local load even when the prime mover is not supplying mechanical power to the induction generator. In such a case, the induction generator should be disconnected from the system to allow the battery to supply the load for longer periods.

A 2-hp prototype was assembled for the validation of the proposed concept. The parameters of the induction machine were obtained experimentally. The effect of the variation of the size of the capacitor bank used for excitation of the generator as well as the load variations on the output voltage were analyzed theoretically. The size of the capacitor bank was selected for a given shaft speed at no-load conditions so that the output voltage is regulated at rated value. The VSI provides the reactive power required for the regulation of the voltage as the load increases or consumes more reactive power. A model for the system was developed and used in the design of the four linear controllers of the VSI. The control logic of the VSI was implemented in a rapid prototyping system from dSPACE. A user interface that allows the monitoring and setting of system parameters was developed in dSPACE control desk. Extensive experimental testing was carried out for two types of prime movers: Impulse type micro hydro and wind turbines. It was shown that the proposed system is effective in regulating the output voltage and frequency for variation in the input power, from the prime movers, and output power consumed by the load.

5.2 SUGGESTIONS FOR FUTURE WORK

(1) Control of the dump load for the start-up of the induction generator.

(2) Control of the dump load during normal operation to consume excess active power produced by the induction generator that is not used by the load and cannot be stored in the battery bank of the VSI that is completely charged.

(3) Detailed theoretical analysis of the effect of varying the wind turbine parameters like inertia, torsional coefficient and damping constant on the regulation of voltage and frequency.

(4) Analysis of the proposed control scheme for the regulation of voltage and frequency considering variable impedance, unbalance and or non-linear loads.

REFERENCES

[1] Twidell J.W. and Weir A.D, "Renewable Energy Resources", E. & F.N. Span Ltd. London, New York, 1996

[2] Johnson G.L, "Wind Energy Systems", Prentice Hall, 1985

[3] Jayadevailah T.S. and Smith R.T, "Generation Schemes for Wind Power Plants", IEEE Trans. on Aero space and electronic systems, Vol. AES-11, No. 4, pp-453-550, July 1975

[4] Hillowala R.M. "Control and Interface of Renewable Energy System", A Ph.D. Thesis, University of Brunswick, 1992

[5] Boyle Godfrey "Renewable Energy, Power for a sustainable future", 1996

[6] Warnick C.C "Hydro Power Engineering", Prentice Hall 1984

[7] Grantham A.C, Rahman F. and Seyoum D. "A Self-Excited Generator with Voltage Regulation for use in Remote area Power Supply", Power electronic and Motion Control Conference, 2000, Proceedings, IPEMC 2000.Vol 2, 15-18 Aug.2000, pp-710-715

[8] Rajakaruna R.M.A.S "Control of a Stand-Alone Self-Excited Induction Generator Driven by an Unregulated Turbine", A Ph.D. Thesis University of Toronto 1993

[9] Gulliver J.S and Arndt R.E.A "Hydro Power Engineering Hand Book", McGraw-Hill, Inc. 1991

[10] Lopes Luiz A.C and Almeida R.G, "Wind-Driven Self-Excited Induction Generator with Voltage and Frequency Regulated by a Reduced-Rating Voltage Source Inverter", IEEE Trans. on Energy Conversion, Vol.21, No.2, June 2006, pp. 297-304

[11] Vaidya Jay "Advanced Electric Generator and Control for High Speed Micro/Mini Turbine Based Power Systems", Earl Gregory, Power Generation, Propulsion Directorate, AFRL/PRPG Wright-Patterson AFB

[12] Ackermann Thomas "Wind Power in Power Systems", John Wiley and Sons Ltd. 2005

[13] Hansen L.H, Blaabjerg F., Christensen H.C. and Linhard U, "Generators and Power Electronics Technology for Wind Turbines", IECON'01: The 27th Annual Conference of the IEEE Industrial electronic Society, 2000

[14] Ghulam Dastagir and Luiz A.C. Lopes "Voltage and Frequency Regulation of Self-excited Induction Generator", Electrical Power Conference, Montreal, 2007

[15] E.D. Basset and F.M. Potter, "Capacitive Excitation for Induction Generators", AIEE Trans. (Elect Engg.), Vol.54, pp. 540-544, May 1935

[16] C.F. Wagner, "Self excitation of Induction Motors", AIEE Trans. (Elect. Engg.) Vol.58, pp. 47-51, February 1939

[17] Mustafa Al-Saffar "Voltage Control of SEIG using a Continuously Controlled Capacitors", A Ph.D Thesis, University of Winconsin-Madison 1997

[18] Murthy S.S, Malik O.P and Tandon A.K "Analysis of Self-Excited Induction Generators", IEE Proceedings C. Generation, Transmission and Distribution, 1982

[19] G.C.D. Souza, Martin F, J.P Rey and J.A Bruinsma, "An Autonomous Induction Generator System with Voltage Regulations", In Proc of the 4th IEEE International on Power Electronics and Drive Systems (PEDS 2001), Indonesia, 22-25 Oct. 2001.Vol.1, pp-94-98

[20] Ping L, Jiang X, Yong K, Hui and Jian C "Synchronous Frame Based Control Method of Voltage Source Converter (SVC) for Prototype Super-Conducting Magnetic Energy Storage (SMES)", in Proc of the 3rd Power Electronics and Motion Control Conference (IPEMC 2001), Vol.2, pp-537-541

[21] A. E. Fitzgerald, Charles Kingsley and Stephen D. Umans, Jr. "Electric Machinery", 6th Edition 2003

[22] Chapman S.J "Electric Machinery Fundamentals", 4th Edition 2005

[23] Bhim Singh Murthy S.S and Sushma Gupta "Analysis and Design of STATCOM-Based Voltage Regulator for Self-Excited Induction Generators", IEEE Trans. on Energy Conversion, Vol.19 No.4, Dec.2004, pp-783-790

[24] Singh S.P, Bhim Singh and Jain M.P "Performance Characteristics and Optimum Utilization of a Cage Machine as Capacitor Excited Induction Generator", IEEE Trans. on Energy Conversion, Vol.5, Dec.1990, pp-679-685

[25] Mohan N. "Electric Drives: An Integrative Approach", 2001

[26] Sun Huili "Performance Assessment of Islanding Detection Methods using the Concepts of Non Detection Zones", An M.A.Sc Thesis, Concordia University 2005

APPENDIX

A-1 PER UNIT REPRESENTATION

Due to the simpler calculations and easier interpretation of the numerical values, all the variables, parameters and equations in the steady-state analysis of SEIG are presented in per unit values. Generally the rated values of voltage, current and frequency of the generator are selected as base values. In this thesis, the rms values of rated line to neutral voltage and the rms value of rated line currents are selected as the base values. The base values of the other system variables are derived by considering their relationships to the selected base values.

Selected Base Values:

Voltage	$V_B = 120\ V$
Current	$I_B = 6.1\ A$
Frequency	$f_B = 60$ Hz
Speed	$\omega_B = 1800$ rpm

Derived Base Values:

Impedance	$Z_B = V_B/I_B = 19.67$ ohms
Power	$S_B = V_B.I_B = 732$ watts

Since the base power is in per phase, then the machine three phase rated power P_{pu} is 3 p.u, but the p.u power used in this steady-state analysis is based on the actual machine rated power $P_{BR} = 1.492$ kW that is equivalent to 2-hp. The new p.u power can

be calculated by, $P_{punew} = P_{puold}\ 3P_B/P_{BR}$. Now, the value of 1.0 p.u of the new P_{pu} is equivalent to the three-phase rated power.

The machine saturation curve measured at synchronous speed is shown in Fig. 3-7, all voltages and currents are in rms values. The relationship between V_g/F and X_m is also shown in (3-11) and given in p.u value. The measured parameters of the induction machine in the per-unit system are given below,

Stator resistance (R_s) = 0.0676 p.u

Rotor resistance (R_r) = 0.0453 p.u

Magnetization reactance (X_m) = 2.2 p.u

Stator and rotor leakage reactances $(X_{ls}=X_{lr})$ = 0.0732 p.u

A-2 DEFINITION OF CONSTANTS

By solving the equivalent circuit of induction generator for the two unknowns X_m and F, following two non-linear equations can be obtained.

$$f(X_m, F) = (A_1 X_m + A_2)F^2 + (A_3 X_m + A_4)F + A_5 = 0$$
$$g(X_m, F) = (B_1 X_m + B_2)F^3 + (B_3 X_m + B_4)F^2 + (B_5 X_m + B_6)F + (B_7 X_m + B_8) = 0$$

Where,

$$A_1 = R_L(R_s + R_r) + 2X_c X_1, \quad A_2 = R_L(R_s + R_r)X_1 + X_c X_1^2$$
$$A_3 = -(R_s R_L + 2X_c X_1)v, \quad A_4 = -(R_s R_L + X_c X_1)X_1 v$$
$$A_5 = -X_c R_L(R_L + R_s)$$
$$B_1 = -2X_1 R_L, \quad B_2 = -X_1^2 R_L, \quad B_3 = -B_1 v, \quad B_4 = -B_2 v$$
$$B_5 = (R_L + R_s + R_r)X_c, \quad B_6 = (R_L + R_s + R_r)X_c X_1 + R_L R_r R_s$$
$$B_7 = -X_c(R_L + R_s)v, \quad B_8 = B_7 X_1$$

For the unknown X_c and F the following equations can be solved,

$$f(X_c, F) = C_1F^3 + C_2F^2 + (C_3X_c + C_4)F + C_5X_c = 0$$

$$g(X_c, F) = (D_1X_c + D_2)F^2 + (D_3X_c + D_4)F + D_5X_c = 0$$

Where,

$$C_1 = -(2X_m + X_1)X_1R_L, \quad C_2 = -C_1v$$
$$C_3 = (R_L + R_s + R_r)(X_1 + X_m), \quad C_4 = R_sR_LR_r$$
$$C_5 = -(R_s + R_L)(X_1 + X_m)v$$
$$D_1 = (2X_m + X_1)X_1, \quad D_2 = R_L(R_s + R_r)(X_1 + X_m)$$
$$D_3 = -D_1v, \quad D_4 = -R_sR_L(X_1 + X_m)v, \quad D_5 = -R_r(R_L + R_s)$$

A-3 ELECTRONIC CIRCUIT FOR THE GATING SIGNALS OF VSI